Title
Slow Magnetic Relaxation in Single-Chain and Light Actuated Single-Molecule Magnets

Author
Feng, Xiaowen

Publication Date
2015

Peer reviewed|Thesis/dissertation

Slow Magnetic Relaxation in Single-Chain and Light-Actuated Single-Molecule Magnets

by

Xiaowen Feng

A dissertation submitted in partial satisfaction of the

requirements for the degree of

Doctor of Philosophy

in

Chemistry

in the

Graduate Division

of the

University of California, Berkeley

Committee in charge:

Professor Jeffrey R. Long, Chair
Professor Richard A. Andersen
Professor Michael F. Crommie

Summer 2015

Abstract

Slow Magnetic Relaxation in Single Chain and Light-Actuated Single Molecule Magnets

By

Xiaowen Feng

Doctor of Philosophy in Chemistry

University of California, Berkeley

Professor Jeffrey R. Long, Chair

The work presented in this dissertation describes the synthesis and characterization of single chain and single molecule magnets that display slow magnetic relaxation at low temperatures. A wide variety of techniques and spectroscopic methods are covered, including SQUID measurements, high field and high frequency EPR spectroscopies, structural analysis, infrared spectroscopies. Chapter one provides a brief introduction to single chain and single molecule magnets, characterization method, and synthetic strategies toward these materials.

In Chapter Two Cyano-bridged single-chain magnets of the type $L_4FeReCl_4(CN)_2$, where L = diethylformamide (DEF) (**1**), dibutylformamide (DBF) (**2**), dimethylformamide (DMF) (**3**), dimethylbutyramide (DMB) (**4**), dimethylpropionamide (DMP) (**5**), and diethylacetamide (DEA) (**6**), have been synthesized to enable a systematic study of the influence of structural perturbations on magnetic exchange and relaxation barrier. Across the series, varying the amide ligand leads to Fe-N-C bond angles ranging from 154.703(7)° in **1** to 180° in **6**.Variable-temperature dc magnetic susceptibility data indicate ferromagnetic exchange coupling in all compounds, with the strength of exchange increasing linearly, from J = +4.2(2) cm^{-1} to +7.2(3) cm^{-1}, with increasing Fe-N-C bond angle. Ac magnetic susceptibility data collected as a function of frequency reveal that the relaxation barriers of the chain compounds rises steeply with increasing exchange strength, from 45 cm^{-1} to 93 cm^{-1}. This examination demonstrates that subtle tuning of orbital overlap, and thus exchange strength, can engender dramatic changes in the relaxation barrier. Indeed, the perfectly linear Fe-N-C bond angle in **6** leads to one of the highest barriers and coercive fields yet observed fora single-chain magnet.

Chapter Three briefly discusses model compounds $(NBu_4)_2[ReCl_4(CN)_2]$ (**1**), $(DMF)_4ZnReCl_4(CN)_2$ (**2**), and $[(PY5Me_2)_2Mn_2ReCl_4(CN)_2]$-$(PF_6)_2$ (**3**) synthesized to probe the origin of the magnetic anisotropy barrier in the one-dimensional coordination solid $(DMF)_4MnReCl_4(CN)_2$ (**4**). High-field EPR spectroscopy reveals the presence of an easy-plane anisotropy ($D > 0$) with a significant transverse component, E, in compounds **1**- **3**. These findings indicate that the onset of one-dimensional spin correlations within the chain compound **4** leads to a suppression of quantum tunneling of the magnetization within the easy-plane, resulting in magnetic bistability and slow relaxation behavior. Within this picture, it is the transverse E term associated with the Re^{IV} centers that determines the easy-axis and the anisotropy energy scale associated with the relaxation barrier. The results demonstrate for the first time that slow magnetic relaxation can be achieved through optimization of the transverse

anisotropy associated with magnetic ions that possess easy-plane anisotropy, thus providing a new direction in the design of single-molecule and single-chain magnets.

In Chapter Four, molecules exhibiting bistability have been proposed as elementary binary units (bits) for information storage, potentially enabling fast and efficient computing. In particular, transition metal complexes can display magnetic bistability via either spin-crossover or single-molecule magnet behavior. I now show that the octahedral iron(II) complexes in the molecular salt $[Fe(1\text{-propyltetrazole})_6](BF_4)_2$, when placed in its high-symmetry form, can combine both types of behavior. Light irradiation under an applied magnetic field enables fully reversible switching between an $S = 0$ state and an $S = 2$ state with either up ($M_S = +2$) or down ($M_S = -2$) polarities. The resulting tristability suggests the possibility of using molecules for ternary information storage in direct analogy to current binary systems that employ magnetic switching and the magneto-optical Kerr effect as write and read mechanisms**.**

In Chapter Five, the mononuclear complex *trans*-$(Bu_4N)_2[Re^{IV}Cl_4(CN)_2]$ ·2DMA (DMA = *N*,*N*-dimethylacetamide) with $D = +11.5$ cm^{-1} (and $|E| = 3.1$ cm^{-1}) is shown to display Orbach-type slow relaxation of magnetization with an energy barrier for spin-reversal of $U_{eff} = 26.7$ cm^{-1} in well agreement with the spectroscopically and magnetically derived energy gap. This energy barrier represents the highest record for 4d/5d mononuclear single-molecule magnets yet observed.

In Chapter Six, one-dimensional chain solid $Co(hfac)_2(NITPhenOMe)(DMF)_x$ is shown to display stronger intrachain interaction between Co(II) and radical centers with J = -97 cm^{-1}, compared to that of -76 cm^{-1} in the original Co(hfac)2(NITPhOMe) compound. Further magnetic measurements revealed a energy barrier of $\Delta_\tau = 251$ cm^{-1} with magnetic blocking up to 12 K. This energy barrier and blocking temperature represents the highest record yet for any single-chain magnets reported.

Table of Contents

Table of Figures

Acknowledgements

Six years were spent on the results presented in this dissertation. After reading enough acknowledgements from previous lab mates (which secretly becomes my favorite habit in lab), I am eventually at the stage of writing my own. Six years ago, as a freshly graduated student from Peking University, I have no idea what my life would be in a completely new country. Also, I did not expect it would take six years for me to get this degree! However, at the end, everything worked out great and worth well.

I will start by acknowledging my advisor, Prof. Jeffrey Long, not because it is standard to thank your advisor first, but because I can't achieve any success in graduate school without his guidance. I appreciate all the resources he provided me during this journey and making the whole lab like a family. No matter where I am in the future, I will always be proud as Long group alumni.

There is another special person I would like to thank, who is my undergraduate advisor, Prof. Song Gao. He allowed me work in his lab since first year of undergrad, and was patient enough to deal all the fundamental questions (and troubles) I had throughout my entire four years at Peking University. He is the first person taught me magnetism and convinced me to become a chemist for my career. When I am depressed, he is always there to give me suggestions to move forward. Without him, I might already become a boring person working for a boring company now.

It seems that I am now moving to the section of thanking my great lab mates. I begin by thanking Prof. T. David Harris. Besides Jeff, Dave is probably the most important person in graduate school for me. He was my coworker and is my lifetime friend. I appreciate his special speech for me every time when I was lazy or depressed. Also, he gave me my first English name "Spanky" as soon as he figured out I don't have one. I appreciate that as well.

Having spent most my time at Berkeley living in 3001 Ellis Street, I would like to thank my roommates Prof. Jeffrey Rinehart and Dr. Brian Wiers. Jeff went to school with me everyday. He was the alarm for me by knocking on my doors every morning telling me it is time to wake up and go to work. We played video games together and discussed chemistry when we were tired of playing. Till today, I still remember his comforting talk to me on the day of my qualifying exam when I felt extremely nervous. Also, I appreciate his continuous support of my research, for example, he was among the 10 audience of my ACS talk at 4:00 pm of the last day. Brian is probably the most interesting American I have ever met, though most of times I don't quite understand his humorous. To me, it seems that he knows everything. He is definitely a great friend to be missed when I move to Boston. Also, Brian is the person to make me to think critically, for example, I am now very careful when I am reading things from Wikipedia.

In 2009, Jeff took four students to his lab, Eric, Katie, Dana, and me. Dr. Eric "Erc" Bloch is the leader of our small team. We worked next to each other at the beginning of graduate school and he took the advantage of that teaching me English, for example, rubber band. I would like to thank him and his wife Lynn for introducing US culture to me when I first came to US. I also appreciate his effort to demonstrate that a tesla coil won't kill a person when he is as big as Dave Harris. I am glad we will become labmates again when I go to Boston. Katie is my magnetism comrade. She is always nice to everyone and everything, though sometimes I don't understand why she call moth cute. I enjoyed all the moments during the past six years and I am glad we both made it to the end! Cheers! By the way, I would like thank to her kept promoting cheese to me who doesn't like cheese at all. Dana is a nice girl working on biochemistry. For most of

times, I don't really understand biology, thanks to all the sleeps I did during my biology classes in high school. Dana did great job working on biology related materials by herself and I believe she will achieve great success. I also enjoyed my time playing intramural soccer with her.

Kenji Sumida is worthy of a significant amount of thanks. He is always helpful throughout graduate school. I appreciate his patience answering all my questions as my GSI, as well as his patience editing my Chinese-accent research papers. He taught me the rules of baseball and that become my favorite sport. I thank Kenji for that as well.

I would also like to thank Joe Zadrozny. Joe is among those people who are never tired of teaching me English and American culture in a special way, for example, changing my homepage or wallpaper of my laptop while I am having lunch. I will always miss our research trips to the high field magnetic national lab and endless discussions about magnetism together.

I also thank Tom Mcdonald. He is an honorary resident of 3001 Ellis Street, approved by all residents at 3001 Ellis Street. I am always curious if he has any inside relationship with one of my favorite fast food restaurant, though I never get a chance ask him. I appreciate his support to me during graduate school. Zoey Herm has always been a kind lab mate and I appreciate the drink she bought me after breaking one of my Champagne bottles. I wish her great success in Europe.

The year after I joined the lab, Jeff brought in big group of students, Jarad Mason, David Zee, and Jordan Axelson. Among these people, I begin by thanking Jarad. Jarad is always willing to help me though 99% of times he will start with "no". No matter how hard he tried to prove he doesn't like me, for example, putting a dead moth on my bench, he failed. Indeed, I always believe he likes me a lot. I appreciate that. David and Jordan work on the water splitting project, which doesn't overlap with my project a lot. But their hard working attitude always inspires me and I wish them big success in the future.

Many talented students joined Jeff's lab after Jarad, David and Jordan. Miguel Gonzales also comes from Asia, but speaks much better English than I am. He provided great help to me discovering the first light actuate single-molecule magnet when I was in France. Dianne is always hard working and I enjoyed working in the same glove box with her. Mike Aubrey is also a great person I will surely miss when I go to Boston. I will recall all the moments we have in the lab, except the night he puked in my BMW after he got super drunk. Lucy and Phil joined the lab three years and have been working in the same subgroup with me since. They fast made great impact to the small group, which is very impressive. Phil is the only person I know from Ohio, except LeBron James. He proved to me that no matter how old you are, you could always get cookies and candies from your grandparents. I thank Phil and his family for the delicious cookies. Lucy comes from south California and I learned people use the word "dude" a lot in SoCal. Matt was a visiting student couple years ago and he joined the Long group for graduate school after college. I appreciate his loyalty to baseball, though I always believe Cardinals is a better team. The other students in the Long group, Jon, Rodi, Mercedes, Julia, Rebecca all will continue to carry the tradition of excellence as the old members do.

Many post-docs have also passed through lab and provide me great help. Prof. Hema Karunadasa, who was also a graduate student in the lab taught me how to use the glovebox properly. I also thank her for the great help of collecting low temperature crystal structures after she become a professor at Stanford University. Hye Jin Choi was a great source of magnetism knowledge. Every time I talked to her, she was always nice and patient. Pierre Dechambeniot taught me how to do layering for crystallization and that make a big impact for my entire research in graduate school. I also thank him for his help when I was doing experiments in

France and sharing his knowledge about wines with me. Prof. Leslie Murray overlapped with me for only one year, but I do enjoy playing fantasy basketball with him. It would even be better if he accepted any of the trade proposals I suggested. Prof. Michael Nippe is great person to talk to when I am depressed by synthesis. He always has great suggestions and ideas and after all of it, I only need to pay him a hotpot dinner. Dr. Selvan Dimir also worked on magnetism and she kepted mazing me by making awesome molecules. Her great synthetic knowledge helped me a lot during the course of pursuing my Ph.D degree.

There are also several undergraduate researchers I would like to thank: Kaithlyn Weeber, Mary Anne Manumpil, David Gygi, Raymond Yu, and Jo Melville. I wish them best luck of the future and I am looking forward to seeing their success.

I have a list of collaborators outside the department to thank. Without them, I can't understand science as nearly to the level as I do now. I learned EPR from Prof. Steve Hill and his student Junjie Liu, which resulted in the work of chapter 3 in this dissertation. Dr. Rodolphe Clérac and Prof. Corine Mathonière helped me apply fellowship to France and the effort eventually resulted in our big discovery of the first light actuated single-molecule magnet. I have special thanks to Rodolphe. He is a probably the best friend and collaborator I could ask for in this field. He always challenges me on my results and discoveries and makes me understand my research in a much deeper level.

Through the ups and downs of my graduate school time, I cannot accomplish anything without the support of my parents. Though I know they never care if I thank them or not, I am always grateful to be their only son and am always thankful for their endless support since I was born.

Much like Jeff whose name always shows at the end of author list of my papers because he has to deal with all the mess I created, I saved my last acknowledgements to a special person: Wenjing Liao. After six years at Berkeley, I couldn't ask for any better ending than this: I got my Ph.D and I found my true love. Although I know Wenjing is always proud of me no matter what I accomplish in graduate school, I hope that she can take some additional pride in knowing that this dissertation, though she won't understand most of it, is for her. During the darkest days of my Ph.D life, she never gave up on me and kept telling me I am the best. Wenjing, I truly thank you for everything.

It seems that I am about running out of space, so I will stop here. To anyone that I may left out, please don't feel offended. The graduate department requires me to stop before this section becomes longer than the real dissertation.

Chapter 1: An Overview of Slow Magnetic Relaxation in Single-Chain Magnets and Light Actuated Single-Molecule Magnets

1.1 Slow Magnetic Relaxation in Single-Molecule and Single-Chain Magnets

Nearly two decades ago, slow magnetic relaxation was observed in the molecular cluster compound $Mn_{12}O_{12}(O_2CCH_3)_{16}(H_2O)_4$ upon removal of an applied dc magnetic field, a phenomenon related to an energy barrier to spin inversion.[1] As shown in Figure 1, the Mn12 cluster consists of a central $Mn^{IV}{}_4O_4$ cubane with oxo-bridges to an outer sphere of eight Mn^{III} ions. At low temperatures, the Mn^{III} ions are anitferromagnetically coupled with the Mn^{IV} ions within the molecule to give an overall S = 10 spin ground state. Owing to the magnetic easy axis, the 21 M_S (M_S = 10, 9, …, -9, -10) levels will then split in the absence of an external magnetic field, with the M_S = ±10 levels lowest in energy and M_S = 0 highest, as is shown by the double-well potential model in Figure 2. Thus, flipping from "spin-up" (M_S = 10) to "spin-down" (M_S = −10) requires overcoming an energy barrier. The height of this energy barrier can be quantified according to the expression $U_{eff} = |D|S^2$ for an integer spin system or the expression $U_{eff} = |D|(S^2\text{-}1/4)$ for a half-integer spin system. Owing to their potential applications in high-density information storage, this remarkable discovery led to significant interest in designing, synthesizing, and studying new single-molecule magnets.[2]

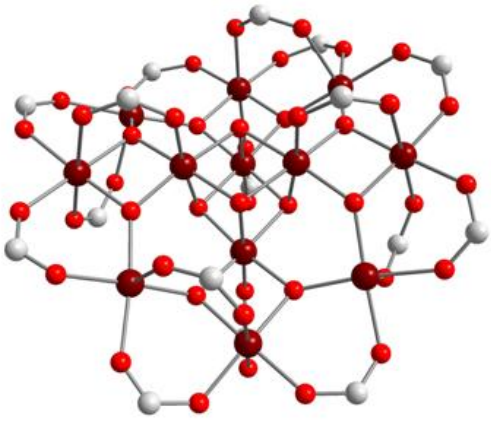

Figure 1. Crystal structure of $Mn_{12}O_{12}(O_2CCH_3)_{16}$. Dark red, red, and gray spheres represent Mn, O, and C atoms, respectively; some C, and H atoms are omitted for clarity

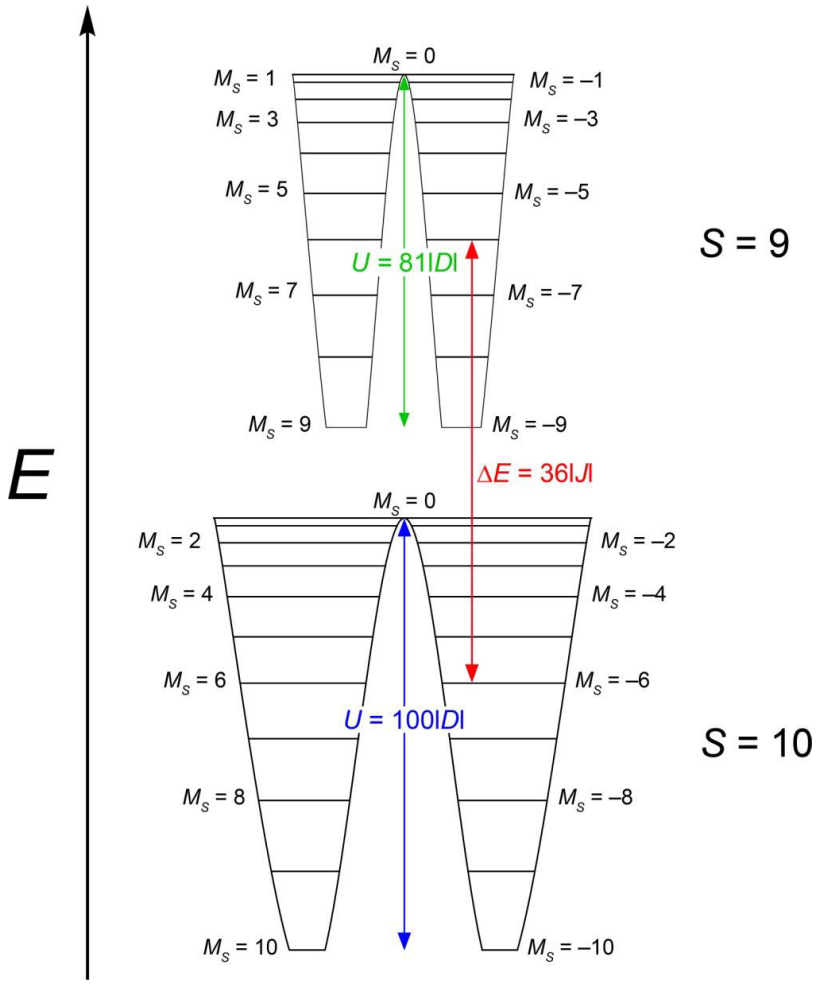

Figure 2. Energy splitting of the ground state and first excited state for an $S = 10$ molecule with uniaxial anisotropy.

Almost ten years after the discovery of $Mn_{12}O_{12}(O_2CCH_3)_{16}$, slow magnetic relaxation was also observed in a one-dimensional chain compound $Co(hfac)_2(NITPhoMe)$, shown in Figure 3, which displays a relaxation barrier of 107 cm^{-1}.[3] Within the chain, the high spin Co(II) (S = 3/2) centers are antiferromagnetically coupled to the nitroxide radical ligands (S = 1/2), leading to a net spin of S =1 per repeating unit. Indeed, this phenomenon was predicted by Roy Glauber over forty years ago and is known as the Glauber mechanism.[4] Shortly after this remarkable discovery, slow magnetic relaxation was also observed in another one-dimensional chain compound $[(saltmen)_2(py)_2Mn^{III}{}_2Ni^{II}(pao)_2]^{2+}$, wherein the trinuclear MnNiMn building units are ferromagnetically coupled, leading to an S = 3 net spin per repeating unit.[5] In this paper, such one-dimensional chain compounds that display slow magnetic relaxation were first termed single-chain magnets.

As evident from the foregoing examples, single-chain magnets display higher energy barriers than in their molecular building units. This increased barrier stems from an additional component to the total energy barrier, which is termed correlation energy. The

magnetic correlation length, ξ, increases exponentially as the temperature is lowered. If one considers flipping the spin in a single-chain magnet, the first energy component is the same anisotropic energy barrier, similar to that of a single-molecule magnet. In addition, as all the spin units within the chain are correlated via magnetic coupling, flipping the spin in single-chain magnets requires overcoming a second energy component that results from creating a new domain wall. Thus, the total relaxation barrier for a single-chain magnet (Δ_τ) may be expressed as $\Delta_\tau = 2\Delta_\xi + \Delta_A$ for an infinite chain. As the temperature is lowered, the correlation length grows exponentially, until it is finally limited by defects within the chain. In this finite-size regime, the expression of the total relaxation barrier is reduced to $\Delta_\tau = \Delta_\xi + \Delta_A$, because only one domain wall will be created at each end of the chain during magnetic relaxation.

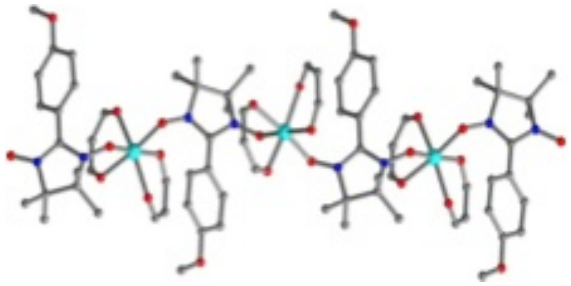

Figure 3. Crystal structure of $Co(hfac)_2NITPhOMe$. Cyan, red, blue, and gray spheres represent Co, O, N, and C atoms, respectively; H atoms are omitted for clarity

After the discovery of the first single-molecule magnet, early research efforts were focused on increasing the energy barrier magnetic relaxation by increasing the spin of the ground state, for instance by creating polynuclear coordination clusters with large magnetic moments.[6] However, results have suggested that any increase in the spin ground state is usually compensated for by a corresponding decrease in total magnetic anisotropy.[7] To overcome this problem, new approaches have emerged, for example by using a molecule that contains a single paramagnetic lanthanide or actinide ion, which can have slow magnetic relaxation resulting form the high spin-orbit coupling of f-element ions.[8] Significantly, the effective energy barrier for such molecules can be as high as 641 cm^{-1}, which is an order of magnitude higher than the original single-molecule magnet $Mn_{12}O_{12}$ and other transition metal clusters.[9] More recently, it has been shown that when placed in an appropriate symmetry, mononuclear first-row transition complexes can display large magnetic anisotropy, originating from a near-degenerate orbital ground term with unquenched orbital angular momentum. Moreover, taking advantage of Kramers Theorem,[10] fast quantum tunneling can be effectively avoided by using half-integer spin metal ions. Following this strategy, a wide range of mononuclear first row transition metal single-molecule magnets have been reported. For example, a linear two-coordinate linear Fe(I) molecule has recently been shown to display a spin reversal barrier of 226 cm^{-1}, and magnetic hysteresis up to 6.5 K.[11]

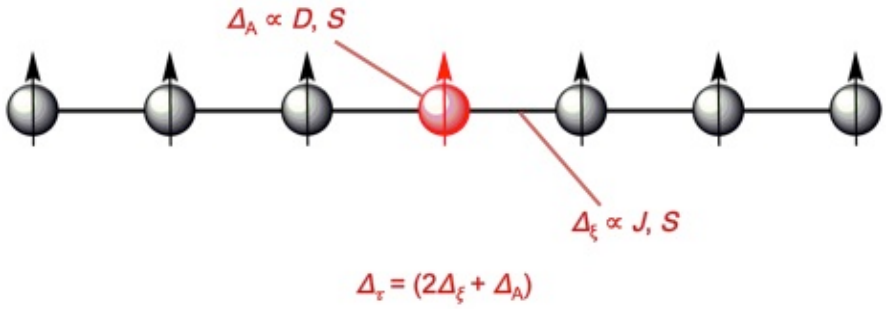

Figure 4. Schematic model of single-chain magnet, illustrating total relaxation barrier $\Delta_\tau = \Delta_A + 2\Delta_\xi$

Unlike the drastic improvements to the energy barrier in single-molecule magnets, efforts toward synthesizing single-chain magnets with large relaxation barriers have yielded limited progress. Indeed, the barrier of the first single-chain magnet, $Co(hfac)_2(NITPhOMe)$, remains the highest ever achieved at 107 cm^{-1}. The limited progress is due in large part to the lack of completed theoretical model for describing the relaxation mechanism in single-chain magnets. Previous work has shown that the correlation energy barrier, Δ_ξ, contributes significantly to the total relaxation barrier. However, studies on how factors, such as magnetic coupling J, and the zero-field splitting parameter D, influence the correlation barrier are in the early stage. Heisenberg and Ising chain models have been used to describe relaxation dynamics in theoretical works, while the study of real systems have suggested a more complicated Hamiltonian model. The Ising model assumes the domain walls within the chain are narrow, with the value of $|D/J|$ is larger than 4/3, and $\Delta_\xi = 4|J|S^2$. In the Heisenberg model, the magnetic anisotropy has to be small as $|D|<<|J|$, with $\Delta_\xi \approx 4S^2(|JD|)^{1/2}$. However, there is an intermediate regime between the Ising and Hersenberg limits, where the domain walls are spread across more than one unit cell. This correlation energy, Δ_ξ, is still under investigation from a fundamental point of view.[12]

1.2 Characterization of Slow Magnetic Relaxation in Single-Chain Magnets

To date, several techniques, including SQUID magnetometry, micro-SQUID, and X-ray magnetic circular dichroism, have been applied to probe slow magnetic relaxation in single-molecule and single-chain magnets. In most of these cases, slow magnetic relaxation occurs at extremely low temperatures (below 10 K) with relaxation times on the order of milliseconds. For such cases, slow magnetic relaxation can be observed by ac susceptibility measurements by applying an oscillating magnetic field at different frequencies. If the chain compound possesses an energy barrier to reorientation of the magnetization, the magnetic susceptibility will show a lag to the applied oscillating field. In this case, the in-phase magnetic susceptibility, χ_M', will decrease, while an out-of-phase susceptibility will grow in, featuring a series of frequency dependent peaks at different temperatures. These frequency dependent peaks can be using a generalized

Debye model to give the total relaxation time τ.[13] In an ideal single-chain magnet, slow magnetic relaxation occurs via thermal excitation over the energy barrier, known as Orbach relaxation, and can be characterized by the following equation:

$$\tau^{-1} = \tau_0^{-1}\exp(-\Delta_\tau/k_B T)$$

Here, τ is the relaxation time of the magnetic moment at the given temperature; Δ_τ is the total relaxation barrier of the single-chain magnet; and τ_0 is the attempt frequency. For a real singe-chain magnet, slow magnetic relaxation should only occur via Orbach relaxation, thus, the plot of $\ln(\tau)$ versus $1/T$ should feature a linear region where the slope of the line is the total relaxation barrier Δ_τ.

Unlike the quantum tunneling always observed in single-molecule magnets, as the chain correlation length grows, quantum tunneling is increasingly suppressed. In fact, the relaxation time due to tunneling should increase exponentially with increasing chain length. One method of visualizing such an effect is to consider the probability that all spins within the chain tunnel simultaneously, as would be required if the total spin were to tunnel coherently. If the probability for one spin to tunnel is considered as P ($P<1$), then the probability for observing quantum tunneling in a chain should be P^n, where n represents the number of the repeating units. Clearly, this probability decreases exponentially with increasing number of spins in the chain. Consequently, in the limit of large correlation length, S can be treated classically.

Another difference between slow magnetic relaxation for a single-chain magnet and that for a single-molecule magnet is the additional energy component, the correlation energy Δ_ξ. Determining the value of correlation energy is the most important aspect of distinguishing single-chain magnets from single-molecule magnets. For any one-dimensional classical system, the $\chi_M T$ product in zero applied field is directly proportional to the correlation length, ξ, in zero applied field. In the particular case of anisotropic Heisenberg or Ising-like one-dimensional behavior, ξ, and thus $\chi_M T$, increases exponentially with decreasing temperature, according to the equation:

$$\chi_M T/C = \exp(\Delta_\xi/k_B T)$$

where C is the effective Curie constant, Δ_ξ is the correlation energy (the energy needed to create a domain wall in the chain), and k_B is the Boltzmann constant.[14] Following from this relationship, a plot of $\ln(\chi_M T)$ vs $1/T$ should display a linear region, with the line of best fit exhibiting a slope corresponding to the correlation energy. Thus, to experimentally probe the one-dimensional nature of a single-chain magnet, variable-temperature ac susceptibility data are collected in the absence of an applied dc field, with an ac field of 4 Oe oscillating at 1 Hz, with the resulting plot of $\ln(\chi'_M T)$ vs $1/T$ featuring a linear region over certain temperature range and yielding the value of Δ_ξ corresponding to the energy required to create a domain wall within the chain.

In conclusion, it is extremely important to fully characterize the magnetic properties, especially the one dimensional nature of a chain compound, before one can define such compounds as single-chain magnets. Although a lot of questions and parameters are still unclear and require theoretical and experimental development, a detailed characterization

is certainly the first step forward toward a better understanding of these promising materials.

1.3 Single-Chain Magnets with Uniaxial Anisotropic Building Units

Considering the relationship between single-molecule and single-chain magnets, a straightforward way of designing single-chain magnets should be by assembling single-molecule magnets with bridging ligands. This strategy has resulted in the discovery of several single-chain magnets, such as the one of the first single-chain magnets, $[(saltmen)_2(py)_2Mn^{III}{}_2Ni^{II}(pao)_2]^{2+}$.[5] However, in practice, the choice of single-molecule magnets capable of assembling into one-dimensional chain compound is quite limited. Indeed, except for a couple examples of $Mn^{III}{}_2$ chains, very few single-chain magnets are synthesized directly from a single-molecule-magnet building unit. An alternative to this approach is to use uniaxial anisotropic building units instead of single-molecule-magnet units. Following this idea, octahedral Co^{II}, Fe^{II}, Mn^{III} or Ln^{III} ions with available coordination sites could be good candidates as the anisotropy building units for single-chain magnets, when they are assembled with appropriate bridging ligands, such as organic radicals. However, one has also to notice that, unlike the single-chain magnets made of single-molecule magnets, for single-chain magnets of this type, it is hard to have a clear expression of anisotropic energy barrier and correlation energy barrier using *S*, *D*,

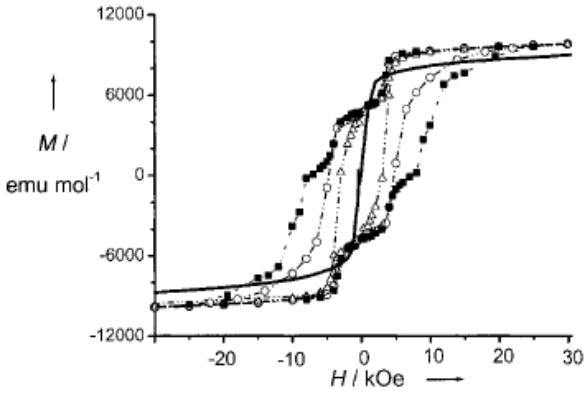

Figure 5. Magnetic hysteresis of $Co(hfac)_2(NITPhOMe)$ at 2.0 K (black solid squares), 3.0 K (circles), and 4.5 K (triangles).

and *J*. Thus, it remains difficult to describe the slow relaxation mechanism, which still requires a lot theoretical effort in this field of research.

The best case representing this type of single-chain magnets is the first example of single-chain magnets, $Co(hfac)_2(NITPhOMe)$, reported by Gatteschi et al. in 2001, shown in Figure 5, which still holds the record of energy barrier for a single-chain magnet.[4] The large Ising type magnetic anisotropy within the chain originates from the strong spin-orbit coupling in six-coordinate octahedral Co(II) centers, as later demonstrated for the mononuclear complex $Co(hfac)_2(NITPhOMe)$.

This approach was then applied to the lanthanides, using a similar radical ligand, as the strong spin-orbit coupling from 4f-orbitals was expected to provide much larger magnetic anisotropy than transition metals. In 2005, Gatteschi and co-workers reported a series of single-chain magnets consisting of [Ln(hfac)$_3$] (Ln = Tb, Dy, Ho, Er), and a nitronyl nitroxide radical.[15] However, the energy barrier is much smaller than the original Co(hfac)$_2$(NITPhOMe) complex. This is largely due to the much smaller magnetic coupling between nitronyl nitroxide radical and Ln(III) centers, as the contracted 4f orbitals do not overlap as strongly with the radical p orbitals. With a much smaller intrachain interaction, the correlation energy required to create domain walls decreases, leading to a drastic decrease in total relaxation barrier. This result suggested that to improve the properties of Ln(III) based single chain magnets, a better radical ligand with more diffused p orbitals and thus stronger magnetic coupling should be used. Recent developments in Ln(III)-radical single-molecule magnets has shown strong magnetic coupling between nitrogen-based radical, such as N_2^{3-}, bipymidine, bipy-based radicals and Ln(III) centers, providing good candidate building units for pursuing single-chain magnets with large magnetic anisotropy.

Another representative example is a zig-zag chain compound [Mn^{III}(TPP)O$_2$PHPh](H$_2$O) report by Bernot and co-workers, as shown in Figure 6.[16] Within the chain, the anisotropic $S = 2$ Mn^{III} centers are canted and antiferromagnetically coupled, with $D_{Mn} = -3.3$ cm^{-1}, $J = 0.47$ cm^{-1}, $\theta = 34.6°$, and $\Delta_\tau = 26$ cm^{-1}. Remarkably, this compound fits well into the Ising chain model, where the theoretical energy barrier calculated by $8|J|S^2\cos\theta + |D|S^2 = 25.7$ cm^{-1} is in good agreement with the experimental barrier.

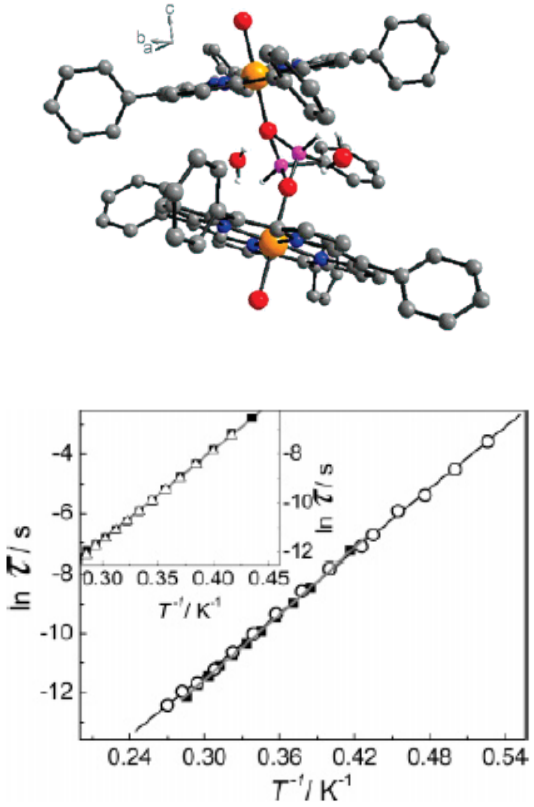

Figure 6. Upper: Crystal structure of [Mn^{III}(TPP)(O$_2$PHPh)](H$_2$O). Yellow, red, purple, and gray

spheres represent Mn, O, P, and C atoms, respectively; H atoms are omitted for clarity. Lower: Arrhenius plot and best fit to powder sample (circles) and crystals (squares), to give $\Delta_\tau = 26$ cm^{-1}.

As discussed above, assembling anisotropic molecular building units, including octahedral cobalt(II), manganese (III), or lanthanides ions, is one of the most rational ways of synthesizing single-chain magnets. As the magnetic anisotropy is assured by the building units, improving the intrachain magnetic coupling between building units is the key factor to increasing the total relaxation barrier, and therefore to increase the blocking temperature.

1.4 Cyano-Bridged Single-Chain Magnets

The family of compounds, known as Prussian Blue analogues, represent one of the most interesting types cyanide-bridged materials.[17] Inspired from the three-dimensional Prussian Blue system with extended M-C-N-M'-N-C- linkages, efforts using six coordinate cyanide building units of the type $[M(L)_x(CN)_{6-x}]^{a-}$, toward one-dimensional chain compound have resulted in many successful cyano-bridged single-chain magnets systems.[18,19,20]

The linear M-CN-M′ interaction (ca. 5.0 Å between M and M') provides an effective pathway for magnetic superexchange coupling within coordination compounds. The nature of nearest-neighbor magnetic interactions is illustrated in Figure 7 for two octahedral metal centers connected through a linear cyanide bridge. Antiferromagnetic exchange coupling is expected for unpaired electrons in symmetry-compatible orbitals ($t_{2g} + t_{2g}$ or $e_g + e_g$), which interact through cyanide π and π* orbitals. Here, mixing of the two compatible interacting orbitals leads to a new lower-energy molecular orbital. The two electrons then occupy the new orbital and adopt an antiparallel configuration, as imposed by the Pauli exclusion principle. Conversely, unpaired electron density in orthogonal metal orbitals ($t_{2g} + e_g$) will leak into orthogonal cyanide-based orbitals, such that no orbital mixing occurs. This absence of an interaction enforces ferromagnetic exchange, in accordance with Hund's rules. In some cases, the ferromagnetic coupling through a cyanide-bridge can be as high as 29 cm^{-1}. Thus, the ability of predicting magnetic coupling and effectiveness of transferring a strong interaction make metal-cyanide complexes good candidate for building units in designing single-chain magnets.

The first example will be focused on the Ising chain compound $[Fe^{III}(bpy)(CN)_4]_2[CoII(H_2O)_2](H_2O)_4$,[18b] with the structure shown in Figure 8. The cyano building unit, $[(bpy)Fe^{III}(CN)_4]^-$, coordinates two of its four cyanide groups in the *cis*-position toward two Co(II) centers. Dc susceptibility measurement revealed ferromagnetic coupling between the low-spin Fe(III) and high-spin Co(II) centers. Slow magnetic relaxation was therefore observed with total relaxation barrier $\Delta_\tau = 99$ cm-1 and $\tau_0 = 9.4\times10^{-12}$ s. It is worth noting that this compound represents the highest energy barrier for a cyano-bridged single-chain magnet.

In selecting a building unit for directing the formation of a single-chain magnet, an ideal structure consists of a metal complex bearing two terminal cyanide ligands oriented trans to one another, as this type of complex can react with another metal species to generate a simple linear chain with alternating MM' composition. The representative example of such system is a series of one-dimensional chain compounds $(DMF)_4MReCl_4(CN)_2$ (M = Mn, Fe, Co, Ni) assembled from paramagnetic dicyanometalate building unit $[ReCl_4(CN)_2]^{2-}$.[18n] Variable-temperature dc susceptibility measurements on the MRe solids revealed the presence of intrachain antiferromagnetic coupling in the Mn analogue and ferromagnetic coupling in the other three solids, giving rise to repeating spin units of S = 1 (Mn), 7/2 (Fe), 3 (Co), and 5/2 (Ni). Fits to plots of $\chi_M T$ vs. T gave coupling constants of -5.4 (Mn), +4.8 (Fe), +2.4 (Co), and +3.7 (Ni) cm^{-1}. In addition, plots of $\ln(\chi_M T)$ vs. $1/T$ constructed for the solids showed linear regions, allowing the extraction of correlation energies of = 19 (Mn), 28 (Fe), 8.5 (Co), and 8.8 (Ni) cm^{-1}. As discussed earlier in the introduction, the correlation energy of a single-chain magnet within the Ising limit is related to the coupling strength by the expression $\Delta_\xi = 4|JS_1S_2|$. However, the calculated correlation barrier using experimental J values and the equation above

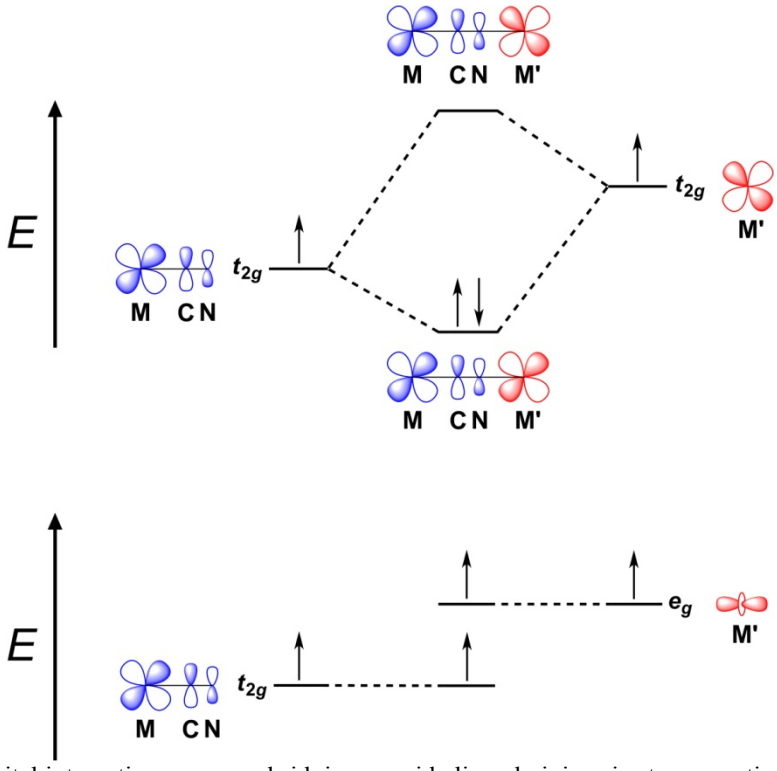

Figure 7. Orbital interactions across a bridging cyanide ligand giving rise to magnetic superexchange. Upper: Unpaired electrons in symmetry compatible t_{2g} orbitals interact through cyanide π* orbitals, resulting in antiferromagnetic coupling (via the Pauli exclusion principle). In actuality, this is a bit of an oversimplification, as electronic structure calculations indicate that the π orbitals of cyanide are responsible to nearly the same extent. Lower: Unpaired electrons from incompatible metal-based orbitals leak over into orthogonal cyanide-based orbitals, resulting in ferromagnetic coupling (via Hund's rules).

yielded strong disagreement with the experimental correlation energy barrier, suggesting

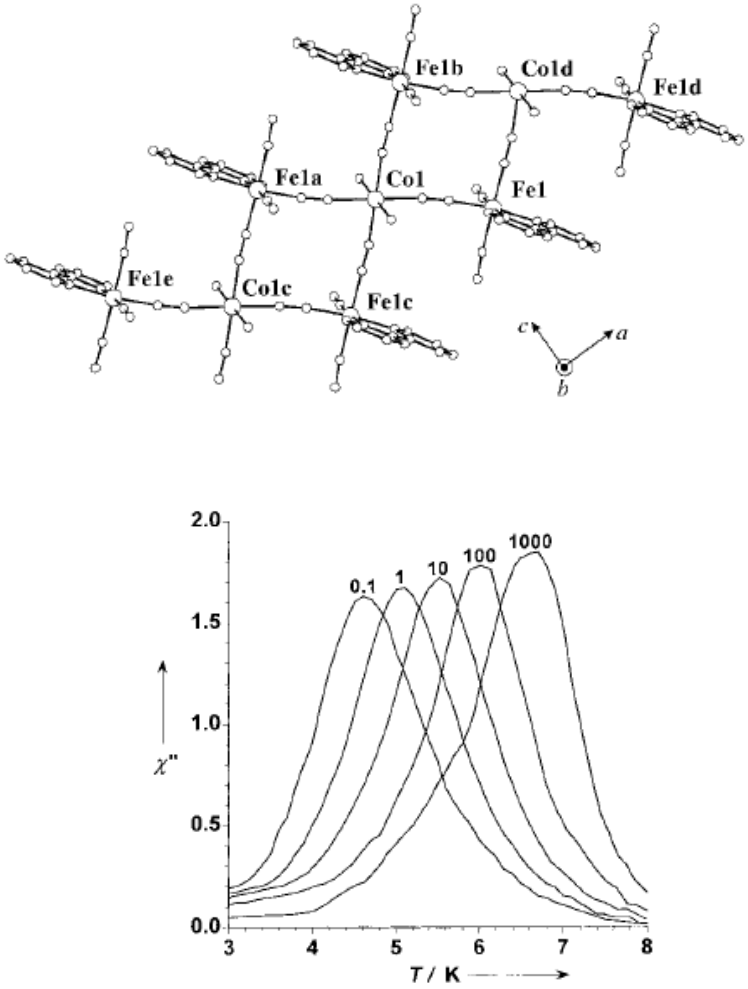

Figure 8. Upper: Perspective view of $\{[Fe(bpy)(CN)_4]_2Co(H_2O)_2\}(H_2O)_4$ parallel to a axis. Uncoordinated water molecules are omitted for clarity. Lower: Temperature dependence of out-of-phase component of single-crystal sample with oscillating field (1 Oe) applied along b axis.

that these chain compounds do not fall within the Ising limit regime with sharp domain walls. For this intermediate regime, efforts to determine an analytic expression for correlation energy are still in progress.

To probe the relaxation dynamics in the MRe solids, ac susceptibility was monitored as a function of both temperature and frequency. The variable-temperature and variable-frequency measurements for all solids showed peaks in χ_M' and χ_M'' that exhibit strong frequency dependence, indicating the presence of slow relaxation along the chains. Indeed, linear fits to Arrhenius plots of the relaxation times derived from these experiments gave relaxation barriers of Δ_τ = 31 (Mn), 56 (Fe), 17 (Co), and 20 (Ni) cm^{-1}. Notably, these barriers correspond to the finite-size regime, as the ac measurements were conducted below the crossover temperatures obtained from $\ln(\chi_M'T)$ data.

The tricyanometalate building unit, $[TpFe(CN)_3]^-$ has also been employed to obtain the single-chain magnets, $Tp_2LCuFe_2(CN)_6$, where L = MeOH[18k], DMF[18l]. The structure of this type of chain compound has been described as a double zig-zag chain (see **Figure 10**). Here, each $[TpFe(CN)_3]^-$ unit is bridged through two of its cyanide ligands to a Cu^{II} ion, while the third cyanide remains terminal. Each Cu^{II} ion resides in a distorted square pyramidal geometry. In the basal plane, two cis coordination sites are bound by the nitrogen ends of cyanide ligands originating from two separate and adjacent $[TpFe(CN)_3]^-$ units, while the other two sites are bound to cyanide ligands of a second pair of $[TpFe(CN)_3]^-$ units. Finally, each Cu^{II} ion features a coordinated MeOH or DMF molecule in the apical position.

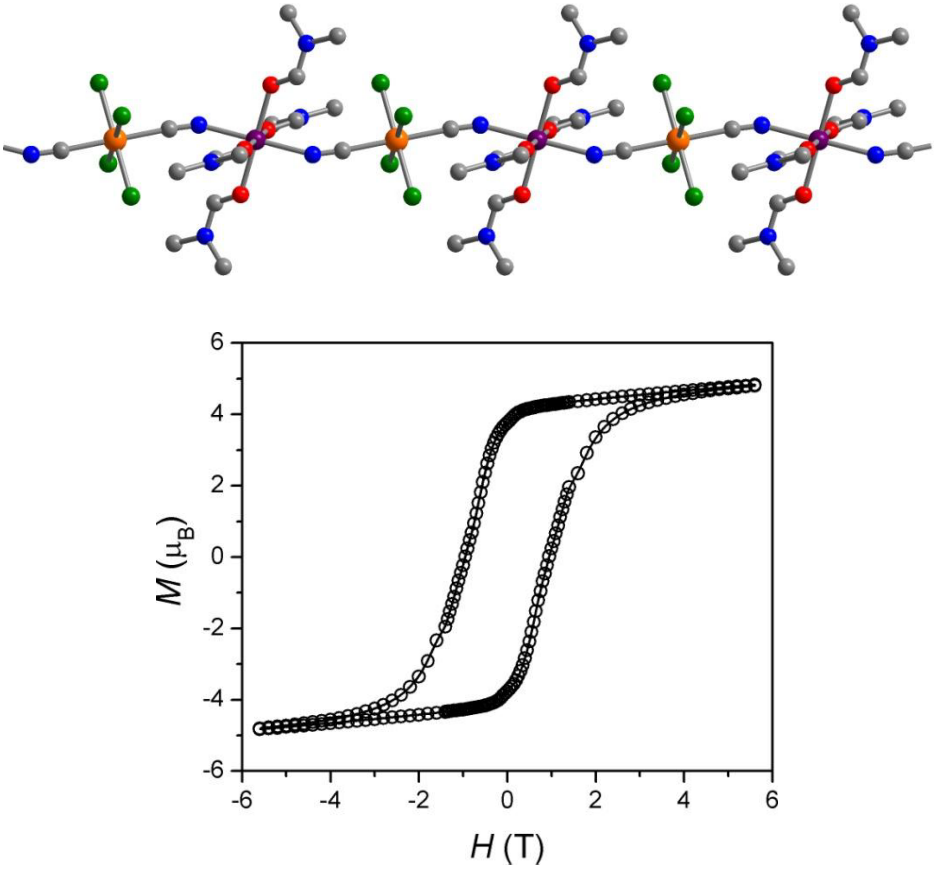

Figure 9. Upper: Crystal structure of the one-dimensional solid $(DMF)_4Fe^{II}Re^{IV}Cl_4(CN)_2$. Orange, purple, green, red, blue, and gray spheres represent Re, Fe, Cl, O, N, and C atoms, respectively; H atoms are omitted for clarity. Lower: Variable-field magnetization data for the FeRe solid, collected at 1.8 K with a sweep rate of 150 Oe/min.

Variable-temperature dc susceptibility data collected for the $CuFe_2$ compounds revealed the presence of ferromagnetic intrachain coupling, as expected between low-spin Fe^{III} (t_{2g}^5) and square-pyramidal Cu^{II} ($e^4b_2^2b_1^2a_1^1$) centers. In order to obtain a fit to these data, each compound was treated as a repeating trinuclear unit. Two distinct coupling constants arise from this approximation, where J_1 corresponds to the interaction within the

trinuclear unit between Fe^{III} and Cu^{II}, and J_2 between trinuclear units. Fits to the data gave exchange parameters of J_1 = +16 cm^{-1} and J_2 = +6.2 cm^{-1} for the MeOH-bound chain and J_1 = +7.5 cm^{-1} and J_2 = +4.9 cm^{-1} for the DMF-bound chain. As the correlation barrier for a single-chain magnet is directly related to the strength of coupling, this difference in magnetic coupling indicates that the MeOH-bound chain should display a higher barrier. Indeed, while no hysteresis was observed in the plot of *M* vs. *H* for the DMF-bound solid down to 1.8 K, the plot obtained for the MeOH-bound solid revealed a hysteresis loop at 1.8 K with a coercive field of H_C = 120 Oe.

To further probe the single-chain magnet behavior in the $CuFe_2$ compounds, variable-

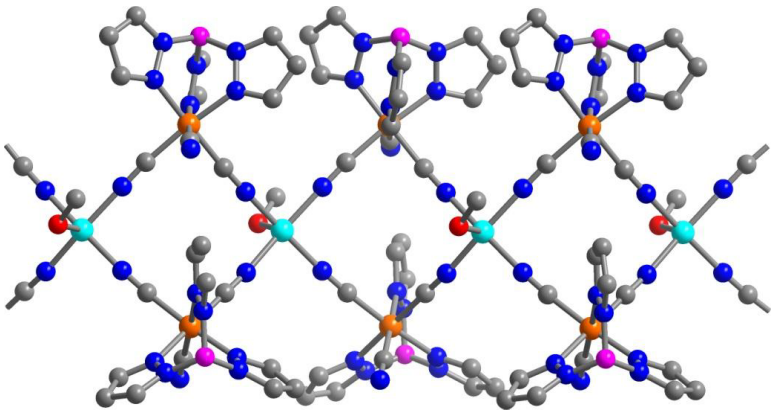

Figure 10. Crystal structure of the one-dimensional solid $Tp_2(CH_3OH)Cu^{II}Fe^{III}{}_2(CN)_6$. Orange, cyan, magenta, red, blue, and gray spheres represent Fe, Cu, B, O, N, and C atoms, respectively; H atoms are omitted for clarity.

temperature ac susceptibility data were collected at different temperatures. Arrhenius fits to the data yielded relaxation barriers of = 78 cm^{-1} for the MeOH-bound chain and 28 cm^{-1} for the DMF-bound chain. The significant difference in barriers is likely a direct result of the disparate *J* values and thus demonstrates the critical role M-N-C angles can play in the relaxation barriers of single-chain magnets. Later in this thesis, I will provide a detailed magneto-structural correlation study on the relationship between energy barriers and M-N-C bond angles in a series of single-chain magnets of type $L_4FeReCl_4(CN)_2$.

Despite the structural and magnetic diversity of cyano-bridged single-chain magnets that have been published, only a few cyanometalate building units have been used in the field, compared to the large number of cyanomatalate compounds that exist. As most of these building units were originally synthesized for a purpose unrelated to magnetism, there may remain a large number of potentially good candidates that have yet to be explored. Indeed, more synthetic efforts seeking new cyanomatalate building unit for single-chain magnets may result in new types of chain structures with larger relaxation barriers. Another direction of the field should focus on increasing the magnetic coupling strength

through cyanide-bridges. A recent result from a zig-zag ReCu chain compound has shown ferromagnetic coupling could be as high as 29 cm^{-1}. As the height of correlation energy barrier is directly related to the strength of magnetic coupling strength, increasing intrachain magnetic coupling would result in a drastic increase in the total relaxation barrier.[21]

1.5 Light-Actuated Single Molecule Magnets

Silicon-based electronics may ultimately be replaced by circuits and devices comprised of molecular-scale components capable of switching between distinct states at high speeds with minimal energy input.[22,23,24,25] As a result, researchers are actively seeking molecules exhibiting bistable physical states that can be interchanged via external stimuli, such as temperature, light, electric or magnetic fields, or pressure. Here, molecules capable of interconverting between two stable magnetic polarization directions, known as single-molecule magnets, are of particular interest, owing to the prominent use of magnetic field-based switching in information storage over the past half-century. The introduction of additional physical states that can be accessed in such molecules via other stimuli stands as a challenge that could enable access to increased information density and, for the interesting case of light-based switching, potentially even result in molecular manifestations of magneto-optical effects observed in solids. In this dissertation, we will provide an initial demonstration of how spin-crossover behavior in a transition metal complex can give rise to a photoswitchable single-molecule magnet exhibiting tristability.

Spin-crossover complexes of $3d^4$ to $3d^7$ metal ions have been a focus of research for nearly eighty years,[26,27,28] due in part to their potential applications as molecular memory media, switches, displays, and sensors.[29] Of these, by far the majority are pseudo-octahedral $3d^6$ iron(II) complexes possessing coordination geometries dominated by N-donor ligands that place the ligand field splitting energy near the spin pairing energy.[30].For molecules of this type, the low-spin $t_{2g}^6e_g^0$ electron configuration with $S = 0$ is the ground state at low temperature, but at higher temperatures the high-spin $t_{2g}^4e_g^2$ electron configuration with $S = 2$ becomes significantly thermally populated, owing to differences in the entropy contributions to the Gibbs free energy associated with the spin degrees of freedom. Importantly, in some instances it is possible to switch between the two states using light irradiation, a phenomenon known as light-induced excited spin state trapping or the LIESST effect.[31,32,33] Thus, certain spin-crossover complexes can offer optically switchable bistability.

Another type of magnetic bistability is found in single-molecule magnets, molecules for which the magnetic dipole associated with a high spin ground state prefers to align along a unique axis.[1] Here, an axial magnetic anisotropy creates an energy barrier for converting between up ($M_S = +S$) and down ($M_S = -S$) orientations of the spin, as described by the zero-field splitting Hamiltonian $H = DS_z^2 + E(S_x^2 - S_y^2)$ with D large and negative and E small. As a result, at low temperatures, these molecules exhibit slow magnetic relaxation and magnetic hysteresis associated with switching between the two

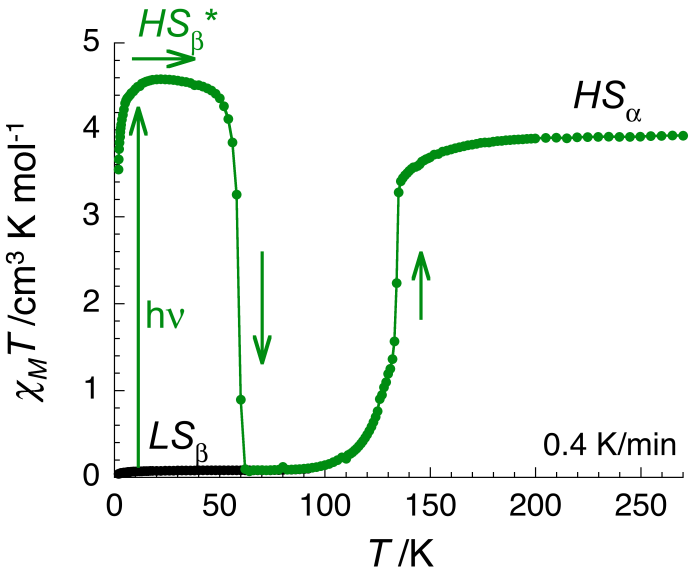

Figure 11. Temperature dependence of $\chi_M T$ product for $Fe(ptz)_6(BF_4)_2$, showing both thermal and light induced spin-crossover.

states via application of a magnetic field. While most single-molecule magnets are

polynuclear complexes, it was recently discovered that high-spin iron(II) complexes with an appropriate axial ligand field could also behave in this fashion.[34,35,36,37,38] These results motivated us to search for photoactive spin-crossover complexes that might additionally behave as single-molecule magnets when switched into their high-spin configuration. In Chapter 4, I will discuss magneto-optical study of $Fe(ptz)_6(BF_4)_2$ salt, the first system ever shown to exhibit the LIESST effect in the solid state. Indeed, this molecular salt now provides the first example of a light actuated single-molecule magnet.

1.6 Acknowledgement

This research was supported by NSF Grant No. CHE-0617063. I thank Prof. R. Clérac for helpful discussions. I also thank Dr. T. David Harris and Dr. J. M. Zadrozny for experimental assistance.

1.7 References

1. (a) Sessoli, R.; Tsai, H. L.; Schake, A. R.; Wang, S.; Vincent, J. B.; Folting, K.; Gatteschi, D.; Christou, G.; Hendrickson, D. N. *J. Am. Chem. Soc.***1993**, *115*, 1804. (b) Sessoli, R.; Gatteschi, D.; Caneschi, A.; Novak, M. A. *Nature* **1993**, *365,* 141. (c) Gatteschi, D.; Sessoli, R.; Villain, J. *Molecular Nanomagnets*, Oxford University Press: New York, 2006 and references therein.
2. (a) Garanin D. A.; Chudnovsky, E. M. *Phys. Rev. B*, **1997**, *56*, 11102; (b) Leuenberger, M. N.; Loss, D. *Nature*, **2001**, *410*, 789; (c) Jo, M. H.; Grose, J. E.; Liang, W.; Baheti, K.; Deshmukh, M. M.; Sokol, J. J.; Rumberger, E. M.; Hendrickson, D. N.; Long, J. R.; Park, H.; Ralph, D. C. *Nano Lett.*, **2006**, *6*, 2014. (d) Ardavan, A.; Rival, O.; Morton, J. J. L.; Blundell, S. J.; Tyryshkin, A. M.; Timco, G. A.; Winpenny, R. E. P. *Phys. Rev. Lett.* **2007**, *98*, 57201. (e) Bogani, L.; Wernsdorfer, W. *Nat. Mater.* 2008, **7**, 179. (f) Stamp, P. C. E.; Gaita-Arino, A. *J. Mater. Chem.* **2009**, *19*, 1718. (g) Loth, S.; von Bergmann, K.; Ternes, M.; Otte, A. F.; Lutz, C. P.; Heinrich, A. J. *Nat. Phys.* **2010**, *6*, 340.
3. Caneschi, A.;Gatteschi, D.; Lalioti, N.; Sangregorio, C.; Sessoli, R.; Venturi, G.; Vindigni, A.; Rettori, A.; Pini, M. G.; Novak, M. A. *Angew. Chem., Int. Ed.* **2001**, *40*, 1760.
4. Glauber, R. J. *J. Math. Phys.* **1963**, *4*, 294.
5. Clérac, R.; Miyasaka, H.; Yamashita, M.; Coulon, C. *J. Am. Chem. Soc.* **2002**, *124*, 12837.
6. Milios, C. J.; Vinslava, A.; Wernsdorfer, W.; Moggach, S.; Parsons, S.; Perlepes, S. P.; Christou, G.; Brechin, E. K. *J. Am. Chem. Soc*., **2007,** *129*, 2754.
7. (a) Neese, F.; Solomon, E. I. *Inorg. Chem.,* 1998, **37**, 6568; (b) Waldmann, O. *Inorg. Chem.*, 2007, **46**, 10035; (c) Neese, F.; Pantazis, D. A. *Faraday Discuss.*, **2011**, *148*, 229.
8. (a) Ishikawa, N.; Sugita, M.; Ishikawa, T.; Koshihara, S. Y.; Kaizu, Y. *J. Am. Chem. Soc.*, **2003**, *125*, 8694. (b) Rinehart, J. D.; Long, J. R. *J. Am. Chem. Soc.*, **2009**, *131*, 12558.
9. (a) Branzoli, F.; Caretta, P.; Filibian, M.; Zoppellaro, G.; Graf, M. J.; Galan-Mascaros, J. R.; Fuhr, O.; Brink, S.; Ruben, M. *J. Am. Chem. Soc.*, **2009**, *131*, 4387; (b) Gonidec, M.; Biagi, R.; Corradini, V.; Moro, F.; De Renzi, V.; del Pennino, U.; Summa, D.; Muccioli, L.; Zannoni, C.; Amabilino, D. B.; Veciana, J. *J. Am. Chem. Soc.*, **2011**,

133, 6603; (c) Jiang, S. D.; Wang, B. W.; Sun, H. L.; Wang, Z. M.; Gao, S. *J. Am. Chem. Soc.*, **2011**, *133*, 4730.
10. Kramers, H. A. *Proc. R. Acad. Sci. Amsterdam*, **1930**, *33*, 959.
11. (a) Zadrozny, J. M.; Long, J. R. *J. Am. Chem. Soc.*, **2011**, *133*, 20732; (b) Mossin, S.; Tran, B. L.; Adhikari, D.; Pink, M.; Heinemann, F. W.; Sutter, J.; Szilagyi, R. K.; Meyer, K.; Mindiola, D. J. *J. Am. Chem. Soc.*, **2012**,*134*, 13651.
12. Miyasaka, H.; Julve, M.; Yamashita, M.; Clérac, R. *Inorg. Chem.* **2009**, *48*, 3420.
13. (a) Cole, K.S.; Cole, R. H. *J. Chem. Phys.* **1941**, *9*, 341. (b) Boettcher, C. J. F. *Theory of Electric Polarisation*; Elsevier: Amsterdam, 1952. (c) Aubin, S. M.; Sun, Z.; Pardi, L.; Krzystek, J.; Folting, K.; Brunel, L. J.; Rheingold, A. L.; Christou, G.; Hendrickson, D. N. *Inorg. Chem.* **1999**, *38*, 5329.
14. (a) Lescouezec, R.; Vaissermann, J.; Ruiz-Perez, C.; Lloret, F.; Carrasco, R.; Julve, M.; Verdaguer, M.; Dromzee, Y.; Gatteschi, D.; Wernsdorfer, W. *Angew. Chem. Int. Ed.* **2003**, *42*, 1483. (b) Loveluck, J. M.; Lovesey, S. W.; Aubry, S. *J. Phys. C: Solid State Phys*. **1975**, *8*, 3841. (c) Nakamura, K.; Sasada, T. *J. Phys. C: Solid State Phys.* **1978**, *11*, 331.
15. (a) Bogani, L.; Sangregorio, C.; Sessoli, R.; Gatteschi, D. Angew. Chem. Int. Ed. **2005**, *44*, 5817. (b) Bernot, K.; Bogani, L.; Caneschi, A.; Gatteschi, D.; Sessoli, R. J. Am. Chem. Soc. **2006**, *128*, 7947.
16. Bernot, K.; Luzon, J.; Sessoli, R.; Vindigni, A.; Thion, J.; Richeter, S.; Leclercq, D.; Larionova, J.; van der Lee, A. *J. Am. Chem. Soc.* **2008**, *130*, 1619.
17. Lescouezec, R.; Toma, L. M.; Vaissermann, J.; Verdaguer, M.; Delgado, F. S.; Ruiz-Perez, C.; Lloret, F.; Julve, M. *Coord. Chem. Rev.* **2005**, *249*, 2691.
18. (a) Toma, L.; Lescoueezec, R.; Vaissermann, J.; Herson, P.; Marvaud, V.; Lloret, F.; Julve, M. *New J. Chem.* **2005**, *29*, 210. (b) Lescoueezec, R.; Vaissermann, J.; Ruiz-Perez, C.; Lloret, F.; Carrasco, R.; Julve, M.; Verdaguer, M.; Dromzee, Y.; Gatteschi, D.; Wernsdorfer, W. *Angew. Chem., Int. Ed.* **2003**, *42*, 1483. (c) Toma, L. M.; Lescouezec, R.; Lloret, F.; Julve, M.; Vaissermann, J.; Verdaguer, M. *Chem. Commun.* **2003**, 1850. (d) Toma, L. M.; Delgado, F. S.; Ruiz-Perez, C.; Carrasco, R.; Cano, J.; Lloret, F.; Julve, M. *Dalton Trans.* **2004**, 2836. (e) Toma, L. M.; Lescouezec, R.; Pasan, J.; Ruiz-Perez, C.; Vaissermann, J.; Cano, J.; Carrasco, R.; Wernsdorfer, W.; Lloret, F.; Julve, M. *J. Am. Chem. Soc*. **2006**, *128*, 4842. (f) Toma, L. M.; Lescouezec, R.; Uriel, S.; Llusar, R.; Ruiz-Perez, C.; Vaissermann, J.; Lloret, F.; Julve, M. *Dalton Trans.* **2007**, 3690. (g) Visinescu, D.; Toma, L. M.; Lloret, F.; Fabelo, O.; Ruiz-Perez, C.; Julve, M. *Dalton Trans.* **2008**, 4103. (h) Lescouezec, R.; Vaissermann, J.; Toma, L. M.; Carrasco, R.; Lloret, F.; Julve, M. *Inorg. Chem.* **2004**, *43*, 2234. (i) Wen, H.-R.; Wang, C.-F.; Zuo, J. L.; Song, Y.; Zeng, X.-R.; You, X.-Z. *Inorg. Chem.* **2006**, *45*, 582. (j) Wang, S.; Zuo, J.-L.; Zhou, H.-C.; Song, Y.; Gao, S.; You, X.-Z. Eur. J. *Inorg. Chem.* **2004**, 3681. (k) Wang, S.; Zuo, J.-L.; Gao, S.; Song, Y.; Zhou, H.-C.; Zhang, Y.- Z.; You, X.-Z. *J. Am. Chem. Soc.* **2004**, *126*, 8900. (l) Wen, H. R.; Wang, C.-F.; Song, Y.; Zuo, J.-L.; You, X.-Z. *Inorg. Chem.* **2006**, *45*, 8942. (m) Costa, V.; Lescouezec, R.; Vaissermann, J.; Herson, P.; Journaux, Y.; Araujo, M. H.; Clemente-Juan, J. M.; Lloret, F.; Julve, M. *Inorg. Chim. Acta* **2008**, *361*, 3912.
19. Harris, T. D.; Bennett, M. V.; Clérac, R.; Long, J. R. *J. Am. Chem. Soc.* **2010**, *132*, 3980-3988.

20. Feng, X.; Harris, T. D.; Long, J. R. *Chem. Sci.* **2011**, *2*, 1688.
21. Harris, T. D.; Coulon, C.; Clérac, R.; Long, J. R. *J. Am. Chem. Soc.* **2011**, *133*, 123-130.
22. Mannini, M.; Pineider, F.; Sainctavit, P.; Danieli, C.; Otero, E. Sciancalepore, C.; Talarico, A. M.; Arrio, M.-A.; Cornia, A.; Gatteschi, D.; Sessoli, R. *Nat. Mater.* **2009**, *8*, 194-197.
23. Mannini, M.; Pineider, F.; Danieli, C.; Totti, F.; Sorace, L.; Sainctavit, P.; Arrio, M.-A.; Otero, E.; Joly, L.; Cezar, J. C.; Cornia, A.; Sessoli, R. *Nature* **2010**, *468*, 417-421.
24. Vincent, R.; Klyatskaya, S.; Ruben, M.; Wernsdorfer, W.; Balestro, F. *Nature* **2012**, *488*, 357-359.
25. Coskun, A.; Spruell, J. M.; Barin, G.; Dichtel, W. R.; Flood, A. H.; Botros, Y. Y.; Stoddart, J. F. *Chem. Soc. Rev.* **2012**, *41*, 4827–4859.
26. Cambi, L.; Szego, L. *Chem. Ber. Dtsch. Ges*. **1931**, *64*, 2591-2598.
27. Franke, P. L.; Haasnoot, J. G.; Zuur, A. P. *Inorg. Chim. Acta.*, **1982** *59*, 5-9.
28. Bousseksou, A.; Molnar, G.; Salmon, L.; Nicolazzi, W. *Chem. Soc. Rev.* **2011**, *40*, 3313-3335.
29. Kahn, O.; Martinez, C. J. *Science* **1998**, *279*, 44-48.
30. Halcrow, M. A. *Polyhedron* **2007**, *26*, 3523-3576.
31. Decurtins, S.; Gütlich, P.; Kohler, C. P.; Spiering, H.; Hauser, A. *Chem. Phys. Lett.* **1984**, *105*, 1-4.
32. Decurtins, S.; Gütlich, P.; Hasselbach, K. M.; Hauser, A.; Spiering, H. *Inorg. Chem.*, **1985**, *24*, 2174-2178.
33. Hauser, A. *Chem. Phys. Lett.* 1986, *124*, 543-548.
34. Freedman, D. E.; Harman, W. H.; Harris, T. D.; Long, G. J.; Chang, C. J.; Long, J. R. *J. Am. Chem. Soc.* **2010**, *132*, 1224-1225.
35. Harman, W. H.; Harris, T. D.; Freeman, D. E.; Fong, H.; Chang, A.; Rinehart, J. D.; Ozarowski, A.; Sougrati, M. T.; Grandjean, F.; Long, G. J.; Long, J. R.; Chang, C. J. *J. Am. Chem. Soc*. **2010**, *132*, 18115-18126.
36. Lin, P. H.; Smythe, N. C.; Gorelsky, S. I.; Maguire, S.; Henson, N. J.; Korobkov, I.; Scott, B. L.; Gordon, J. C.; Baker, R. T.; Murugesu, M. *J. Am. Chem. Soc*. **2011**, *133*, 15806-15809.
37. Weismann, D.; Sun, Y.; Lan, Y.; Wolmershauser, G.; Powell, A. K.; Sitzmann, H. *Chem. Eur. J.* **2011**, *17*, 4700-4704.
38. Zadrozny, J. M.; Atanasov, M.; Bryan, A. M.; Lin, C.-Y.; Rekken, B. D.; Power, P. P.; Neese, F.; Long, J. R. *Chem. Sci.* **2012**, *4*, 125-138.

Chapter 2: Influence of Structure on Exchange Strength and Relaxation Barrier in a Series of $FeRe(CN)_2$ Single-Chain Magnets

2.1 Introduction

Over the past decade, a number of magnetic chain compounds have been shown to retain their magnetization upon removal of an applied field,[1] a phenomenon predicted by Glauber nearly half a century ago for chains of ferromagnetically coupled anisotropic spins.[2] This dynamic behavior is analogous to that observed in single-molecule magnets,[3] and, consequently, chain compounds that exhibit slow magnetic relaxation have come to be known as single-chain magnets.[1b] While the relaxation dynamics of single-molecule and single-chain magnets share several key characteristics, one pronounced difference is that single-chain magnets tend to display much higher relaxation barriers than do their molecular counterparts. As a result, these chain compounds have received considerable recent attention, owing to their potential utility in applications such as spin-based high-density information storage.[4]

The propensity for single-chain magnets to exhibit higher relaxation barriers than single-molecule magnets can be attributed to short range magnetic correlation along individual chains. In a single-molecule magnet, the magnitude of the relaxation barrier, Δ_A, is governed by the equation $\Delta_A = S^2|D|$, where S is the spin ground state and D is the axial zero-field splitting parameter. In a single-chain magnet, the barrier similarly depends on S and D of the repeating spin unit, but additionally this value scales with the strength of magnetic exchange, J, between spin units. Indeed, the overall relaxation has been theoretically predicted[1g,2,5] and experimentally demonstrated[1f,5b,6] to follow the expression $\Delta_\tau = (8J + D)S^2$ for systems falling within the Ising limit.[7] Thus, increasing the strength of exchange along a chain represents an important route toward achieving high magnetic relaxation barriers in single-chain magnets.

An ideal system for installing strong magnetic exchange along a chain would feature a synthetically adjustable component to enable facile tuning of J. Along these lines, cyano-bridged chain compounds offer themselves as attractive candidates, owing to the predictability of both structure and magnetic exchange afforded by the M-CN-M′ linkage.[8] In particular, numerous investigations have shown that the strength of magnetic exchange between two metal centers through cyanide stems directly from the M′-N-C angle and can often be explained through simple molecular orbital considerations.[9] As such, controlling the M′-N-C angle should also provide a convenient handle through which to adjust and maximize the magnitude of the relaxation barrier.

Recently, we reported the synthesis of a series of cyano-bridged single-chain magnets of the type $(DMF)_4MReCl_4(CN)_2$ (M = Mn, Fe, Co, Ni).[10] The structures of these compounds feature considerably bent M-N-C angles (155.8(1)°-159.4(1)°), resulting from solid-state packing effects. We were intrigued by the possibility of constructing a series of related chain compounds, where only the identity of the amide ligand is varied across the series. The different steric and electronic properties of the amides, along with the associated alterations to solid-state packing, should provide a means through which to adjust the M-N-C angle and thereby enhance significantly the intrachain exchange strength and relaxation barrier. Herein, we demonstrate that this is indeed feasible

through the synthesis and characterization of a series of $L_4FeReCl_4(CN)_2$ chain compounds, where L = diethylformamide(DEF) (**1**), dibutylformamide (DBF) (**2**),dimethylformamide(DMF) (**3**), dimethylbutyramide (DMB) (**4**), dimethylpropionamide (DMP) (**5**), and diethylacetamide (DEA) (**6**).

2.2 Experimental Section

Preparation of Compounds: The compounds $(Bu_4N)_2[trans\text{-}ReCl_4(CN)_2]\bullet 2DMA$ and $(DMF)_4FeReCl_4(CN)_2$ (**3**) were synthesized as described previously.[10] Solid $(Bu_4N)CN$ was dried in vacuo ($P < 10^{-3}$ Torr) for 36 h using a trap containing P_2O_5 prior to use. All other reagents were obtained from commercial sources and used without further purification. *Caution!* Although we have experienced no problems while working with them, perchlorate salts are potentially explosive and should be handled with extreme care and only in small quantities.

$(DEF)_4FeReCl_4(CN)_2$ (1). A solution containing $Fe(ClO_4)_2\bullet 6H_2O$ (0.020 g, 0.078 mmol) in 2 mL of diethylformamide (DEF) was added to a solution of $(Bu_4N)_2[ReCl_4(CN)_2]\bullet 2DMA$ (0.030 g, 0.035 mmol) in 2 mL of DEF. The resulting deep blue solution was allowed to stand for 12 h to afford blue plated-shaped crystals, suitable for single-crystal X-ray diffraction. The crystals were collected by filtration, washed with successive aliquots of DEF (3 × 1 mL) and Et_2O (3 × 5 mL), and then were allowed to dry in air to give **1** (0.018 g, 59%) as a dark blue solid. IR: ν_{CN} 2151cm^{-1}. Anal. Calcd for $C_{22}H_{44}Cl_4FeN_6O_4Re$: C, 31.44; H, 5.28; N, 10.00; Found: C, 31.27; H, 5.38; N, 10.32.

$(DBF)_4FeReCl_4(CN)_2$ (2). A solution containing $(Bu_4N)_2[ReCl_4(CN)_2]\bullet 2DMA$ (0.040 g, 0.038 mmol) in 3 mL of dibutylformamide (DBF) was carefully layered on top of a solution containing $Fe(ClO_4)_2\bullet 6H_2O$ (0.020 g, 0.078 mmol) in 3 mL of DBF. Upon standing for two days, dark blue block-shaped crystals, suitable for single-crystal X-ray diffraction, formed from the layering. The crystals were collected by filtration, washed with Et_2O (3 × 2 mL), and dried in air to give **2** (0.012 g, 35%) as a dark blue solid. IR: ν_{CN} 2155 cm^{-1}. Anal. Calcd for $C_{38}H_{76}Cl_4FeN_6O_4Re$: C, 43.93; H, 7.37; N, 8.09; Found: C, 44.25; H, 7.62; N, 8.78.

$(DMB)_4FeReCl_4(CN)_2$ (4). A solution containing $(Bu_4N)_2[ReCl_4(CN)_2]\bullet 2DMA$ (0.040 g, 0.038 mmol) in 2 mL of dimethylbutyramide (DMB) was carefully layered on top of a solution containing $Fe(ClO_4)_2\bullet 6H_2O$ (0.020 g, 0.078 mmol) in 2 mL of DMB. Upon standing for one day, dark blue plate-shaped crystals, suitable for single-crystal X-ray diffraction, formed from the layering. The crystals were collected by filtration, washed with Et_2O (3 × 2 mL), and dried in air to give **4** (0.010 g, 29%) as a dark blue solid. IR: ν_{CN} 2158 cm^{-1}. Anal. Calcd for $C_{26}H_{52}Cl_4FeN_6O_4Re$: C, 34.83 H, 5.85; N, 9.38; Found: C, 34.65; H, 5.55; N, 9.25.

$(DMP)_4FeReCl_4(CN)_2$ (5). A solution containing $(Bu_4N)_2[ReCl_4(CN)_2]\bullet 2DMA$ (0.044 g, 0.042 mmol) in 2 mL of dimethylpropionamide (DMP) was carefully layered on top of a solution containing $Fe(ClO_4)_2\bullet 6H_2O$ (0.014 g, 0.055 mmol) in 2 mL of DMP. Upon standing for one day, dark blue plate-shaped crystals, suitable for single-crystal X-ray diffraction, formed from the layering. The crystals were collected by filtration, washed with Et_2O (3 × 2 mL), and dried in air to give **4** (0.011 g, 33%) as a dark blue solid. IR: ν_{CN} 2160 cm^{-1}, Anal. Calcd for $C_{22}H_{44}Cl_4FeN_6O_4Re$: C, 33.67 H, 5.65; N, 10.71; Found: C, 33.65; H, 5.78; N, 10.82.

$(DEA)_4FeReCl_4(CN)_2$ (6). A solution containing $(Bu_4N)_2[ReCl_4(CN)_2]\bullet 2DMA$ (0.040 g, 0.038 mmol) in 3 mL of diethylacetamide (DEA) was carefully layered on top of a

solution containing $Fe(ClO_4)_2 \cdot 6H_2O$ (0.027 g, 0.11 mmol) in 3 mL of DEA. Upon standing for 3 days, dark blue block-shaped crystals, suitable for single-crystal X-ray diffraction, formed from the layering. The crystals were collected by filtration, washed with Et_2O (3 × 2 mL), and dried in air to give **4** (0.012 g, 35%) as a dark blue solid. IR: ν_{CN} 2162 cm^{-1}, Anal. Calcd for $C_{32}H_{65}Cl_4FeN_7O_4Re$: C, 31.44; H, 5.28; N, 10.00; Found: C, 31.69; H, 5.24; N, 9.95.

X-Ray Structure Determinations. Single crystals of compounds **1**, **2, 4, 5** and **6** were coated with Paratone-N oil and mounted on glass fibers or Kaptan loops. The crystals were then quickly transferred to a Bruker APEX or Bruker MICROSTAR diffractometer, and cooled in a stream of nitrogen gas. Preliminary cell data were collected, giving unit cells with the triclinic, monoclinic, or tetragonal Laue group for all compounds, using the SMART[1] or APEX2[2] program package. The unit cell parameters were later refined against all data. A full hemisphere of data was collected for all compounds. None of the crystals showed significant decay during data collection. Data were integrated and corrected for Lorentz and polarization effects using SAINT[3] and were corrected for absorption effects using SADABS[4].

Space group assignments were based upon systematic absences, *E*-statistics, and successful refinement of the structures. Structures were solved by direct methods and expanded through successive difference Fourier maps. They were refined against all data using the SHELXTL[5] program. Thermal parameters for all non-hydrogen atoms were refined anisotropically in all compounds. Table 1 summarizes the unit cell and structure refinement parameters for compounds **1**, **2**, and **4**-**6**.

Magnetic Susceptibility Measurements. Magnetic data were collected on a Quantum Design MPMS-XL SQUID magnetometer. Dc susceptibility, dc magnetization and ac susceptibility measurements for **6** were obtained for a microcrystalline powder restrained in its frozen mother liquor within a sealed quartz tubes to prevent sample decomposition. All measurements of compounds **1**, **2**, **4** and **5** were obtained for microcrystalline powders restrained in a frozen polyethylene bag. Dc magnetization data were collected at 1.8 K while sweeping the magnetic field between 7 and –7 T. Ac magnetic susceptibility data were collected in zero dc field in the temperature range 1.7-10 K, under an ac field of 4 Oe oscillating at frequencies in the range 0.5-1488 Hz. For compound **4**, ac magnetic susceptibility data were also collected under a dc field of 1000 Oe. All data were corrected for diamagnetic contributions from the sample holder, as well as for the core diamagnetism of each sample (estimated using Pascal's constants).

Other Physical Measurements. Infrared spectra were obtained on a Nicolet Avatar 360 FTIR with an attenuated total reflectance accessory (ATR). Carbon, hydrogen, and nitrogen analyses were obtained from the Microanalytical Laboratory of the University of California, Berkeley. X-ray powder diffraction data were collected using Cu Kα (λ = 1.5406 Å) radiation on a Siemens D5000 diffractometer.

2.3 Results and Discussion

2.3.1 Syntheses and Structures. In general, the chain compounds were prepared by combining $[ReCl_4(CN)_2]^{2-}$and $[Fe(amide)_6]^{2+}$ in neat amide (see Scheme 1). In the case of **1**, the reaction solution produced single crystals upon standing. In contrast, for **2** and **4**-**6**, direct combination of solutions containing the precursor complexes resulted in the immediate precipitation of product mixtures. In each of these cases, a layering technique was employed to obtain single crystals. Here, a solution containing $[ReCl_4(CN)_2]^{2-}$in the

appropriate amide was carefully added to the top of a solution containing $[Fe(amide)_6]^{2+}$ ions in the amide. Over the course of days, each layering produced single crystals of the intended chain compounds.

Table 1. Selected Mean Inter atomic Bond Distances (Å) and Angles (°) for the Compounds $L_4FeReCl_4(CN)_2$, where L = DEF (**1**), DBF (**2**), DMF (**3**), DMB (**4**), DMP (**5**), DEA (**6**).

compound	∠Fe-N-C	∠Re-C-N	shortest interchain M-M	Re-C	Fe-N	Fe-O
1	154.703(7)	173.265(7)	8.6226(8)	2.1124(2)	2.1529(2)	2.1253(2)
2	157.562(6)	173.233(5)	8.9348(5)	2.1182(5)	2.1443(5)	2.1138(6)
3[9]	157.968(5)	175.259(6)	8.3027(6)	2.1177(1)	2.1546(1)	2.1339(1)
4	164.374(4)	179.685(4)	9.477(6)	2.1217(4)	2.1736(4)	2.1095(4)
5	170.579(3)	176.564(3)	9.976(6)	2.1132(3)	2.1293(3)	2.1227(3)
6	180	180	9.902(4)	2.1084(3)	2.0753(3)	2.1170(2)

Single-crystal x-ray analyses of compounds **1**-**6** revealed the structures to consist of parallel one-dimensional chains, where each chain features alternating $[ReCl_4(CN)_2]^{2-}$ and$[Fe(amide)_4]^{2+}$ units connected through Re-CN-Fe linkages (see Figures 1 and S1-S4 in the Supplementary Information). The local coordination environment of the Re^{IV} center is preserved across the series of compounds and does not significantly deviate from that observed in the structure of$(Bu_4N)_2[ReCl_4(CN)_2]\cdot 2DMA$.[10]Similarly, each Fe^{II} center resides in an approximate octahedral coordination environment, with slight variations in the Fe-N and Fe-O distances (see Table 1). Specifically, the Fe-N distances range from 2.0753(3) to 2.1736(4) Å, consistent with a high-spin (S = 2) electron configuration for Fe^{II}.[11] In addition, the Fe-O distances range from 2.1095(4) to 2.1339(1), consistent with other high-spin Fe^{II} complexes featuring amide ligands.[13]Within each structure, individual chains are well separated, with the shortest interchain metal-metal distances ranging from 8.3027(6) Å in **3** to 9.976(6) Å in **5** Additionally, no significant hydrogen bonding contacts between chains are evident in any of the structures.

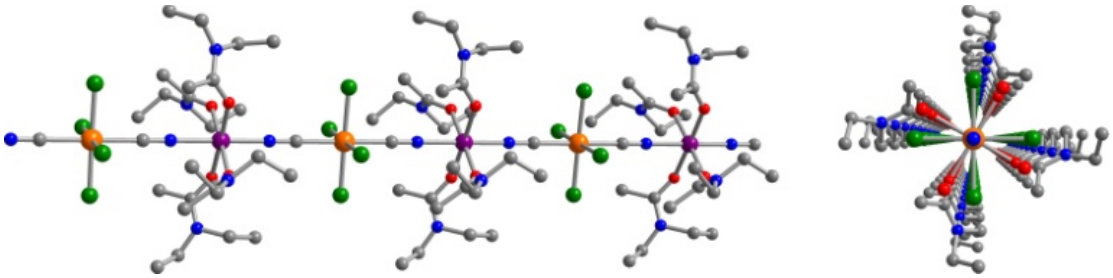

Figure 1. Left: Crystal structure of $(DEA)_4FeReCl_4(CN)_2$ (**6**). Orange, purple, green, red, blue, and gray spheres represent rhenium, iron, chlorine, oxygen, nitrogen, and carbon atoms, respectively; hydrogen atoms are omitted for clarity. Right: View down the four-fold crystallographic axis of the chain, demonstrating linear Re-C-N and Fe-N-C angles.

Scheme 1.

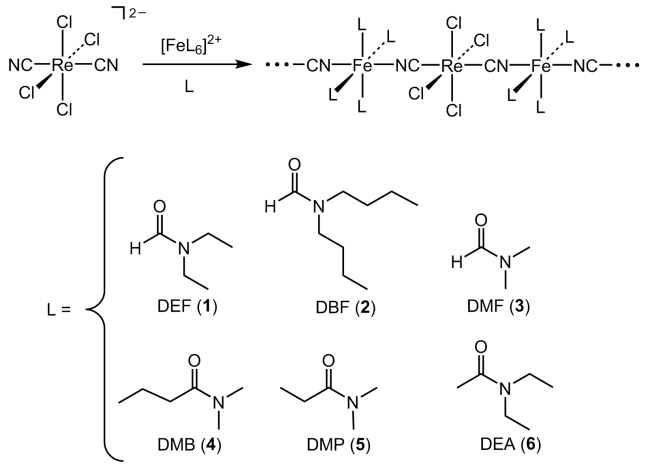

Across the series of compounds, only a subtle variation is observed in the mean Re-C-N angle, which changes from 173.233(5)° in **2** to 180° in **6**. Note that the space group *P*4/*n* adopted by **6** positions the Re-CN-Fe linkages along a crystallographic four-fold axis, thereby imposing perfectly linear Re-C-N and Fe-N-C angles. In contrast, the Fe-N-C angle varies much more drastically across the series, from 154.703(7)° in **1** to 180° in **6**. Such deviation from linearity is common for Fe-N-C angles in metal-cyanide compounds and is thought to stem primarily from crystal packing and steric conflicts imposed by ligands.[14] However, perfectly linear angles are rare in Fe-N-C linkages and have only been observed in several compounds featuring Au^{I}-CN-Fe^{II} linkages.[12] Here, no clear correlation is observed between Fe-N-C angle and extent of ligand steric bulk or electronic character across the series, indicating that slight differences in crystal packing likely give rise to the bent angles.

2.3.2 Magnetic Exchange Interactions. With crystallographic data for the FeRe chain compounds in hand, we set out to examine the influence of structure on exchange coupling between the Fe^{II} and Re^{IV} centers through the cyanide bridge. Toward this end, variable-temperature dc magnetic susceptibility data were collected for compounds **1**-**6** under an applied field of 1000 Oe. The corresponding plots of $\chi_M T$ vs. T, as exemplified in the data for **6** shown in Figure 2, exhibit a common general profile (see also Figures S5-S8). At 300 K, $\chi_M T$ = 5.09, 4.33, 5.46,[10] 5.09, 5.04, 4.56 cm^3·K/mol for **1**-**6**, respectively, slightly higher than the value of $\chi_M T$ = 4.28 cm^3·K/mol that would be expected for magnetically isolated Re^{IV} ($S = {}^3/_2$, g = 1.66) and Fe^{II} (S = 2, g = 2.00) ions. Across the series, $\chi_M T$ rises with decreasing temperature, gradually at first, then more abruptly below 50 K. This temperature dependence indicates the presence of intrachain ferromagnetic coupling between neighboring Re^{IV} and Fe^{II} centers. Finally, below 20 K, $\chi_M T$ for each compound undergoes a precipitous downturn, likely due to a combination of magnetic anisotropy of the Re^{IV} and Fe^{II} centers and weak interchain antiferromagnetic interactions.

In order to quantify the exchange between neighboring Re^{IV} and Fe^{II} centers in each chain, the $c_M T$ vs. T data were modeled according to the following spin Hamiltonian for an alternating classical-spin Heisenberg chain:

$$H = -2J\sum_{i}^{\infty}(S_i s_i + S_i s_{i+1})$$

where J represents the exchange coupling constant for the interaction between Re^{IV} and Fe^{II} centers, and S and s are the local spins of Re^{IV} ($S = {}^3/_2$) and Fe^{II} ($S = 2$), respectively. The data were fit with an expression previously used to describe an alternating chain,[15] to give the values of J and g listed in Table 2. Across the series, the exchange constant varies from $J = +4.2(2)$ cm^{-1} for **1** to $J = +7.2(3)$ cm^{-1} for **6**.[16] Inspection of Table 2 and Figure 3 reveals an important correlation between these values and the solid-state structures of the respective chain compounds. Indeed, across the series, the magnitude of J scales linearly with the Fe-N-C bond angle. Specifically, the ferromagnetic exchange becomes stronger as the Fe-N-C linkage becomes more linear. Overall, a 16% increase in Fe-N-C from **1** to **6** leads to a 71% increase in J.

Based on simple molecular orbital considerations, magnetic exchange through cyanide between octahedral metal centers with and $t_{2g}{}^3$ electronic configurations is expected to be governed by multiple exchange pathways.[17,18] First, two π-π interactions occur in symmetry compatible Re^{IV} t_{2g} orbitals through cyanide π* orbitals with the Fe^{II} orbitals of t_{2g} symmetry resulting in antiferromagnetic coupling (via the Pauli exclusion principle).In opposition to this, two σ-π interactions between electrons in orthogonal e_g and t_{2g} orbitals, respectively, should give rise to ferromagnetic exchange as per Hund's rules. Such competitive interactions generally lead to net ferromagnetic coupling , as σ-type bonding is invariably stronger than π-type bonding. Indeed, ferromagnetic exchange has been observed in several compounds containing Cr^{III}-CN-Fe^{II} [19] and Re^{IV}-CN-Fe^{II}[10,20] linkages. In the case of the Cr^{III}-CN-Fe^{II} linkage, this behavior has been attributed to a kinetic exchange mechanism, where partial electron transfer from an Fe^{II} t_2 orbital into a Cr^{III} t_2 orbital enforces a parallel alignment of spins.[21] Given the isoelectronic nature of Cr^{III} and Re^{IV} ions, such a mechanism may also dominate in the FeRe chain compounds. If a $t_{2g} \rightarrow t_{2g}$ electron transfer is responsible for the ferromagnetic interaction, then the magnitude of the exchange should be maximized when overlap between the cyanide π* and $Fe^{II}t_{2g}$ orbitals is maximized. Indeed, this is exactly the case in **1**-**6**, where the compound exhibiting a linear Re-CN-Fe fragment (**6**) demonstrates the strongest

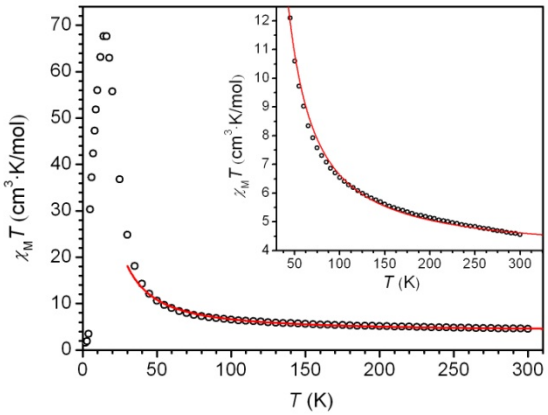

Figure 2. Variable-temperature dc magnetic susceptibility data for **6**, collected in an applied field of 1000 Oe. The solid red line corresponds to a fit to the data, as described in the text. Inset: Expanded view of the data and fit, highlighting the presence of intrachain ferromagnetic coupling.

ferromagnetic interaction. Accordingly, the ferromagnetic interaction decreases in magnitude from 7.2(3) cm^{-1} to 4.2(2) cm^{-1} as the Fe-N-C angle undergoes subsequent bending, as overlap between the π-type orbitals is progressively reduced. These values of *J* are similar to those previously reported for molecular clusters featuring Cr^{III}-CN-Fe^{II} [19c] and Re^{IV}-CN-Fe^{II} [20]. Additionally, while no *J* value has been extracted, the Prussian blue analogue $Fe_3[Cr(CN)_6]_2 \cdot 15H_2O$ undergoes ferromagnetic ordering below T_C = 21 K.[19a] We note that this is the first example of a magnetostructural correlation observed through cyanide between metal centers with $t_{2g}^4e_g^2$ and t_{2g}^3 electronic configurations. Similar dependence of *J* on M-N-C angle has been reported in compounds featuring Fe^{III}-CN-Mn^{III}, M^{III}-CN-Cu^{II} (M = Cr, Mn and Fe) and Cr^{III}-CN-Ni^{II} linkages.[9adg] For instance, in the the series of Fe^{III}-CN-Mn^{III} compounds, *J* was shown to scale linearly with Mn-N-C angle, with a crossover from positive to negative *J* occurring at a critical angle.[9g] This phenomenon was attributed to increasing overlap between magnetic Fe^{III} and Mn^{III} dπ orbitals.

Table 2. Summary of Magnetic Data for $L_4FeReCl_4(CN)_2$, where L = DEF (**1**), DBF (**2**), DMF (**3**), DMB (**4**), DMP (**5**), DEA (**6**).

	∠Fe-N-C	*g*	*J* (cm^{-1})	Δ_t(cm^{-1})	τ_0 (s)
1	154.703(7)	2.21	4.2(2)	45	4.2×10^{-10}
2	157.562(6)	1.84	4.5(2)	55	9.0×10^{-11}
3	157.968(5)	1.96	4.8(4)	56	1.0×10^{-10}
4	164.374(4)	2.14	5.6(3)	49	8.6×10^{-10}
5	170.579(3)	1.84	6.3(2)	53	3.9×10^{-10}
6	180	1.78	7.2(3)	93	8.7×10^{-11}

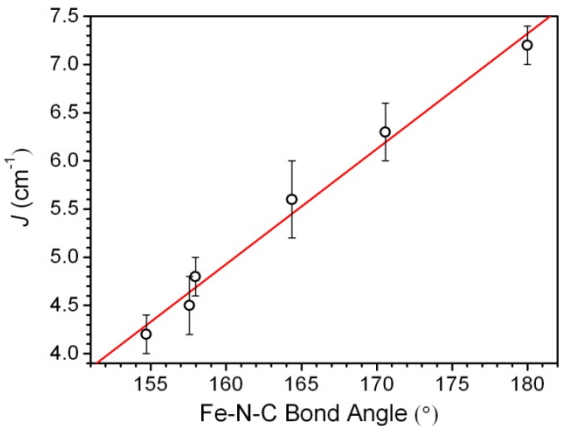

Figure 3. Dependence of exchange strength (*J*) on Fe-N-C angle in **1**-**6** (left to right data points, respectively). The solid red line corresponds to a line of best fit through the data.

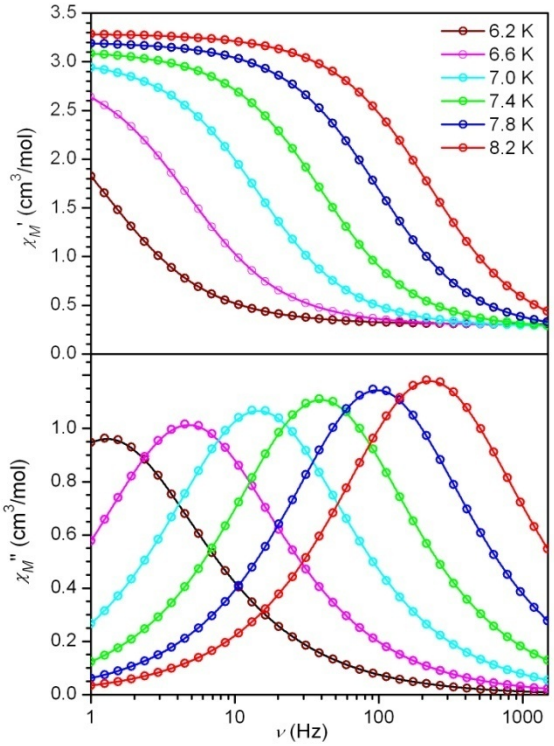

Figure 4. Variable-frequency in-phase (upper) and out-of-phase (lower) components of the ac magnetic susceptibility data for **6**, collected in a 4 Oe ac field at selected temperatures. Solid lines correspond to fits to the data, as described in the text.

2.3.3 Magnetization Dynamics. To probe slow magnetic relaxation in the chain compounds, variable-frequency ac susceptibility data were collected for **1-6**at multiple temperatures under zero applied dc field. Data collected for all compounds show frequency dependence in both the in-phase (χ_M') and out-of-phase (χ_M'') components of the susceptibility. Moreover, plots of χ_M' vs. ν and χ_M'' vs. ν show a feature that shifts position as the temperature is varied (see Figures 4 and S9-S13). From these data, Cole-Cole plots of χ_M'' vs. χ_M' were constructed and fit to a generalized Debye model to obtain α values and relaxation times (τ) at each temperature (see Figures S14-S18).[22] Here, α provides a quantitative measure of how closely the Cole-Cole plot resembles a semicircle, and this value provides some insight into the distribution of relaxation times. Across the series, α ranges from 0.16 to 0.20, indicating a relatively narrow distribution of relaxation times. In the cases of **1-3**, **5**, and **6**, Arrhenius plots of $\ln\tau$ vs. $1/T$ each show a linear arrangement of data, as expected for a single-chain magnet (see Figures 5, S19, S20, and S23). Accordingly, considering the expression $\tau = \tau_0\exp(\Delta_\tau/k_BT)$, fits to the data provide relaxation barriers of Δ_τ = 45, 55, 56, 53, and 93 cm^{-1} for compounds **1-3**, **5**, and **6**, respectively (see Table 2). In addition, values of attempt time vary from $\tau_0 = 8.7 \times 10^{-11}$ s for **6** to 4.2×10^{-10} s for **1**, within the range typically observed for single-chain magnets.

Notably, the relaxation barrier observed for **6** is among the highest yet observed for single-chain magnets.[1ac] In comparison, the radical bridged chain compound Co(hfac)$_2$(*p*-butoxyphenyl-NN) was shown to exhibit a relaxation barrier of Δ_τ = 243 cm^{-1}, but with a

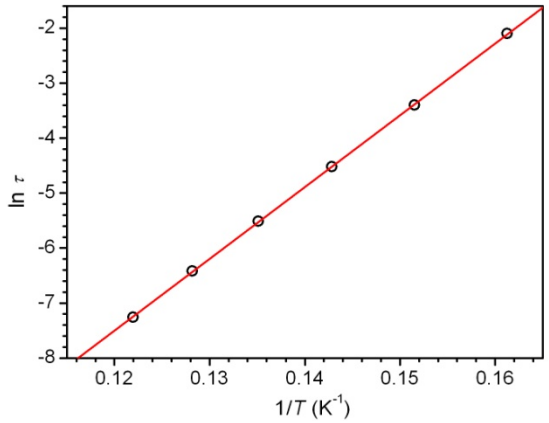

Figure 5.Arrhenius plot of relaxation time for **6**. The solid red line corresponds to a linear fit to the data, giving $\Delta_\tau = 93$ cm^{-1}.

much smaller attempt time ($\tau_0 = 6.8 \times 10^{-13}$ s).[23] The authors note that the small τ_0 may be diagnostic of spin glass behavior caused by interchain interactions. Indeed, this hypothesis is supported by a lack frequency dependence in the ac susceptibility upon application of a 500 Oe dc field. Another compound, $(bpy)_2(H_2O)Co^{II}Fe^{III}{}_2(CN)_8$, was reported to exhibit a barrier of $\Delta_\tau = 106$ cm^{-1}.[24] However, this large barrier is misleading, as it is associated with an extremely small attempt time of ($\tau_0 = 1.5 \times 10^{-17}$ s). As the authors note, this value is much smaller than is to be expected, and this compound deserves further study. Considering chain compounds that show attempt times within the range typically observed for superparamagnets and do not exhibit anomalous relaxation behavior, the highest barrier yet reported belongs to the radical-bridged chain compound $Co(hfac)_2(NITPhOMe)$.[1a] This compound, which was also the first reported example of a single-chain magnet, displays a relaxation barrier of$\Delta_\tau = 107$ cm^{-1}. [1a,25] In addition, the double-zigzag chain compound $[Fe^{III}(bpy)(CN)_4]_2Co^{II}(H_2O)_2$, the first example of a cyano-bridged single-chain magnet, exhibits ferromagnetic coupling between Fe^{III} and Co^{II} centers and an overall relaxation barrier of $\Delta_\tau = 99$ cm^{-1}.[1c] As such, compound **6** exhibits, to our knowledge, the second highest barrier for a cyano-bridged single-chain magnet and the third highest barrier among all single-chain magnets.

Finally, note that plots of χ_M' vs. T for the compounds exhibit maxima at ca. 10 K, likely stemming from weak interchain interactions and/or a magnetic phase transition (see Figures S24, S25, S27, and S28). Nevertheless, the above analysis of the ac susceptibility clearly shows the presence of single-chain magnet behavior, which may occur within either an ordered or a simply paramagnetic phase.[26]

In the case of compound **4**, the relaxation time does not follow Arrhenius behavior under zero applied dc field (see Figure S21). Moreover, the plot of χ_M' vs. T exhibits a sharp maximum at ca. 10 K, which may be the mark of a magnetic phase transition as described above (see Figure S26). As such, the ac susceptibility data were recollected under an applied dc field of 1000 Oe in order to suppress the phase transition. Indeed, relaxation times acquired from these data clearly exhibit Arrhenius behavior, and a linear fit to the data provides values of $\Delta_\tau = 49$ cm^{-1} and $\tau_0 = 8.6 \times 10^{-10}$ s (see Figure S22).

Table 2 summarizes the correlation between Fe-N-C angle, exchange strength, and relaxation barrier. Remarkably, the barrier is more than doubled across the series, from Δ_τ = 45 cm^{-1} in **1** to 93 cm^{-1} in **6**. This dramatic increase in barrier is directly linked to the enhancement in magnetic correlation afforded by increasing exchange strength. Overall, the 71% increase in J leads to a 107% increase in Δ_τ. Inspection of Figure 6 reveals that for compounds **1-3** and **6**, the relaxation barrier increases with increasing J in a moderately linear progression. In contrast, the barriers observed for compounds **4** and **5** do not fall along this line. The anomalous behavior in **4** may arise due to the application of a dc field in the data collection to suppress interchain effects. Along those lines, interchain interactions in **5** may also affect the overall barrier. It is not immediately clear why such similar interchain interactions would affect the chain compounds disproportionately. Note, however, that while interchain exchange may affect the relaxation barrier, J values were obtained from data fit well above the temperatures at which maxima in χ' are observed. As such, these interactions should not bear a significant effect on determinations of exchange strength.

2.4 Conclusion and Outlook

The foregoing results demonstrate that subtle structural perturbations can give rise to dramatic increases in exchange strength and relaxation barrier in single-chain magnets. Specifically, a series of cyano-bridged FeRe chain compounds has been synthesized in which the Fe-N-C angle varies from 154.703(7)° to 180°. Fits to dc susceptibility data across the series reveal that the strength of ferromagnetic exchange between Re^{IV} and Fe^{II} ions increases linearly with increasing Fe-N-C angle, from J = +4.2(2) to +7.2(3) cm^{-1}. Moreover, ac susceptibility measurements show a pronounced effect of exchange strength on relaxation barrier, with Arrhenius fits of relaxation time providing values of ranging from Δ_τ = 45 to 93 cm^{-1}. Notably, the high relaxation barrier, along with the significant magnetic hysteresis at low temperature, establishes compound **6** as one of the strongest low-dimensional magnets yet observed.

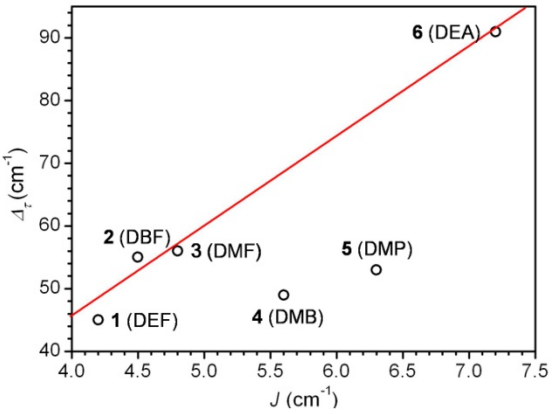

Figure 6. Dependence of relaxation barrier (Δ_τ) on exchange strength (J) for **1**-**6**. The solid red line corresponds to a line of best fit through data for compounds **1**-**3** and **6**.

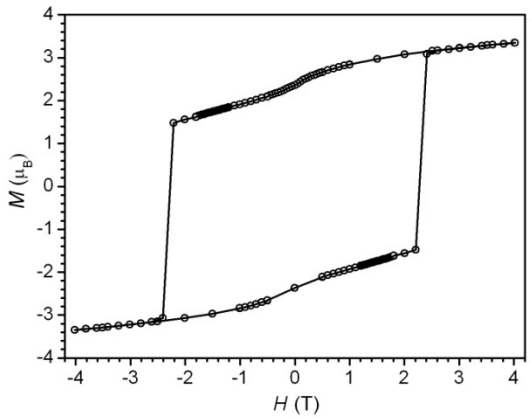

Figure 7. Variable-field magnetization data for **6**, collected at 1.8 K under a sweep-rate of 100 Oe/min. The solid lie is a guide to the eye.

Efforts are underway to pursue other routes toward magnetic chain compounds with strong intrachain exchange. Indeed, we recently reported a related CuRe chain compound that exhibits the strongest ferromagnetic coupling (29 cm^{-1}) yet observed through cyanide.[27] Unfortunately, the zig-zag arrangement of the chain acts to minimize the overall anisotropy. As an extension of that discovery, future work will seek to tune construct linear chain compounds, such as the ones presented above, that feature Re-CN-Cu linkages. In addition to the Re-CN-Cu system, we will also target chain compounds where $[ReCl_4(CN)_2]^{2-}$ units are linked to second- and third-row transition metals, in an effort to impart stronger single-ion anisotropy exchange coupling.

2.5 Acknowledgement

This research was supported by NSF Grant No. CHE-0617063. I thank Prof. R. Clérac for helpful discussions. I also thank Dr. T. David Harris and Dr. J. M. Zadrozny for experimental assistance.

2.6 Reference

1 (a) Caneschi, A.; Gatteschi, D.; Lalioti, N.; Sangregorio, C.; Sessoli, R.; Venturi, G.; Vindigni, A.; Rettori, A.; Pini, M. G.; Novak, M. A. *Angew. Chem., Int. Ed.* **2001**, *40*, 1760. (b) Clérac, R.; Miyasaka, H.; Yamashita, M.; Coulon, C. *J. Am. Chem. Soc.* **2002**, *124*, 12837. (c) Lescouëzec, R.; Vaissermann, J.; Ruiz-Pérez, C.; Lloret, F.; Carrasco, R.; Julve, M.; Verdaguer, M.; Dromzée, Y.; Gatteschi, D.; Wernsdorfer, W. *Angew. Chem., Int. Ed.* **2003**, *42*, 1483. (d) Liu, T. F.; Fu, D.; Gao, S.; Zhang, Y. Z.; Sun, H. L.; Su, G.; Liu, Y. J. *J. Am. Chem. Soc.* **2003**, *125*, 13976. (e) Wang, S.; Zuo, J.-L.; Gao, S.; Song, Y.; Zhou, H.-C.; Zhang, Y.-Z.; You, X.-Z. *J. Am. Chem. Soc.* **2004**, *126*, 8900. (f) Ferbinteanu, M.; Miyasaka, H.; Wernsdorfer, W.; Nakata, K.; Sugiura, K.; Yamashita, M.; Coulon, C.; Clérac, R. *J. Am. Chem. Soc.* **2005**, *127*, 3090. (g) Coulon, C.; Miyasaka, H.; Clérac, R. *Struct. Bonding (Berlin)* **2006**, *122*, 163. (h) Bernot, K.; Bogani, L.; Caneschi, A.; Gatteschi, D.; Sessoli, R. *J. Am. Chem. Soc.* **2006**, *128*, 7947. (i) Miyasaka, H.; Madanbashi, T.; Sugimoto, K.; Nakazawa, Y.; Wernsdorfer, W.; Sugiura, K.; Yamashita, M.; Coulon, C.; Clérac, R. *Chem.−Eur. J.* **2006**, *12*, 7028. (j) Miyasaka, H.; Julve, M.; Yamashita, M.; Clérac, R. *Inorg. Chem.* **2009**, *48*, 3420 and references therein. (k) Venkatakrishnan, T. S.; Sahoo, S.; Brefuel, B.; Duhayon, C.; Paulsen, C.; Barra, A.; Ramasesha, S.; Sutter, J. *J. Am. Chem. Soc.* **2010**, *132*, 6047.

2 Glauber, R. J. *J. Math. Phys.* 1963, **4**, 294.

3 (a) Sessoli, R.; Tsai, H. L.; Schake, A. R.; Wang, S.; Vincent, J. B.; Folting, K.; Gatteschi, D.; Christou, G.; Hendrickson, D. N. *J. Am. Chem. Soc.***1993**, *115*, 1804. (b) Sessoli, R.; Gatteschi, D.; Caneschi, A.; Novak, M. A. *Nature* **1993**, *365*, 141. (c) Gatteschi, D.; Sessoli, R.; Villain, J. *Molecular Nanomagnets*, Oxford University Press: New York, **2006** and references therein. (d) Schelter, E. J.; Prosvirin, A. V.; Dunbar, K. R. *J. Am. Chem. Soc.* **2004**, *126*, 15004. (e) Milios, C. J.; Vinslava, A.; Wernsdorfer, W.; Moggach, S.; Parsons, S.; Perlepes, S. P.; Christou, G.; Brechin, E. K. *J. Am. Chem. Soc.* **2007**, *129*, 2754. (f) Freedman, D. E.; Jenkins, D. M.; Iavarone, A. T.; Long, J. R. *J. Am. Chem. Soc.***2008**, *130*, 2884. (g) Yoshihara, D.; Karasawa, S.; Koga, N. *J. Am. Chem. Soc.***2008**, *130*, 10460. (h) Lin, P.-H.; Burchell, T. J.; Ungur, L.; Chibotaru, L.; Wernsdorfer, W.; Murugesu, M. *Angew. Chem. Int. Ed.*, **2009**, *48*, 9489.

4 (a) Garanin D. A. and Chudnovsky, E. M. *Phys. Rev. B*, **1997**, *56*, 11102; (b) Leuenberger M. N. and Loss, D. *Nature*, 2001, **410**, 789; (c) Jo, M.-H.; Grose, J. E.; Liang, W.; Baheti, K.; Deshmukh, M. M.; Sokol, J. J.; Rumberger, E. M.; Hendrickson, D. N.; Long, J. R.; Park H.; Ralph, D. C. *Nano Lett.*, **2006**, *6*, 2014. (d) Ardavan, A.; Rival, O.; Morton, J. J. L.; Blundell, S. J.; Tyryshkin, A. M.; Timco, G. A.; Winpenny, R. E. P. *Phys. Rev. Lett.* **2007**, *98*, 57201. (e) Bogani, L.; Wernsdorfer, W. *Nat. Mater.* 2008, **7**, 179. (f) Stamp, P. C. E.; Gaita-Arino, A. *J. Mater. Chem.* **2009**, *19*, 1718. (g) Loth, S.; von Bergmann, K.; Ternes, M.; Otte, A. F.; Lutz, C. P.; Heinrich, A. J. *Nat. Phys.* **2010**, *6*, 340.

5 (a) Suzuki, M. and Kubo, R *J. Phys. Soc. Jpn.*, **1968**, *24*, 51. (b) Coulon, C.; Clérac, R.; Lecren, L.; Wernsdorfer, W.; Miyasaka, H. *Phys. Rev. B* **2004**, *69,* 132408.

6 Saitoh, A.; Miyasaka, H.; Yamashita, M.; Clérac, R. *J. Mater. Chem.* **2007**, *17*, 2002.

7 This equation applies in the infinite-size regime for an Ising-type single-chain magnet considering the following Hamiltonian:

$$H = -2J\sum_{-\infty}^{+\infty}\vec{S}_i\vec{S}_{i+1} + D\sum_{-\infty}^{+\infty}\vec{S}_{iz}^2$$

and in the $|D/J| > {}^4/_3$ Ising limit, where Δ_τ is the overall relaxation barrier, and S and D are the spin ground state and magnetic anisotropy parameter of the repeating unit, respectively. See Reference 5b.

8 (a) Dunbar, K. R.; Heintz, R. A. *Prog. Inorg. Chem.* **1997**, *45*, 283, and references therein. (b) Beltran, L. M. C.; Long, J. R. *Acc. Chem. Res.* **2005**, *38*, 325. (c) Shatruk, M.; Avendano, C.; Dunbar, K. *Progress in Inorganic Chemistry*; Karlin, K. D.; John Wiley & Sons: Amsterdam, **2009**; *56*, pp 155, and references therein.

9 (a) Rodriguez-Fortea, A.; Alemany, P.; Alvarez, S.; Ruiz, E. *Inorg. Chem.* **2001**, *40*, 5868-5877; (b) Bond, A. D.; Derossi, S.; Harding, C. J.; McInnes, E. J. L.; McKee, V.; McKenzie, C. J.; Nelson, J.; Wolowska, J. *Dalton Trans*, **2005**, 2403-2409; (c) Miyasaka, H.; Takahashi, H.; Madanbashi, T.; Suguira, K.; Clérac, R.; Nojiri, H. *Inorg. Chem.* **2005**, *44*, 5969-5971; (d) Atanasov, M.; Comba, P.; Daul, C. A. *J. Phys. Chem. A.***2006**, *110*, 13332-13340; (e) Gu, J.; Jiang, L.; Tan, M.; Lu, T. *J. Mol. Struct.* **2008**, *890*, 24; (f) Visinescu, D.; Toma, M.; Cano, J.; Fabelo, O.; Ruiz-Perez, C.; Labrador, A.; Lloret, F.; Julve, M. *Dalton Trans.* **2010**, *39*, 5028-5038. (g)

Kwak, H. Y.; Ryu, D. W.; Lee, J. W.; Yoon, J. H.; Kim, H. C.; Koh, E. W.; Krinsky, J.; Hong, C. S. *Inorg. Chem*. **2010**, *49*, 4632-4642.

10 Harris, T. D.; Bennett, M. V.; Clérac, R.; Long, J. R. *J. Am. Chem. Soc.* 2010, **132**, 3980.

11 (a) Soula, B. ; Galibert, A. M. ; Donnadieu, B. ; Fabre, P. L. *Dalton Trans*., **2003**, 2449; (b) Guionneau, P. ; Marchivie, M. ; Bravic, G. ; Letard, J. F. ; Chasseau, D. *Top. Cuur. Chem.*, **2004**, *234*, 97; (c) Lefebvre, E. ; Conan, F. ; Cosquer, N. ; Kerbaol, J. ; Marchivie, M. ; Sala-Pala, J. ; Kubicki, M. M.; Vigier, E. ; Garcia, C. J. G. *New. J. Chem.*, **2006**, *30*, 1197.

12 (a) Seredyuk, M.; Haukka, H.; Fritsky, I. O.; Kozlowski, H.; Kramer, R.; Pavlenko, V. A.; Gutlich, P. *Dalton Trans.* **2007**, 3183 ; (b) Galet, A. ; Manoz, M. C. ; Martinez, V. ; Real, J. A. *Chem. Commun,* **2004**, 2268-2269.

13 Baumgatner, O. *Z. Kristallogr.***1986**, *174*, 253; Marchetti, F.; Marchetti, F. ; Melai, B. ; Pampaloni, G. ; Zacchini, S. *Inorg. Chem*. **2007**, *46*, 3378; Albinati, A.; Calderazzo, F.; Marchetti, F.; Mason, S. A.; Melai, B.; Pampaloni, G.; Rizzato, S. *Inorg. Chem. Commun*. **2007**, *10*, 902.

14 (a) Shatruk, M.; Draguloscu-Andrasi, A.; Chambers, K. E.; Stoian, S. A.; Bominaar, E. L.; Achim, C.; Dunbar, K. R. *J. Am. Chem. Soc.* **2007**, *129*, 6104; (b) Niel, V.; Munoz, M. C.; Gaspar, A. B.; Galet, A.; Levchenko, G.; Real, J. A. *Chem. –Eur. J.* **2002**, *8*, 2446; (c) Zhang, Y.; Liu, T.; Kanegawa, S.; Sato, O, *J. Am. Chem. Soc.* **2009**, *131*, 7942; (d) Jacob, V.; Huttner, G.; Kaifer, E.; Kircher, P.; Rutsch, P. *Eur. J. Inorg. Chem.* **2001**, 2783; (e) Hilfiger, M. G.; Chen, M.; T. Brinzari, V.; Shatruk, M.; Petasis, D. T.; Musfeldt, J. L.; Achim, C.; Dunbar, K. R. *Angew. Chem. Int. Ed.*, **2010**, *49*, 1410.

15 Drillon, M.; Coronado, E.; Beltran, D.; Georges, R. *Chem. Phys.***1983**, *79*, 449. (b) Georges, R.; Borras-Almenar, J. J.; Coronado, E.; Curely, J.; Drillon, M. *Magnetism: Molecules to Materials I: Models and Experiments*, Eds. Miller, J. S.; Drillon, M.; Wiley-VCH: Verlag, **2002**. The expression used to describe the magnetic susceptibility follows:

$$\chi_0 = \frac{N_A\mu_B^2}{6k_BT}\left[(M_a+M_b)^2\frac{1+P}{1-P}+(M_a-M_b)^2\frac{1-P}{1+P}\right],\ \text{where } M_i = g_i\sqrt{S_i(S_i+1)},$$

$$P = \coth\left(\frac{2J\sqrt{S_a(S_a+1)S_b(S_b+1)}}{k_BT}\right)-\left(\frac{k_BT}{2J\sqrt{S_a(S_a+1)S_b(S_b+1)}}\right),\ S_a = S_{Re}\ \text{and}\ S_b = S_{Fe}$$

$$\chi_0 = \frac{N_A\mu_B{}^2}{6k_BT}\left[(M_a + M_b)^2\frac{(1+P)}{(1-P)} + (M_a\text{-}M_b)^2\frac{(1-P)}{(1+P)}\right]$$

16 The $\chi_M T$ vs. T data for complexes **1** and **3-6** were fit applying the constraint $g_{Re} = g_{Fe}$, as the fitting procedure was unable to independently and accurately determine the two g parameters independently.

17 Here, O_h symmetry is considered to approximate the local coordination environments of the Re^{IV} and Fe^{II} ions.

18 Entley, W. R.; Trentway, C. R.; Girolami, G. S. *Mol. Cryst. Liq. Cryst*. **1995**, *273*, 153; Weihe, H.; Gudel, H. U. *Comments Inorg. Chem*. **2000**, *22*, 75.

19 (a) Ohkoshi, S. ; Yorozu, S.; Sato, O.; Iyoda, T.; Fujishima, A.; Hashimoto, K. *Appl. Phys. Lett*. **1997**, *70*, 1040. (b) Gao, B.; Yao, J.; Xue, D. J. *Magn. Magn. Mater.*

2010, *322*, 2505. (c) Zhang, Y.-Z.; Wang, B. -W.; Sato, O.; Gao, S. *Chem. Commun* .**2010**, *46*, 6959.
20 Harris, T. D. ; Soo, H.; Chang, C. J.; Long, J. R. *Inorg. Chim. Acta.* **2010**, *369*, 91.
21 Palii, A. V.; Tsukerblat, B. S.; Verdaguer, M. *J. Chem. Phys.* **2002**, *117*, 7896.
22 (a) Cole, K. S.; Cole, R. H. *J. Chem. Phys.* **1941**, *9*, 341. (b) Boettcher, C. J. F. *Theory of Electric Polarisation*; Elsevier: Amsterdam, **1952**. (c) Aubin, S. M.; Sun, Z.; Pardi, L.; Krzystek, J.; Folting, K.; Brunel, L.-J.; Rheingold, A. L.; Christou, G.; Hendrickson, D. N. *Inorg. Chem.* 1999, **38**, 5329.
23 Ishii, N.; Okamura, Y.; Chiba, S.; Nogami, T.; Ishida, T. *J. Am. Chem. Soc.* **2008**, *130*, 24.
24 Toma, L. M. ; Lescouëzec, R. ; Lloret, F. ; Julve, M. ; Vaissermann, J. ; Verdaguer, M. *Chem. Commun.* **2003**, 1850-1851.
25 Note that this the term "single-chain magnet" was not used to describe this compound. Rather, the term first appeared in Ref. 1b.
26 (a) Coulon, C.; Clérac, R.; Wernsdorfer, W.; Colin, T.; Miyasaka, H. *Phys. Rev. Lett.* **2009**, *102*, 167204/1–4. (b) Miyasaka, H. ; Takayama, K.; Saitoh, A.; Furukawa, S.; Yamashita, M.; Clérac, R. *Chem.−Eur. J.* **2010**, 3656.
27 Harris, T. D. ; Coulon, C.; Clérac, R.; Long, J. R. *J. Am. Chem. Soc.***2011**, *133*, 123.

2.8 Supporting Information

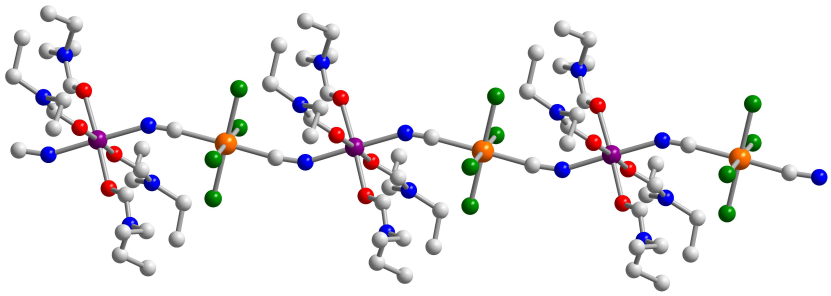

Figure S1. Crystal structure of $(DEF)_4FeReCl_4(CN)_2$ **1** chain. Orange, purple, green, red, blue, and gray spheres represent rhenium, iron, chlorine, oxygen, nitrogen, and carbon atoms, respectively; hydrogen atoms have been omitted for clarity.

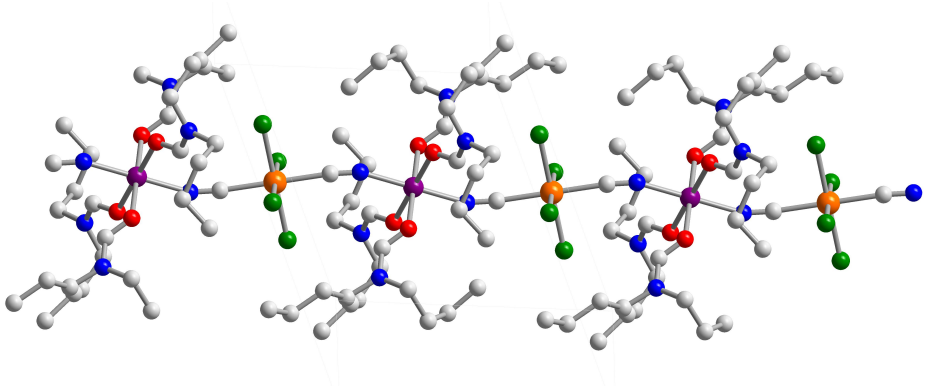

Figure S2. Crystal structure of $(DBF)_4FeReCl_4(CN)_2$ **2** chain. Orange, purple, green, red, blue, and gray spheres represent rhenium, iron, chlorine, oxygen, nitrogen, and carbon atoms, respectively; hydrogen atoms have been omitted for clarity.

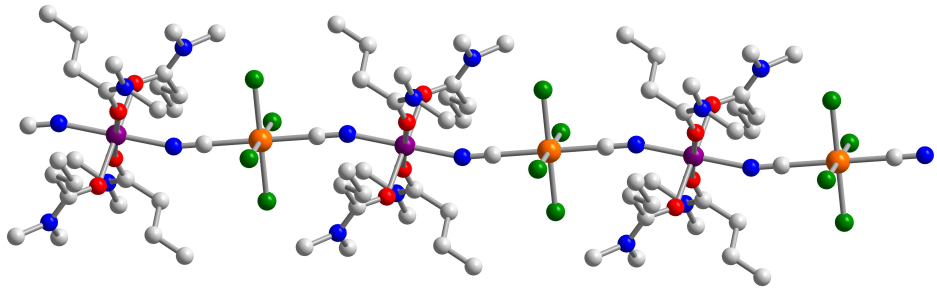

Figure S3. Crystal structure of $(DMB)_4FeReCl_4(CN)_2$ **4** chain. Orange, purple, green, red, blue, and gray spheres represent rhenium, iron, chlorine, oxygen, nitrogen, and carbon atoms, respectively; hydrogen atoms have been omitted for clarity.

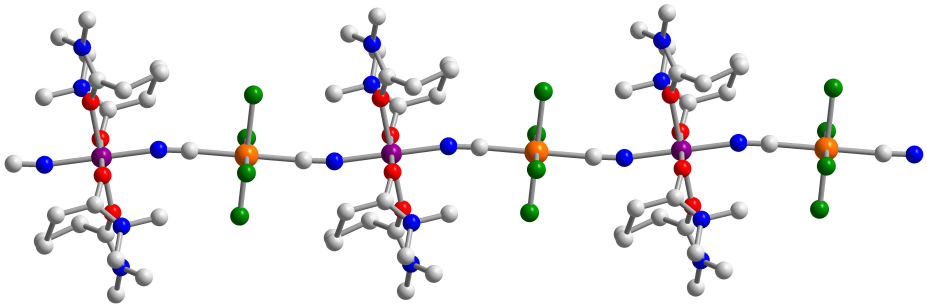

Figure S4. Crystal structure of $(DMP)_4FeReCl_4(CN)_2$ **5** chain. Orange, purple, green, red, blue, and gray spheres represent rhenium, iron, chlorine, oxygen, nitrogen, and carbon atoms, respectively; hydrogen atoms have been omitted for clarity.

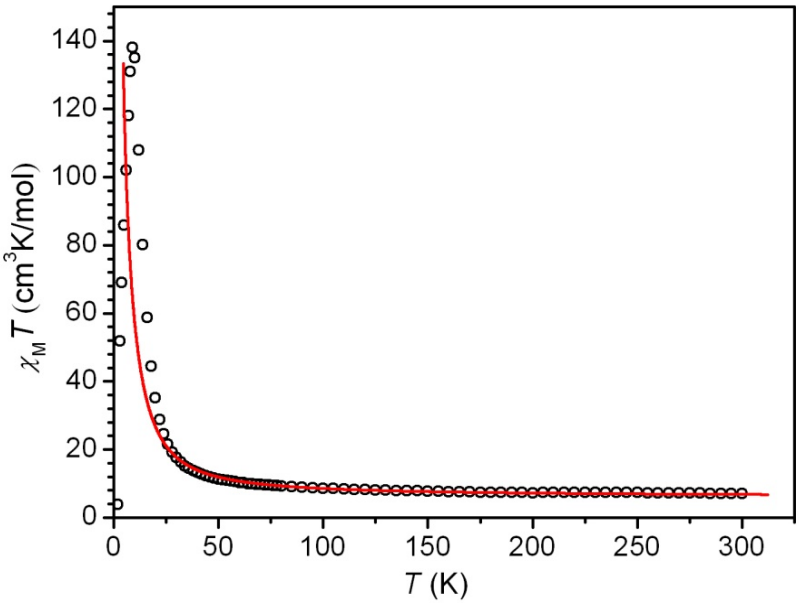

Figure S5. Variable-temperature dc magnetic susceptibility data for **1**, collected in an applied field of 1000 Oe. The solid red line corresponds to a fit to the data, as described in the text.

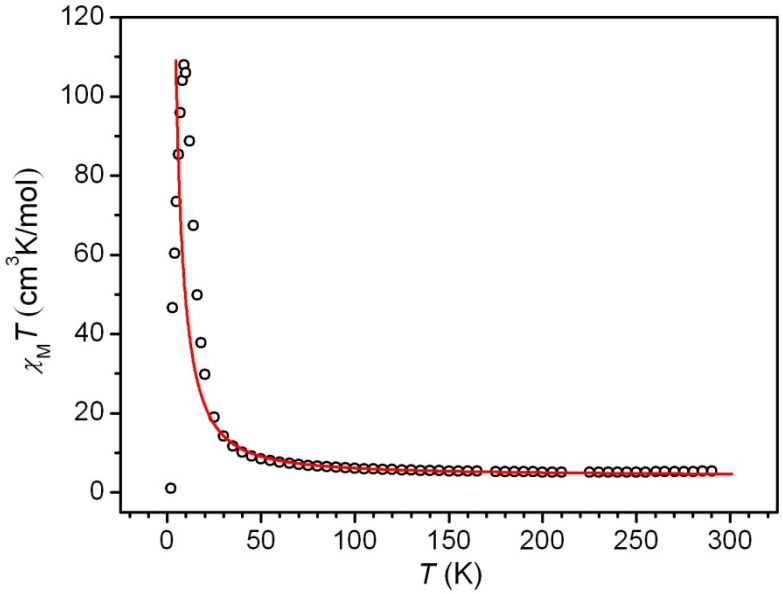

Figure S6. Variable-temperature dc magnetic susceptibility data for **2**, collected in an applied field of 1000 Oe. The solid red line corresponds to a fit to the data, as described in the text.

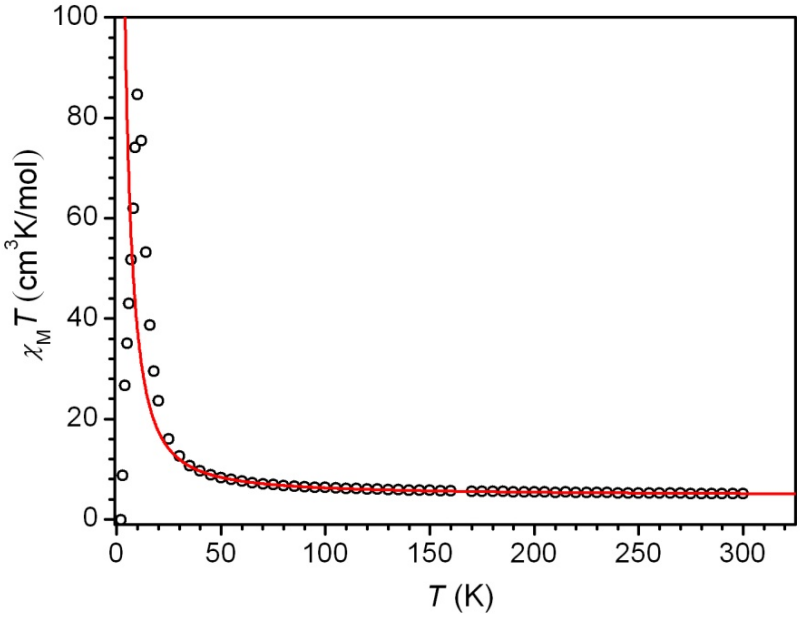

Figure S7. Variable-temperature dc magnetic susceptibility data for **4**, collected in an applied field of 1000 Oe. The solid red line corresponds to a fit to the data, as described in the text.

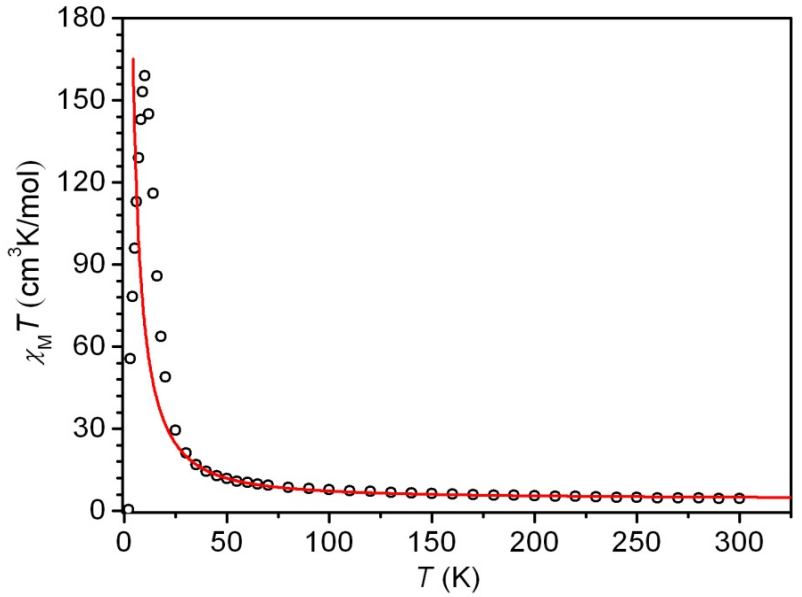

Figure S8. Variable-temperature dc magnetic susceptibility data for **5**, collected in an applied field of 1000 Oe. The solid red line corresponds to a fit to the data, as described in the text.

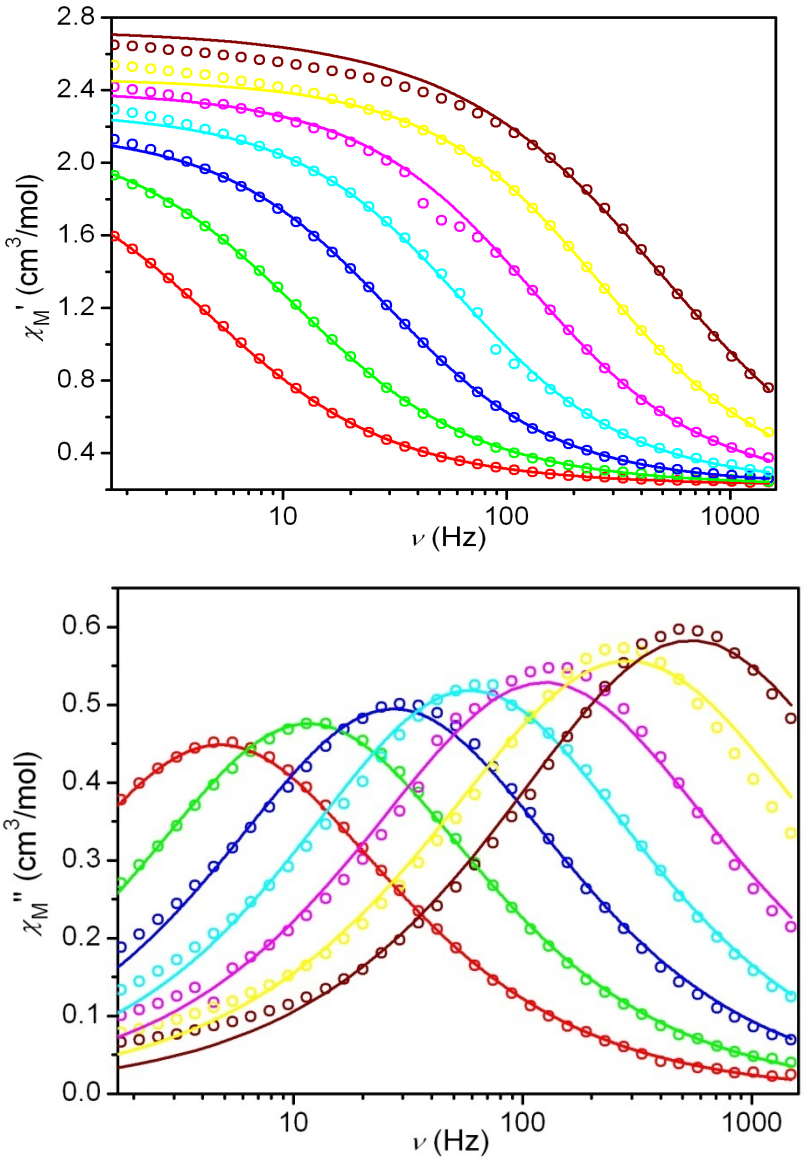

Figure S9. Variable-frequency in-phase (upper) and out-of-phase (lower) components of the ac magnetic susceptibility data for **1**, collected in a 4 Oe ac field at temperatures of 3.6 (red), 3.8 (green), 4.0 (blue), 4.2 (cyan), 4.4 (magenta), 4.6 (yellow) and 4.8 (wine) K. The solid lines correspond to the fits to the data, as described in the text.

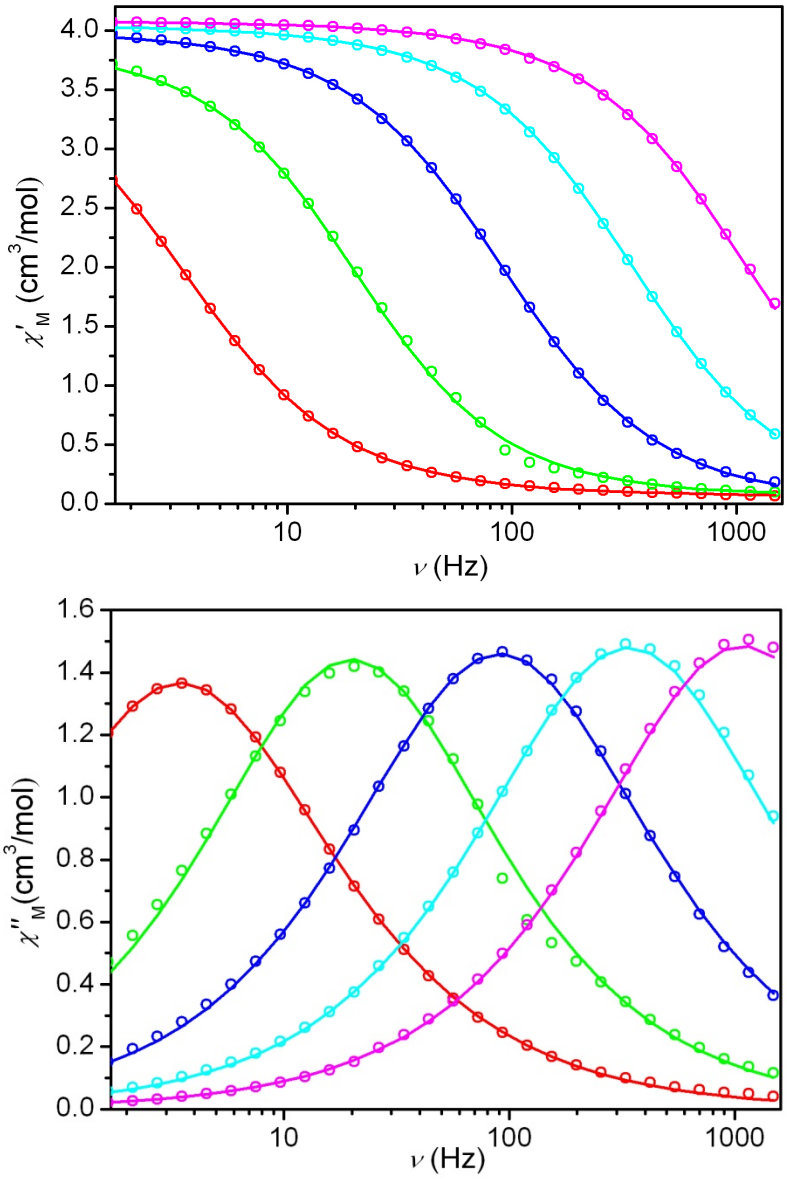

Figure S10. Variable-frequency in-phase (upper) and out-of-phase (lower) components of the ac magnetic susceptibility data for **2**, collected in a 4 Oe ac field at temperatures of 4.0 (red), 4.4 (green), 4.8 (blue) and 5.2 (cyan) and 5.6 (magenta) K. The solid lines correspond to the fits to the data, as described in the text.

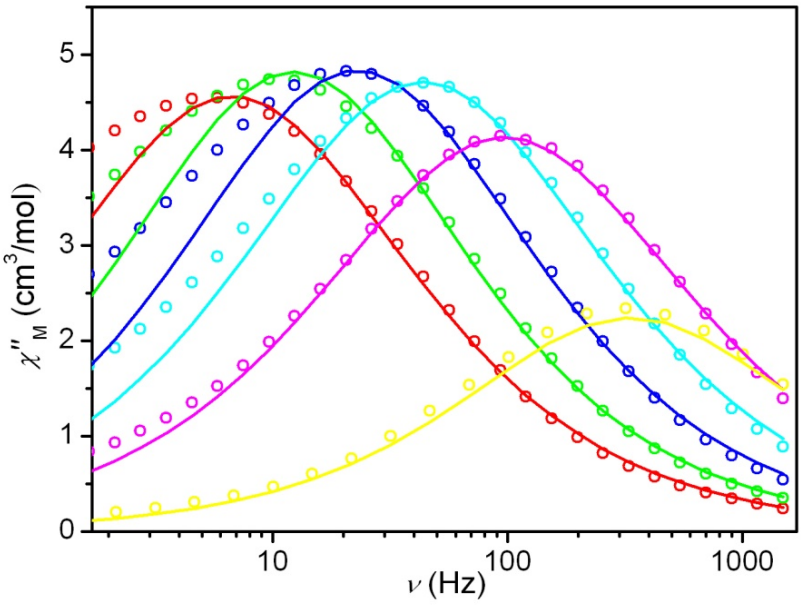

Figure S11. Variable-frequency out-of-phase components of the ac magnetic susceptibility data for **4**, collected under 0 Oe dc field, in a 4 Oe ac field oscillating at temperatures of 9 (red), 9.3 (green), 9.6 (blue), 9.9 (cyan), 10.2 (magenta), and 10.5 (yellow) K. The solid lines correspond to the fits to the data, as described in the text.

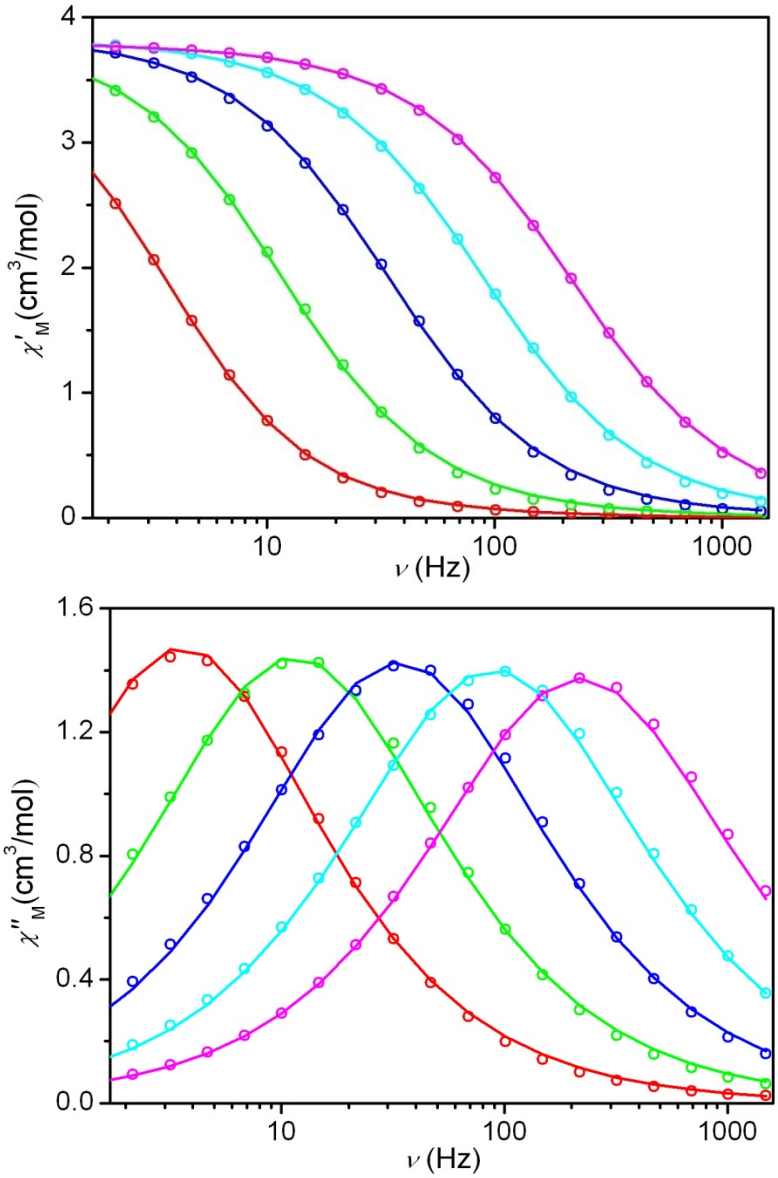

Figure S12. Variable-frequency in-phase (upper) and out-of-phase (lower) components of the ac magnetic susceptibility data for **4**, under a 1000 Oe dc field, collected in a 4 Oe ac field at temperatures of 4 (red), 4.3 (green), 4.6 (blue), 4.9 (cyan) and 5.2 (magenta) K. The solid lines correspond to the fits to the data, as described in the text.

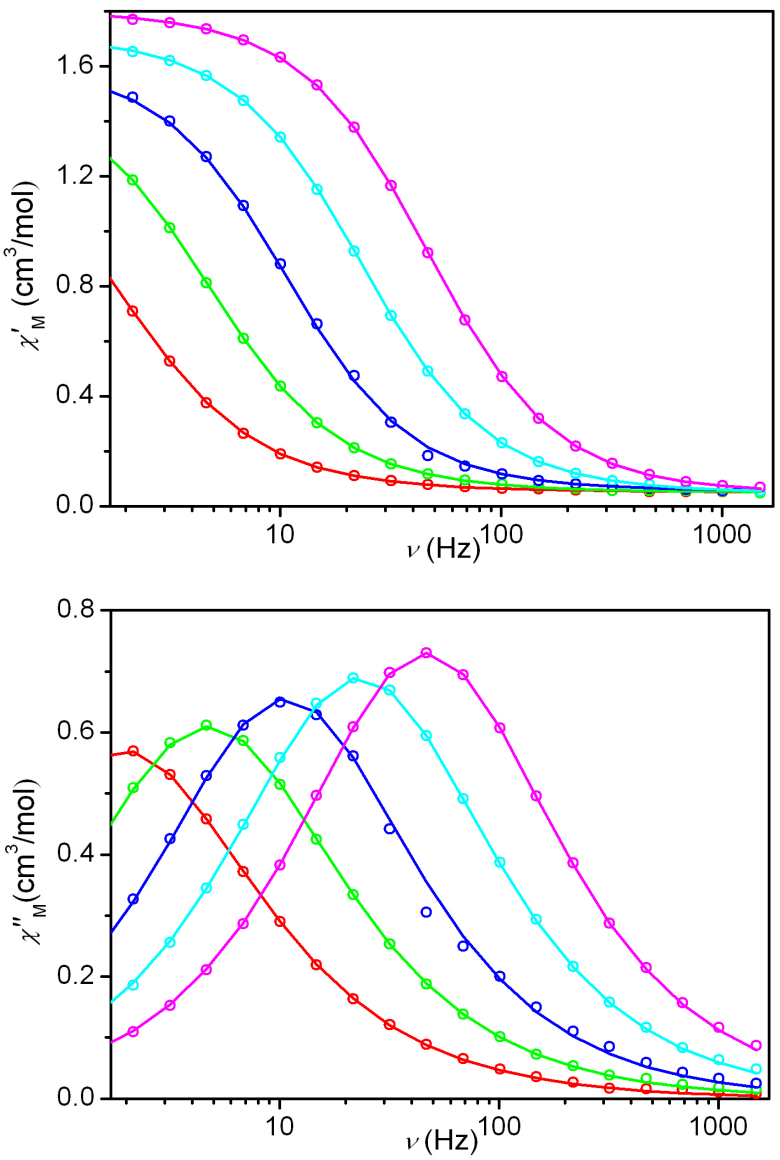

Figure S13. Variable-frequency in-phase (upper) and out-of-phase (lower) components of the ac magnetic susceptibility data for **5**, collected in a 4 Oe ac field at temperatures of 4 (red), 4.2 (green), 4.4 (blue), 4.6 (cyan) and 4.8 (magenta) K. The solid lines correspond to the fits to the data, as described in the text.

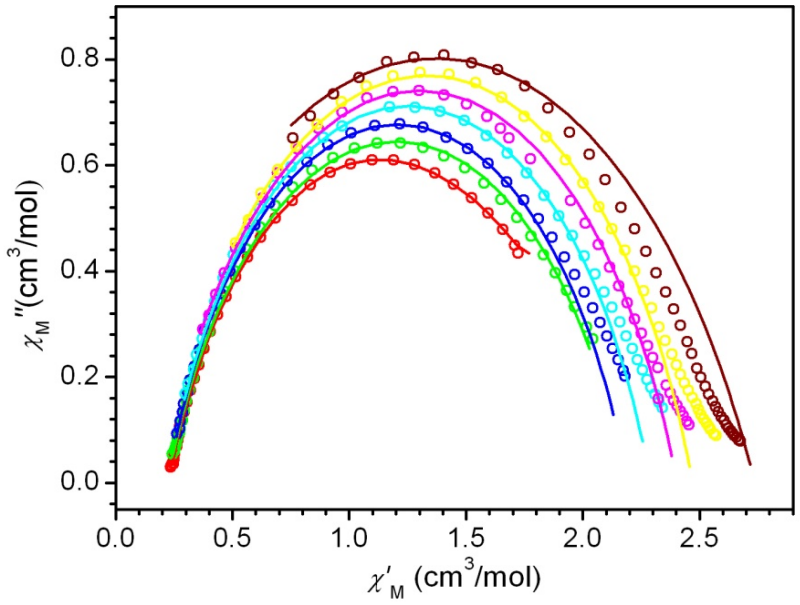

Figure S14. Cole-Cole plots for **1** at temperatures of 3.6 (red), 3.8 (green), 4.0 (blue), 4.2 (cyan), 4.4 (magenta), 4.6 (yellow) and 4.8 (wine) K. The solid lines correspond to the fits to the data, as described in the text.

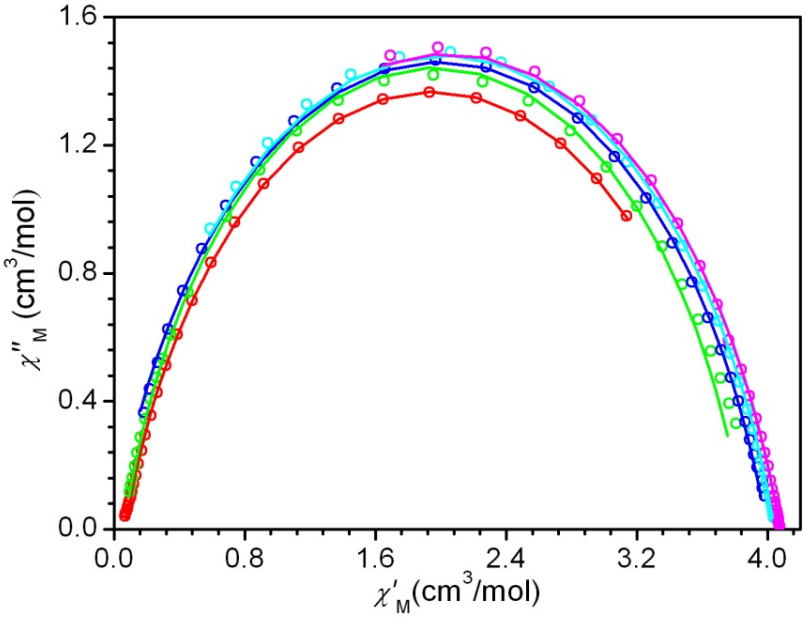

Figure S15. Cole-Cole plots for **2** at temperatures of 4.0 (red), 4.4 (green), 4.8 (blue) and 5.2 (cyan) and 5.6 (magenta) K. The solid lines correspond to the fits to the data, as described in the text.

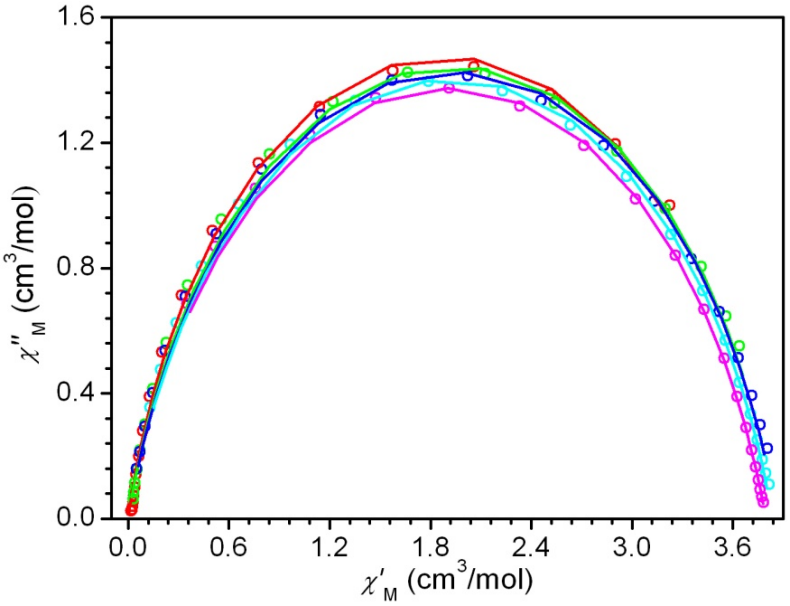

Figure S16. Cole-Cole plots for **4**, constructed from data collected under a 1000 Oe dc field, at temperatures of 4 (red), 4.3 (green), 4.6 (blue), 4.9 (cyan) and 5.2 (magenta) K. The solid lines correspond to the fits to the data, as described in the text.

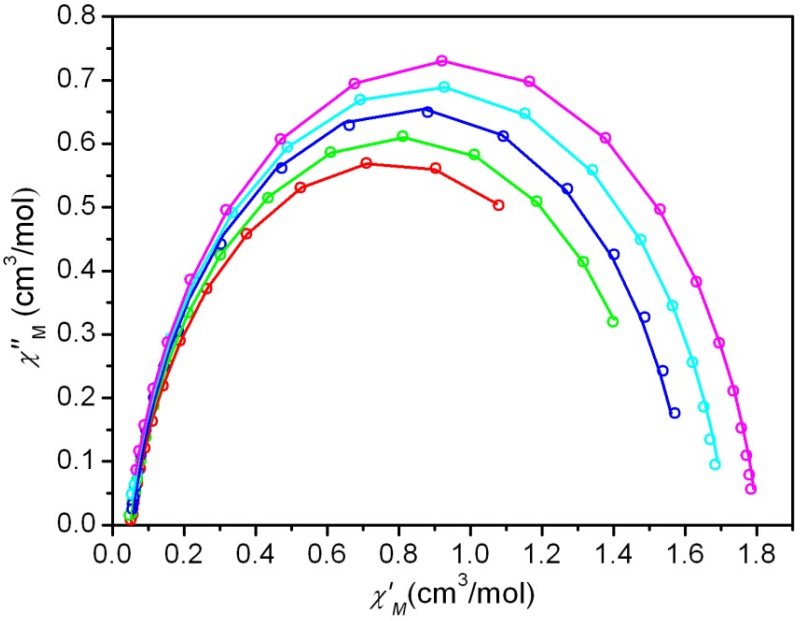

Figure S17. Cole-Cole plots for **5** at temperatures of 4 (red), 4.2 (green), 4.4 (blue), 4.6 (cyan) and 4.8 (magenta) K. The solid lines correspond to the fits to the data, as described in the text.

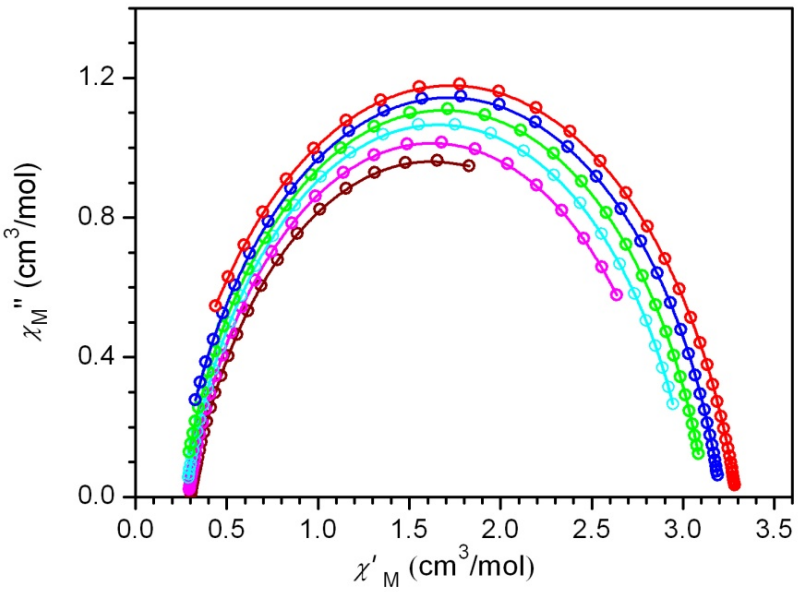

Figure S18. Cole-Cole plots for **6** at temperatures of 6.2 (wine), 6.6 (magenta), 7.0 (cyan), 7.4 (green), 7.8 (blue), and 8.2 (red) K. The solid lines correspond to the fits to the data, as described in the text.

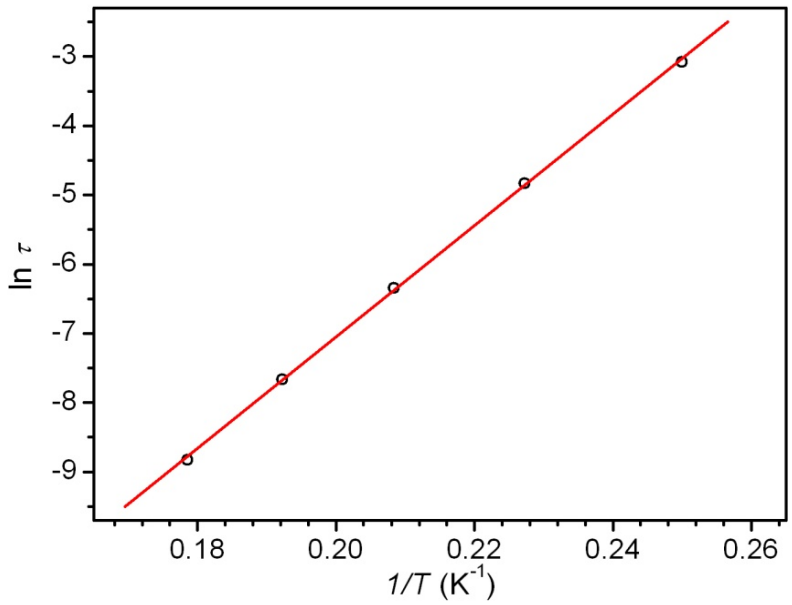

Figure S20. Arrhenius plot of relaxation time for **2**.

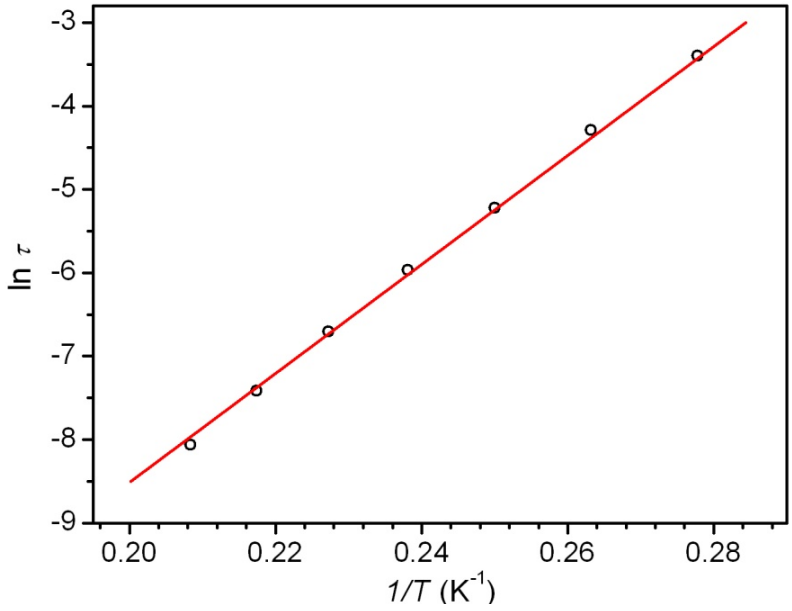

Figure S19. Arrhenius plot of relaxation time for **1**.

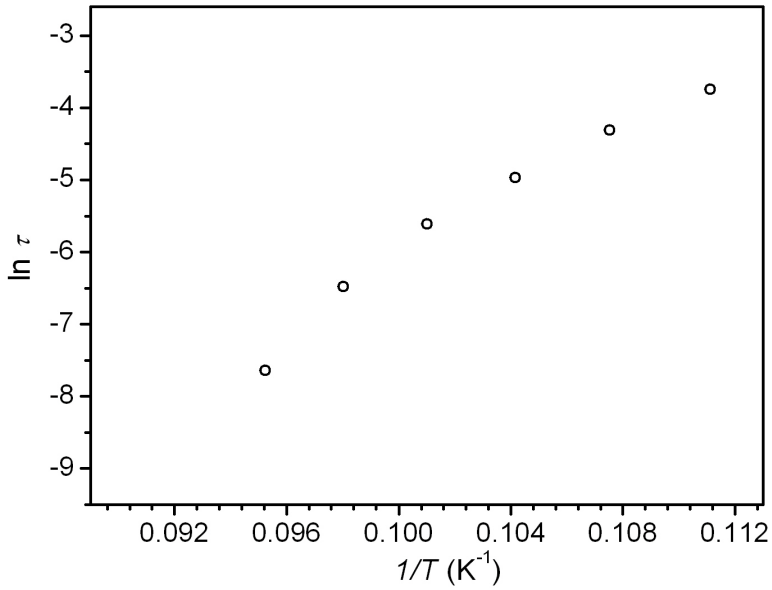

Figure S21. Arrhenius plot of relaxation time for **4**, under a zero dc field.

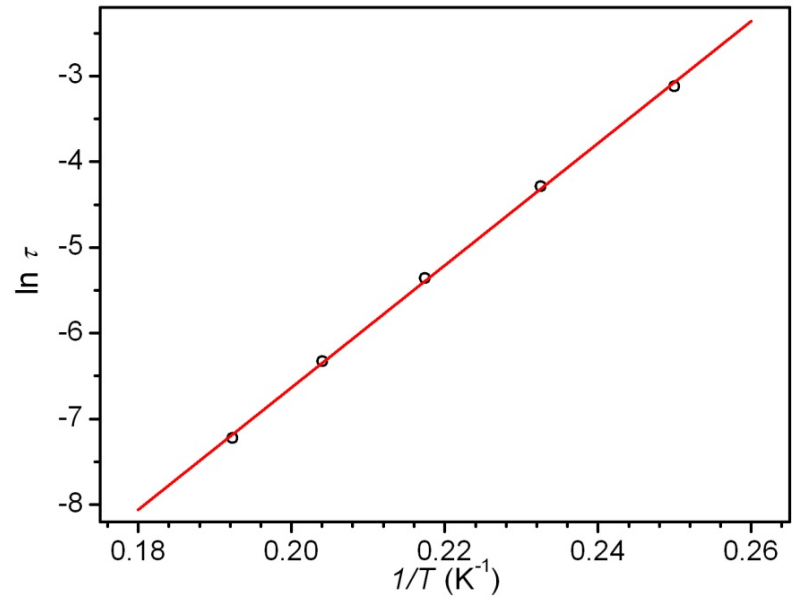

Figure S22. Arrhenius plot of relaxation time for **4**, under a 1000 Oe dc field.

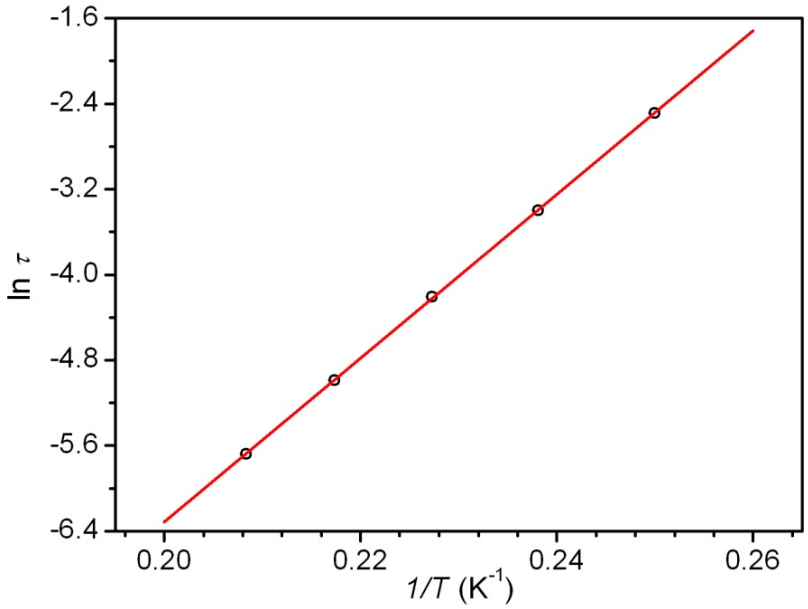

Figure S23. Arrhenius plot of relaxation time for **5**.

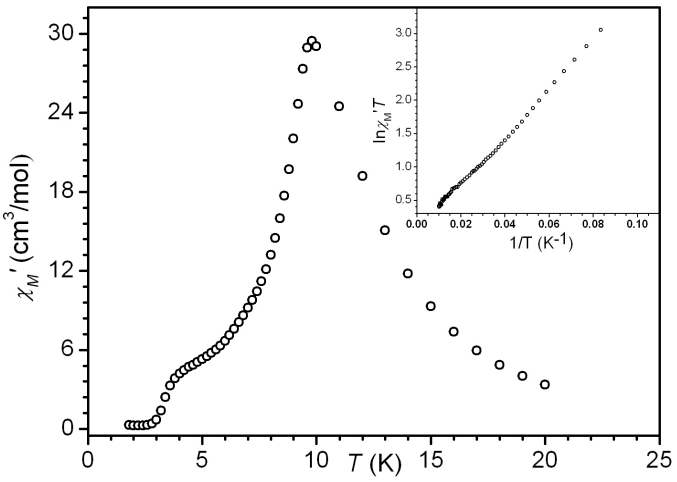

Figure S24. Variable-temperature in-phase component of ac susceptibility of **1**, collected in a 4 Oe ac field oscillating at 1 Hz. Inset: Plot of In($c_M'T$) vs 1/T for **1**, from 10 K to 100 K

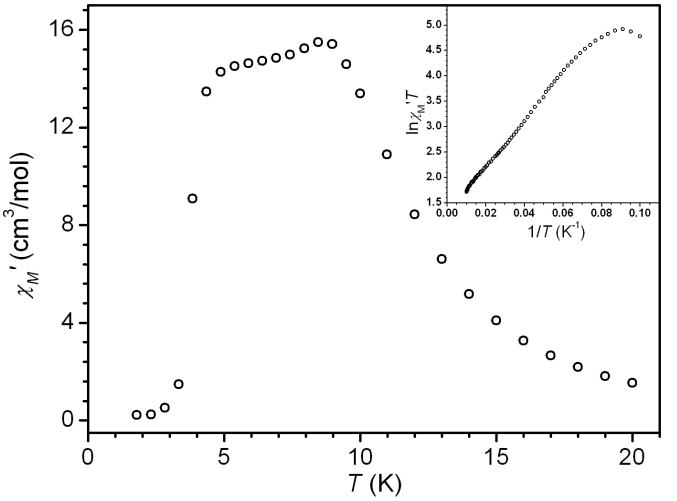

Figure S25. Variable-temperature in-phase component of ac susceptibility of **2**, collected in a 4 Oe ac field oscillating at 1 Hz. Inset: Plot of In($c_M'T$) vs 1/T for **2**, from 10 K to 100 K

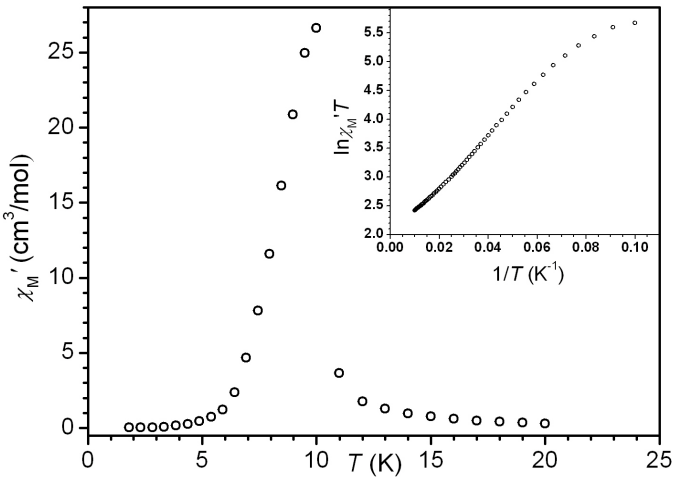

Figure S26. Variable-temperature in-phase component of ac susceptibility of **4**, collected in a 4 Oe ac field oscillating at 1 Hz. Inset: Plot of In($c_M'T$) vs 1/T for **4**, from 10 K to 100 K

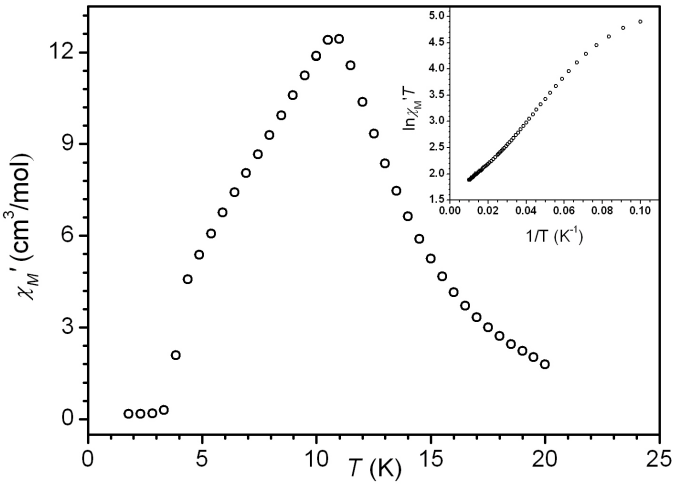

Figure S27. Variable-temperature in-phase component of ac susceptibility of **5**, collected in a 4 Oe ac field oscillating at 1 Hz. Inset: Plot of In($c_M'T$) vs 1/T for **5**, from 10 K to 100 K

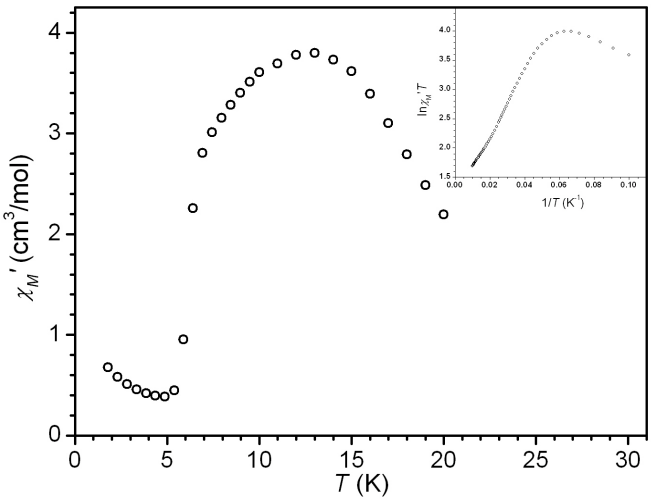

Figure S28. Variable-temperature in-phase component of ac susceptibility of **6**, collected in a 4 Oe ac field oscillating at 1 Hz. Inset: Plot of In($c_M'T$) vs 1/T for **6**, from 10 K to 100 K

Chapter 3: Slow Magnetic Relaxation Induced by a Large Transverse Zero-Field Splitting in a $Mn^{II}Re^{IV}(CN)_2$ Single-Chain Magnet

3.1 Introduction

Molecules that exhibit slow magnetic relaxation upon removal from a polarizing magnetic field, referred to as single-molecule magnets,[1] have received considerable attention owing to their potential utility in applications such as spin-based information storage.[2] In these systems, the slow relaxation arises from the action of a uniaxial magnetic anisotropy, quantified by the axial zero-field splitting parameter, D, on a high-spin ground state, S. This phenomenon engenders a magnetic anisotropy energy barrier, Δ_A, with respect to reversal of the spin of the molecule, where $\Delta_A = S^2|D|$ for integer S and $(S^2 - {}^1/_4)|D|$ for half-integer S. For practical applications of single-molecule magnets to be fully realized, the relaxation barrier must be large enough to ensure stability of the moment orientation to thermal and quantum fluctuations.

Analogous relaxation behavior has been observed more recently in one-dimensional coordination compounds, known as single-chain magnets,[3,4] which consist of paramagnetic ions linked together via bridging ligands. Considering the pursuit of high relaxation barriers in low-dimensional paramagnets, single-chain magnets possess a distinct advantage over single-molecule magnets. The advantage stems from the exchange coupling (J) between the magnetic ions, which adds an additional energy term known as the correlation energy, $\Delta\xi$, to the expression for the relaxation barrier. Assuming a $-2JS_1 \cdot S_2$ interaction between neighboring spin units, the magnitude of the correlation energy for a chain is $\Delta\xi = 4|J|S^2$ in the Ising limit, where $|D/J| > 4/3$, while $\Delta\xi = 4S^2 (|JD|)^{1/2}$ in the Heisenberg limit, where $|D| << |J|$. The total energy barrier with respect to spin reversal can then be expressed as $\Delta\tau = \Delta_A + 2\Delta\xi$ for an infinite chain in which the nucleation of reversed spins necessarily requires the creation of two propagating domain walls.[3g,5,6] In contrast, nucleation from the ends of finite length chains gives rise to an expression for the total energy of $\Delta\tau = \Delta_A + \Delta\xi$. At low temperatures, the relaxation dynamics of single-chain magnets typically fall into the latter category, where the finite chain lengths are caused by crystalline defects.

A negative D value assures that states with maximum spin projection ($M_S = \pm S$) along the z-axis lie lowest in energy, while intermediate spin projections lie higher in energy, such that a classical rotation of the moment from $M_s = +S$ to $-S$ requires excitation over an energy barrier. In the absence of quantum tunneling, which is typically weak for large values of S, it is this anisotropy that gives rise to a magnetically bistable ground state. In contrast, a positive D value and magnetic bistability are widely regarded as being antagonistic, as the ground state in this situation (a singlet for integer S and a Kramers doublet for half-integer S) has minimal spin projection onto the z-axis. Moreover, for the purely axial case, the spin has no preferred orientation within the easy- (xy-) plane. Even in cases involving appreciable transverse (xy) anisotropy, $E(S_x^2 - S_y^2)$, quantum tunneling, which is severe for states that are close in energy, prevents localization of the spin along a preferred direction within the easy-plane. In this context, it is not surprising that it is a commonly held principle that negative D values are essential in the design of single-molecule and single-chain magnets.[7,8]

As noted above, quantum tunneling prevents localization of a magnetic moment along a preferred axis in the case of a quantum spin subjected to easy-plane anisotropy, a simple manifestation of the fact that S_x and S_y do not commute with S_z. However, the situation is quite different in the classical limit, where the magnetic moment associated with a macroscopic easy-plane system may have a preferred (easy-) axis when factoring in any transverse anisotropy of the form $E(S_x^2 - S_y^2)$. In this scenario, the easy-axis would lie along either the *x* or *y* direction, depending on the sign of *E*, and a highly anisotropic energy barrier would prevent rotation of the moment from $+x$ to $-x$ (or $+y$ to $-y$). Furthermore, the maximum barrier height, corresponding to rotation of the moment through *z*, would be dictated by *D*, while the barrier height corresponding to rotation within the *xy*-plane would be dictated instead by *E*. Such a scenario has, so far, not been considered as a possible source of slow magnetic relaxation behavior in either single-molecule or single-chain magnets.

Recently we reported the synthesis of the series of cyano-bridged single-chain magnets $(DMF)_4MReCl_4(CN)_2$ (M = Mn, Fe, Co, Ni), assembled from the building unit $[ReCl_4(CN)_2]^{2-}$.[4] Magnetic analyses revealed that these chain compounds lie in neither the Ising nor Heisenberg limits, which complicates the comparison of the observed $\Delta\tau$ values with those calculated via the experimentally determined *J* and *D* values. Given that the magnetic behavior of the compounds results from a combination of the magnetic anisotropy of the individual spin centers and the interactions between adjacent spin centers, the study of molecules mimicking small fragments of the chain may afford insight into the mechanisms leading to slow magnetic relaxation.

Herein, we report detailed high-frequency, high-field EPR studies of three compounds, $(Bu_4N)_2$[*trans*-$ReCl_4(CN)_2$]·2DMA (**1**), $(DMF)_4ZnReCl_4(CN)_2$ (**2**), and $[(PY5Me_2Mn)_2ReCl_4(CN)_2](PF_6)_2$ (**3**; $PY5Me_2$ = 2,6-bis(1,1-bis(2-pyridyl)ethyl)pyridine), elucidating the influence of metal coordination environment and magnetic interactions on *D*, in order to study the magnetic anisotropy of the chain compound $(DMF)_4MnReCl_4(CN)_2$ (**4**). Surprisingly, **1**-**3** exhibit significant biaxiality, with positive *D* values and a large *E*, suggesting similar properties in compound **4**. We also describe a mechanism for slow magnetic relaxation in a single-chain magnet that arises due to a barrier created by the transverse anisotropy *E* rather than the axial anisotropy *D*. To the best of our knowledge, this is the first observation of slow relaxation arising from *E* in any coordination compound.

3.2 Experimental Section

3.2.1 Preparation of Compounds: The compounds$[(PY5Me_2)Mn(CH_3CN)](PF_6)_2$and $(Bu_4N)_2$[*trans*-$ReCl_4(CN)_2$]·2DMA(**1**) and $(DMF)_4MnReCl_4(CN)_2$ (**4**) were synthesized as described previously.[1e,4] Solid $(Bu_4N)CN$ was dried *in vacuo* ($P < 10^{-3}$ Torr) for 36 h using a trap containing P_2O_5 prior to use. All other reagents were obtained from commercial sources and used without further purification. *Caution!* Although we have experienced no problems while working with them, perchlorate salts are potentially explosive and should be handled with extreme care and only in small quantities.

$(DMF)_4ZnReCl_4(CN)_2$ (2). A solution of $Zn(BF_4)_2·H_2O$ (0.014 g, 0.078 mmol) in 2 mL of DMF was added to a solution of **1** (0.030 g, 0.035 mmol) in 2 mL of DMF. The resulting light green solution was allowed to stand for 2 h to afford green plated-shaped crystals suitable for x-ray analysis. The crystals were collected by filtration, washed with

successive aliquots of DMF (3 × 1 mL) and Et_2O (3 × 5 mL), and dried in air to afford 0.018 g (70%) of product as a light green solid. IR (neat): ν_{CN} 2170 cm^{-1}. Anal. Calcd for $C_{14}H_{28}Cl_4N_6O_4ReZn$: C, 22.80; H, 1.91; N, 11.40; Found: C, 22.90; H, 1.88; N, 11.32.

$[(PY5Me_2)Mn]_2[ReCl_4(CN)_2](PF_6)_2$ (3). A solution of $[(PY5Me_2)Mn(CH_3CN)](PF_6)_2$ (0.035 g, 0.052 mmol) in 2 mL of acetonitrile to a solution of **1** (0.020 g, 0.023 mmol) in 2 mL of acetonitrile. The resulting bright yellow solution was filtered through diatomaceous earth. Diffusion of diethylether vapor into the filtrate afforded yellow blade-shaped crystals suitable for x-ray analysis. The crystals were collected by filtration, washed with successive aliquots of Et_2O (3 × 5 mL), and dried in air to give 0.022 g (62%) of product as a light green solid. IR (neat): ν_{CN} 2156 cm^{-1}. Anal. Calcd for $C_{56}H_{50}Cl_4F_{12}Mn_2N_{12}P_2Re$: C, 41.54; H, 3.11; N, 10.38; Found: C, 41.27; H, 3.65; N, 10.88.

3.2.2 X-Ray Structure Determinations. Single crystals of compounds **2** and **3** were coated with Paratone-N oil and mounted on glass fibers or Kaptan loops. The crystals were then quickly transferred to Bruker MICROSTAR diffractometer, and cooled in a stream of nitrogen gas. Preliminary cell data were collected, giving unit cells with a triclinic or monoclinic Laue group, as established using the SMART[9] or APEX2[10] program package. The unit cell parameters were later refined against all data. A full hemisphere of data was collected for all compounds. None of the crystals showed significant decay during data collection. Data were integrated and corrected for Lorentz and polarization effects using SAINT[11] and were corrected for absorption effects using SADABS.[12]

Space group assignments were based upon systematic absences, *E*-statistics, and successful refinement of the structures. Structures were solved by direct methods and expanded through successive difference Fourier maps. They were refined against all data using the SHELXTL[13] program. Thermal parameters for all non-hydrogen atoms were refined anisotropically in all compounds. Table S1 summarizes the unit cell and structure refinement parameters for compounds **2** and **3**.

3.2.3 Magnetic Susceptibility Measurements. Magnetic data were collected on a Quantum Design MPMS-XL SQUID magnetometer. Dc susceptibility measurements for **2** were obtained for a microcrystalline powder restrained in its frozen mother liquor within a sealed fused silica tube to prevent sample decomposition. Measurements for compound **3** were performed on microcrystalline powders restrained in a frozen polyethylene bag. All data were corrected for diamagnetic contributions from the sample holder, as well as for the core diamagnetism of each sample (estimated using Pascal's constants).

3.2.4 Electron Paramagnetic Resonance. Single-crystal high-field EPR measurements were carried out in a 35 T resistive magnet. A Millimeter Vector Network Analyzer and several different multipliers were used as a microwave source and detector. Powder EPR data were collected in a transmission-type spectrometer based on a 17 T superconducting magnet. A phase-locked Virginia Diodes solid-state source, followed by a cascade of multipliers and amplifiers, was employed as the microwave source.

3.2.5 Other Physical Measurements. Infrared spectra were obtained on a Nicolet Avatar 360 FTIR with an attenuated total reflectance (ATR) accessory. Carbon, hydrogen, and nitrogen analyses were obtained from the Micro analytical Laboratory of the University

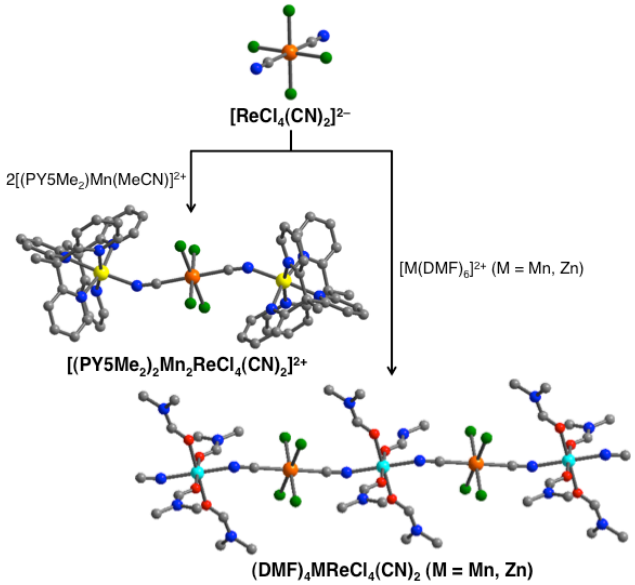

Figure 1. Reaction of *trans*-$[ReCl_4(CN)_2]^{2-}$ (upper) with $[Zn(DMF)_6]^{2+}$ to form the one-dimensional solids $(DMF)_4ZnReCl_4(CN)_2$ (left), with $[PY5Me_2Mn(CH_3CN)]^{2+}$ to form cluster $[(PY5Me_2)_2Mn_2ReCl_4(CN)_2]^{2+}$. Orange, yellow, cyan, green, red, blue, and gray spheres represent Re,Mn, Zn, Cl, O, N, and C atoms, respectively; H atoms have been omitted for clarity

of California, Berkeley. X-ray powder diffraction data were collected using Cu Ka (λ = 1.5406 Å) radiation on a Siemens D5000 diffractometer.

3.3 Results and Discussion

3.3.1 Synthesis and Structures. Compounds **1-3** were synthesized in order to help understand the magnetic anisotropy of chain compound**4**. Here, **1** contains the $[ReCl_4(CN)_2]^{2-}$ fragment of **4**, while **2** is isostructural to **4** with S = 0 Zn^{II} centers replacing the S= $^5/_2$ Mn^{II} centers in the chain. Lastly, the trinuclear cyano-bridged complex of **3** represents an excised fragment of **4**, where the chain is terminated on each end by the pentadentate capping ligand $PY5Me_2$.

The new compounds **2** and **3** were synthesized through direct combination of $[ReCl_4(CN)_2]^{2-}$ and either $[Zn(DMF)_6]^{2+}$ in DMF for **2** or $[(PY5Me_2)Mn]^{2+}$ inMeCN for **3** (see Figure 1). The crystal structures of **1-4** reveal an octahedral coordination geometry at the Re^{IV} center, with four chloride ligands in the equatorial positions and two axial cyanide ligands (see Figures 1, S1, and S2). In all structures, the C-Re-Cl and Cl-Re-Cl bond angles are close to 90° (see Table 1). The mean Re-C distances are slightly shorter in the multinuclear species (2.123(6) Å for **2**, 2.134(5) Å for **3**, and 2.125(1) Å for **4**) than the separation of 2.148(4) Å in the molecular salt**1**. Likewise, the mean Re-Cl distances are also longest in **1**, at 2.346(1) Å, compared to 2.313(4) Å in **2**, 2.330(1) Å in **3**, and 2.341(1) Å in **4**. The Re-C-N angles are all close to 180°, while the M-N-C angles (M = Zn, Mn) in **2-4** deviate significantly from linearity, being 158.7(1)° in **2**, 154.1(1)° in **3**, and 158.8(1)° in **4**. Such deviations are often observed for M^{II} centers coordinated at the nitrogen end of cyanide, and likely arise due to crystal packing forces.[3k,4]

Close comparison of the structures of **1-3** with that of **4** were necessary to evaluate the viability of **1-3** as models for the chain compound **4**. Inspection of the Re^{IV} coordination

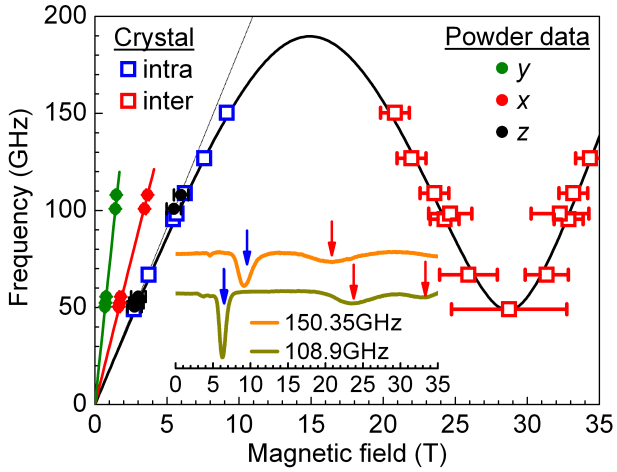

Figure 2. Main panel: EPR peak positions observed for a single crystal of **1** at 1.3 K with the field aligned 3° away from the molecular *z*-axis; intra- and inter-Kramers transitions are marked with blue and red data points, respectively. Powder EPR data are included in the low field region; three components are observed at each frequency, corresponding to the three components of the effective Landé *g* tensor associated with the lowest Kramers doublet (see legend). The solid lines represent the best simulation of the combined data sets (both single crystal and powder measurements), employing Eq. 1 and the single set of Hamiltonian and parameters given in the main text. The thin gray line would be the expectation for the intra-Kramers transition in the absence of rhombic anisotropy (E = 0); the data clearly depart from this expectation, providing a constraint on the E parameter. Inset: Representative single-crystal EPR spectra for **1** collected at 1.3K, demonstrating the observation of three ground state resonances. Intra- and inter-Kramers transitions are marked with blue and red arrows, respectively.

spheres in each structure reveals that the local coordination environment of the Re^{IV} ion is essentially constant for all compounds, providing evidence that **1**- **3** are indeed suitable models of **4**. Additionally, within each structure, no significant hydrogen bonding contacts between chains or molecules are evident in any of the structures, ruling out the presence of any significant pathways for long-range magnetic interactions not present in **4**.

3.3.2 EPR Spectroscopy of 1. Previous fits to variable-temperature dc magnetic susceptibility and magnetization data for **1** suggested significant easy-axis anisotropy with $D = -14.4$ cm^{-1}.[4] However, extracting the sign of D from magnetic data can often be unreliable. Consequently, in order to obtain a definitive determination of the magnetic anisotropy of the $[Re(CN)_2Cl_4]^{2-}$ building block (**1**), single-crystal, high-field EPR measurements were performed; experimental details can be found elsewhere.[14] The EPR data can be described by the following effective spin Hamiltonian:

$$\hat{H} = D\hat{S}_z^2 + E(\hat{S}_x^2 - \hat{S}_y^2) + \mu_B \boldsymbol{B} \cdot \tilde{g} \cdot \hat{\boldsymbol{S}}, \quad (1)$$

with $S = {}^3/_2$(5d^3, with $S = {}^3/_2$ and $L = 0$)and $0 < |E| < |D|/3$. Figure 2 plots the peak positions of EPR transitions observed via high-field studies at 1.3K (see also Figure S3). In this experiment, the crystal was oriented so that the field was aligned close to one of the principal axes of the magneto-anisotropy tensor, determined to be the magnetic hard (*z*-) axis (see below). The most notable feature of these low-temperature spectra is the fact that three resonances are observed in the frequency range from 60 to 130 GHz (see Figure 2, inset). The sharp peak at low field, marked by a blue arrow, corresponds to a

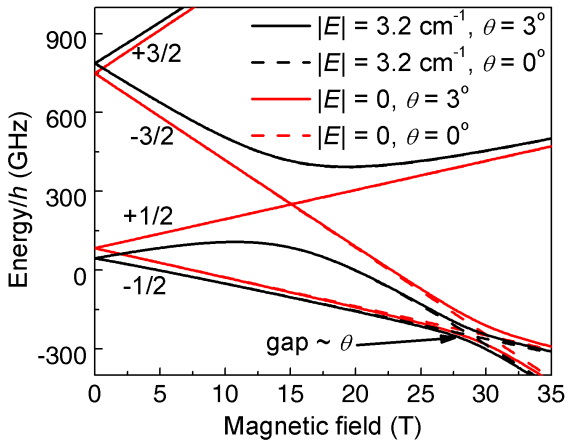

Figure 3. Zeeman diagram for compound**1** generated from Eq. 1with D = +11 cm^{-1} andg_z = 1.58, considering different E values and field misalignment angles θ (see legend), where θ= 0 corresponds to $B//z$. The approximate spin projection (m_s) of each state is labeled in the low-field region of the figure. The figure demonstrates that the avoided crossing at ~15T is determined entirely by E, while the one at ~28T is determined solely by θ. Consequently, different regions of the data in Figure 2 constrain these two parameters.

transition within the lowest Kramers doublet, while the broad peaks at high field, marked by red arrows, correspond to inter-Kramers transitions. The differences in line width can be explained on the basis of D- and E-strain, which primarily influence inter-Kramers transitions.[15] Variable-temperature studies at 126.9 GHz (see Figure S4) indicate that all three resonances correspond to excitations from the lowest-lying energy level within the S=$^3/_2$ manifold.

Two possible scenarios, both involving significant biaxiality where an E term approaches $|D|/3$, could account for the high-field single-crystal data in Figure 2. Indeed, acceptable simulations can be obtained with both positive and negative D parameters (see Figure S5). In order to discriminate between these two cases, low-field powder EPR measurements were performed (see Figure S6); data points corresponding to the three components of the effective g-tensor associated with the lowest Kramers doublet are included in the low field portion of Figure 2. First, note that the highest field (lowest effective g) data points for the powder overlay exactly on the single crystal data, thus confirming that the field was well aligned with the hard axis for the high-field measurements. The thick solid curves in Figure 2 correspond to the best simulations of the combined data sets using Eq. 1, assuming a positive D value and a spin of S = $^3/_2$. The resulting parameters are: D = +11 cm^{-1}, $|E|$ = 3.2 cm^{-1}, g_x = g_y = 1.89, and g_z = 1.58. A reasonable simulation can be obtained for the negative D case as well. However, it yields g values greater than 2.00 (g_y = 2.50 and g_{av} = 2.13), whereas the principal Landé values must be less than 2.00 for an orbitally non-degenerate atom with less than a half-filled d shell, as is the case for octahedrally coordinated Re^{IV}, i.e., L = 0. In other words, the negative D (easy-axis) simulation is physically unreasonable. We thus conclude that the D value is positive for **1**, and we shall see below that the situation is even more definitive in the case of compound **2**.

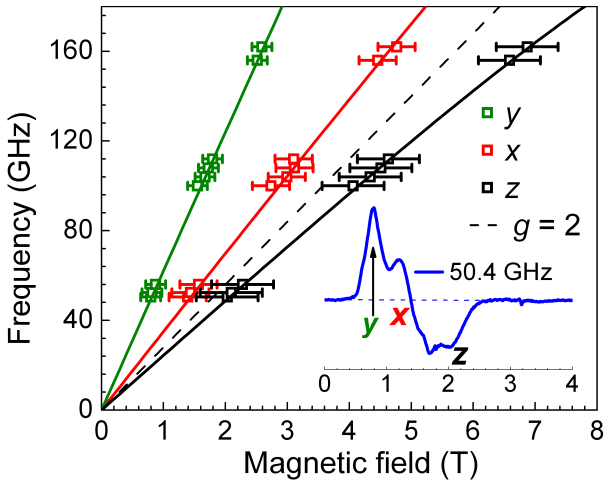

Figure 4. Frequency dependence of the EPR peak positions deduced from powder studies of compound **2** at 5K; the inset shows a representative powder spectrum. Three resonance branches are observed, corresponding to the three principal components of the effective Lande-*g* tensor associated with the lowest Kramers doublet (field parallel to *x*, *y* and *z*). The solid lines are best simulations employing Eq. 1 and the parameters discussed in the main text. The dashed line represents the $g = 2.00$ position. The observation of one resonance above $g = 2.00$,and two below, is indicative of easy-plane-type anisotropy (see main text for further explanation).

Returning to the discussion of the high-field single-crystal measurements, it is notable that the low-field intra-Kramers transitions in Figure 2 do not lie on a straight line that intersects the origin (thin gray line). This may be understood in terms of an avoided level crossing caused by the rhombic *E* term in Eq. 1, as illustrated in Figure 3. Moreover, this situation also explains the broadening of the intra-Kramers resonance with increasing frequency. In the absence of an *E* term, there would be no interaction between the $M_S = -^3/_2$ and $+^1/_2$ states and the spectrum would be linear in B_z (red curves in Figure 3), and the intra-Kramers data would lie on a straight line passing through the origin. Consequently, the departure of the low-field data from the gray line in Figure 2 provides one of the main constraints on *E*, the other being the splitting between the *x* and *y* components of the powder spectrum. Meanwhile, the inter-Kramers transitions above 15 T primarily constrain *D* and g_z. Finally, a small field misalignment was unavoidable due to the fact that a single-axis crystal rotation does not guarantee exact coincidence with the molecular *z*-axis. This misalignment is solely responsible for the second avoided crossing (and the magnitude of the resultant gap, see Figure 3) at ~28T, but it does not affect the low field data significantly. Therefore, the deduced misalignment angle of $q = 3°$ was constrained very precisely from the 28 T minimum seen in the fit to the single-crystal data in Figure 2. Thus, even though the high-field simulation contains four variables (*D*, *E*, g_z and θ), the obtained parameters are very well constrained. Moreover, they are further constrained by the powder measurements.

The *E* parameter obtained from the preceding analysis is quite substantial, corresponding to $|E/D| = 0.294$, which is very close to the maximum allowable value of 1/3. For the extreme biaxial case in which $E = |D|/3$, the $D>0$ and $D<0$ parameterizations are in fact equivalent. It is precisely for this reason that good simulations can be obtained for both cases. In other words, the two parameterizations are similar (see Figure S5), although it should be stressed that the powder measurements clearly favor the positive *D* scenario. Nevertheless, the underlying magnetic properties resulting from either biaxial parameterization would be expected to be quite similar.

3.3.3 Magnetometry and EPR Spectroscopy of 2 and 3. Due to the difficulty associated with interpreting EPR data from a dynamic chain system, where collective spin wave resonance is observed instead of discrete paramagnetic resonance,[16] zero-field splitting parameters for Re^{IV} were not directly obtained from the EPR data for the chain compound **4**. As a means of isolating the magnetic contribution of the Re^{IV} ions within the chain, the isostructural compound **2** was prepared. Here, the paramagnetic Mn^{II} ions have been replaced by diamagnetic Zn^{II} ions in order to prevent significant exchange interactions involving the Re^{IV} centers, while preserving any effects that stem from connecting $[ReCl_4(CN)_2]^{2-}$ units to other metal centers via the cyanide ligands. To confirm the magnetic isolation of the Re^{IV} centers, variable-temperature dc magnetic susceptibility data were collected for a microcrystalline sample of **2**. At 300 K, $\chi_M T$ = 1.30 cm^3K/mol, a value that is expected for an $S = {}^3/_2$ spin center with g = 1.66. In addition, this g value is in good agreement with that previously obtained from magnetization data for **1** (g = 1.65).[4] For temperatures below 70 K, $\chi_M T$ starts to drop, continuing all the way to the minimum measurement temperature 1.8 K. Close inspection of the dc magnetic susceptibility data for **2** and **1** (see Figure S7) reveals virtually identical behavior. Indeed, the $\chi_M T$ vs T plots of **1** and **2** are essentially super imposable, indicating an absence of inter- and/or intra-chain magnetic interactions in **2**. As such, the downturn in $\chi_M T$ can be attributed to the magnetic anisotropy of the Re^{IV} center. Importantly, ac magnetic susceptibility measurements as a function of both frequency and temperature on a polycrystalline sample of **2** revealed no slow relaxation behavior at or above 1.8 K.

To further investigate the magnetic anisotropy in **2**, EPR measurements were carried out on a powder sample (see Figure 4). Analogous to the data obtained for compound **1**, three spectral features are resolved, corresponding to the principal components of the effective g-tensor associated with the lowest Kramers doublet. In the case of easy-plane anisotropy ($D > 0$), the x- and y-components should occur at fields below the spin-only g = 2.00 position (dashed line), while the z-component should occur above; the opposite would hold for the easy-axis ($D < 0$) case. As seen in Figure 4, the powder measurements clearly indicate easy-plane-type anisotropy with $D > 0$, although they do not permit a direct determination of the magnitude of D. Meanwhile, the sizeable splitting between the x and y components of the spectrum again signifies appreciable biaxiality, corresponding to a significant E term. Attempts to detect inter-Kramers transitions were unsuccessful, as sufficiently-sized single crystals have thus far not been obtainable. Therefore, for the purposes of simulation, we were forced to adopt the value of D = +11 cm^{-1} obtained for **1**. The solid curves in Figure 4 represent the best simulation of the peak positions employing Eq. 1 with $|E|$ = 2.1 cm^{-1}, $g_x = g_y$ = 1.78, and g_z = 1.94. As noted already, it is impossible to obtain any reasonable simulation with $D < 0$. However, the E value obtained is rather well constrained by the splitting between the x and y components of the powder spectrum. Therefore, these simulations unambiguously demonstrate that **2** possesses easy-plane-type anisotropy and appreciable transverse anisotropy, in analogy with **1**.

To exclude the possibility that magnetic exchange coupling may act to invert the sign of D in the chain compound **4** relative to its constituent $[ReCl_4(CN)_2]^{2-}$ units, compound **3** was prepared and investigated. In particular, magnetic and EPR measurements were

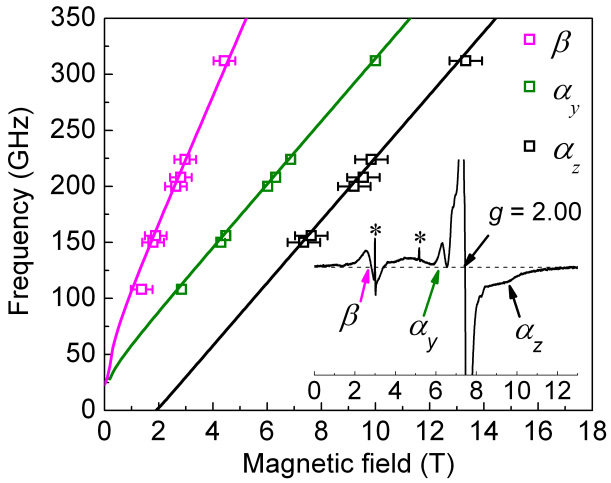

Figure 5. Frequency dependence of the EPR peak positions obtained from studies of a powder sample of **3** at 3.5 K. The solid lines are the best simulations employing Eq. 1 and the parameters discussed in the main text; the inset displays a representative spectrum collected in first-derivative mode at 208 GHz. The strong truncated feature at g = 2.00 is likely due to paramagnetic impurities and/or uncoupled Mn^{II} centers, while the sharp signals marked with asterisks are impurity signals from molecular oxygen absorbed in the sample holder. The broader anisotropic signals labeled α correspond to conventional ΔM_S = 1 transitions, while the β resonance corresponds to a double quantum transition (see main text for a detailed explanation).

carried out on polycrystalline samples of **3** to study the zero-field splitting parameters of the Re^{IV} center in the presence of magnetic exchange coupling (see Figure S8). First, the exchange coupling was probed through variable-temperature dc magnetic susceptibility measurements. At 300 K, $\chi_M T$ = 9.53 cm^3K/mol, slightly lower than the calculated value of $\chi_M T$ = 10.62 cm^3K/mol for an isolated Re^{IV} ($S = {}^3/_2$) center and two Mn^{II} ($S = {}^5/_2$) centers with g_{av} = 2.00. As the temperature is lowered, the value of $\chi_M T$ begins to drop, gradually at first, then abruptly below 70 K. This decrease with lowering temperature indicates the presence of antiferromagnetic interactions between the Re^{IV} and Mn^{II} centers within the molecule. A fit to the data for **3**, employing the program MAGFIT 3.1[17] and the Hamiltonian $\hat{H} = -2J(\hat{S}_{Re}\cdot\hat{S}_{Mn1}+\hat{S}_{Re}\cdot\hat{S}_{Mn2})$, afforded $J = -3.0(4)$ cm^{-1} and g = 1.98. These values are comparable to those of $J = -5.4(4)$ cm^{-1} and g = 1.88 obtained for compound **4**. The slight difference in the magnitude of J may be due to the differences in the ligand field of Mn^{II} and the small variation in the Mn-N-C angles. Considering the very similar metal coordination environments in **3** and **4**, compound **3** should provide a reasonable model of the Mn···Re···Mn motif in **4**. Finally, we note that slow relaxation was not observed in the variable frequency ac susceptibility measurements at temperatures above 1.8 K, even in the presence of an applied dc field.

EPR studies performed on **3** confirm that the Re^{IV} center possesses a positive D parameter, lending further weight to arguments that **4** also experiences easy-plane-type anisotropy. Figure 5 plots the frequency dependence of high-frequency EPR peak positions obtained from studies of a powder sample of **3** at 3.5 K, with the inset displaying a representative spectrum collected in first-derivative mode at 208 GHz. Three relatively strong features are observed, labeled as α_y, α_z and β. At high fields and frequencies, the slopes of the α_y and α_z branches agree with expectations for standard EPR transitions with DM_S = 1 and $g \approx 2$. Meanwhile, the slope associated with the β

branch suggests that it is a double quantum transition with DM_S = 2 and g≈4. We associate the α_y and α_z branches with the parallel (z) and perpendicular (y) extremes of the high-field spectrum. Note that the low-field spectrum would be rather more complex, thereby illustrating the importance of high-field measurements.

Unlike the powder results for compounds **1** and **2**, the α_y and α_z resonance branches correspond to excitations within a coupled molecular spin state experiencing zero-field-splitting. It is for this reason that the high-field portions of the spectrum extrapolate to finite zero-field offsets, unlike the transitions within the lowest Kramers doublet in the case of **1** and **2**. Most importantly, the zero-field offsets deduced from Figure 5 provide direct information on the anisotropy associated with the $ReMn_2$ molecular units of **3**. The results may be interpreted by treating the molecule according to its approximate $S_{total} = S_{Mn1} + S_{Mn2} - S_{Re} = {}^5/_2 + {}^5/_2 - {}^3/_2 = {}^7/_2$ ground state that arises from antiferromagnetic coupling between Re^{IV} and Mn^{II} centers. The solid curves are the simulations obtained employing Eq. 1and the molecular zero-field-splitting parameters D = +0.3 cm^{-1}, $|E|$ = 0.03 cm^{-1} and g = 2.00, with $S = {}^7/_2$. As noted above, the α_z branch corresponds to the ground state transition ($M_S \approx -{}^7/_2$ to $-{}^5/_2$) with the field being parallel to the molecular z-axis, while α_y corresponds to the same transition but with the field parallel to y. The x-component is buried within the very large signal close to g = 2.00. The simulations also successfully account for the double quantum transition (β, or $M_S \approx -{}^7/_2$ to $-{}^3/_2$), assuming

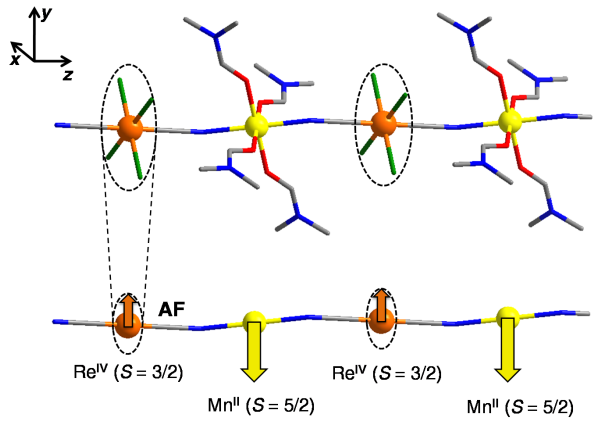

Figure 6. Structure (upper) and spin arrangement (lower) of chain compound **4**. The atoms are colored as follows: Re^{IV} = orange, Mn^{II} = yellow, Cl = green, N = blue, and C = gray. The black dashed circles denote the local xy-plane of each Re^{IV} center, which is determined by the four coplanar chlorine atoms; the z-axis is parallel to the chain direction. In the classical ground state, the Mn^{II} spins (yellow arrows) are locked into an anti parallel arrangement relative to those of the Re^{IV} spins (orange arrows); the easy-plane anisotropy associated with the Re^{IV} centers then constrains the spins within the xy-plane on both sub-lattices

that it belongs to the y-component of the spectrum. It is noteworthy that double quantum transitions usually appear when the field is applied perpendicular to the dominant quantization axis (z-axis), which is consistent with our observations and provides further confirmation for the peak assignments.

Although fine structure peaks are not resolved, observation of the y and z extrema provide a very robust constraint on the sign of the D parameter. Indeed, the fact that the shift of the z-component to the high-field side of the isotropic g = 2.00 position is

substantially greater than that of the *y*-component to the low field side can be taken as unambiguous evidence that the molecular anisotropy is of the easy-plane type, i.e., $D > 0$. One could question the validity of the preceding analysis for a molecule in which the exchange coupling is weak in comparison to the anisotropy ($J < D$). However, extensive studies on other simple trinuclear and tetranuclear molecules have shown that EPR spectra essentially retain the characteristics of a giant spin, particularly at the low- and high-field extremes that dominate at low temperatures, i.e., the same regions of the powder spectrum that we focus on here.[18]

We can make a rough estimate of the anisotropy parameters associated with the Re^{IV} center using the projection method.[19] The zero-field splitting associated with octahedrally coordinated high-spin Mn^{II} may be assumed to be negligible,[20] such that the anisotropy of **3** will be dominated by Re^{IV}. The projection method then gives $\vec{D}_{mol} = 0.0143 \times \vec{D}_{Re}$, where $\vec{D}_{mol}$ and $\vec{D}_{Re}$ are the anisotropy tenors of the $ReMn_2$ molecule and the Re^{IV} center, respectively. We thus estimate that $D_{Re} \approx +21$ cm^{-1} and $E_{Re} \approx 2.1$ cm^{-1}. However, due to the significant uncertainty associated with the resonance positions in Figure 5 and the many simplifying assumptions made in the analysis, these values should be considered as only approximate. Nevertheless, the data once again confirm a positive *D* parameter with considerable rhombicity.

3.3.4 Discussion of the Magnetic Relaxation Process. High-spin Mn^{II} complexes typically possess nearly negligible magnetic anisotropy.[20] As such, the magnetic relaxation barrier in **4**must arise primarily from the anisotropy of the Re^{IV} centers. However, the EPR studies reported here clearly indicate the presence of a positive *D* for Re^{IV}. Moreover, the theoretical anisotropy relaxation barriers of $|D|S^2 = 25$ and 32 cm^{-1} for **4** obtained using the magnitude of *D* (assuming *D* is negative) deduced both by EPR and magnetic measurements, respectively, are in stark disagreement with the experimental barrier of 12 cm^{-1}. These curious factors suggest that new physics may be at play in governing the magnetic relaxation of **4**.

If one considers the doubly degenerate $M_S = \pm{}^1/_2$ ground levels of an isolated $S = {}^3/_2$ molecule with positive *D*, then extreme quantum tunneling effects prevent localization of the molecular magnetic moment within the *xy*-plane, i.e. $\langle \hat{S}_x \rangle = \langle \hat{S}_y \rangle = 0$. However, the coupling of such spins, one-by-one, to form a ferrimagnetic chain, results in a gradual suppression of these tunneling effects. In such a description, the chain possesses a giant spin, *S*, which scales with the chain correlation length, l_ξ. In the case of **4**, the coordination environments of the Re^{IV} centers are collinear throughout the chains, with the *z* direction parallel to the direction of chain propagation. As such, the preferred orientation of the giant spin, *S*, lies in the plane perpendicular to the chain (see Figure 6). A transverse anisotropy then creates a preferred axis within this plane, although quantum tunneling may still prevent localization of *S* for small chain lengths. However, as the chain correlation length grows, these fluctuations diminish as the quantum tunneling is increasingly suppressed. In fact, the relaxation time due to tunneling, t_0, should increase exponentially with increasing chain length. One method of visualizing such an effect is to consider the probability that all spins within the chain tunnel simultaneously, as would be required if the total spin were to tunnel coherently. Clearly, this probability decreases exponentially with increasing number of spins in the chain. Consequently, in the limit of large correlation length, *S* can be treated classically.

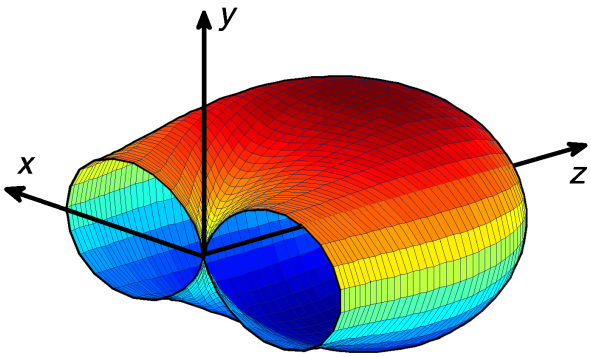

Figure 7. Classical magneto-anisotropy energy surface corresponding to the zero-field operator equivalent terms given in Eqn. (1), with $D > 0$ and $|E|/|D|$ equal to the ratio found from the present EPR experiments on complex **2**. The radial distance to the surface represents the energy of a spin as a function of its orientation; zero energy has been chosen to correspond to the case when the spin is parallel to y, and only the $z > 0$ surface is shown in order to aid viewing of the cross-section in the xy-plane. As can be seen, the spin experiences an anisotropic kinetic barrier against reversal from $+y$ to $-y$, with the barrier minimum occurring along $\pm x$.

Figure 7 depicts the classical potential energy surface in spin space corresponding to the zero-field operator equivalent terms given in Eq. 1, with $D > 0$ and $|E/D|$ equal to the ratio found from the present EPR experiments. The radial distance to the surface represents the energy of a spin as a function of its orientation. The minimum energy occurs when the spin points along $\pm y$, with an energy barrier separating these two orientations. The barrier maximum occurs in the yz-plane, and is determined by D. Meanwhile, it is E that sets the energy scale of the barrier minimum for rotation in the xy-plane. In the large l_z limit, the anisotropy barrier against coherent rotation of an entire chain will be quite considerable, because the anisotropies of the individual Re^{IV} centers sum together. Nevertheless, we propose that magnetization dynamics can still proceed via the usual Glauber mechanism,[5] except that the relevant anisotropy energy scale is determined by E rather than D. As such, the anisotropy energy associated with the reversal of a single Re^{IV} spin within the chain is given by $D_A = 2|E|S^2$. Considering the value of $|E| = 2.1\text{cm}^{-1}$ deduced from the EPR measurements on **2**, the anisotropy energy of **4** can be estimated at $D_A = 9.5\ \text{cm}^{-1}$. Using the previously obtained value of the correlation energy of $D\xi = 19\ \text{cm}^{-1}$ along with the expression for the overall relaxation barrier for a chain in the finite-size limit $D\tau = D_A + D\xi$, a value of $D\tau = 29\ \text{cm}^{-1}$ is obtained for **4**. Remarkably, this value is in excellent agreement with the experimentally determined value of $D\tau = 31\ \text{cm}^{-1}$, which has heretofore been unexplainable in terms of magnetic anisotropy and correlation. Moreover, in our previous work on the isostructural chain compounds $(DMF)_4MReCl_4(CN)_2$ (M = Mn, Fe, Co, Ni), the experimental correlation energy of $(DMF)_4NiReCl_4(CN)_2$was found to be $D\xi = 8.8\ \text{cm}^{-1}$. Taking the small contribution of the zero-field splitting of octahedral Ni^{II} ions and the anisotropy barrier ($\Delta_A = 9.5\ \text{cm}^{-1}$) estimated from EPR data into account, the overall relaxation barrier $D\tau = D_A + D\xi = 18.3\ \text{cm}^{-1}$ agrees very well with the experimental value of $D\tau = 20\ \text{cm}^{-1}$, giving further evidence for the relaxation process via transverse anisotropy. Finally, note that the anisotropy energy of the CoRe and FeRe chain compounds are different, as the important contribution of zero-field splitting from high-spin Co^{II} and Fe^{II} enables a more complicated relaxation mechanism.

A small number of previous studies have uncovered the presence of slow magnetic relaxation in single-molecule and single-chain magnets with $D > 0$. For instance, a mixed-valence alternating high-spin Fe^{II}, low-spin Fe^{III} chain compound was shown to exhibit slow magnetization reversal with easy-plane anisotropy.[21] Here, the authors attributed the relaxation behavior to a mutually orthogonal arrangement of the Fe^{II} molecular axes, which serves to induce Ising interactions along the chain. In another instance, a trinuclear Cu_3 single-molecule magnet was reported to display easy-plane anisotropy, with $U_{eff} = 5$ cm^{-1}.[22] In this work, the authors pointed out that the relaxation follows an Orbach process involving the exchange coupled excited states of the cluster. Similarly, we recently reported the observation of slow magnetic relaxation in a pseudotetrahedral Co^{II} complex with easy plane anisotropy.[23] For the reported molecule, a field-induced bottleneck of the direct relaxation between the $M_S = \pm^1/_2$ levels generated Orbach relaxation pathways through the excited $M_S = 3/2$ levels. Finally, a Fe_3Cr cluster that features constituent Cr^{III} and Fe^{III} centers with hard-axis anisotropy was shown to display single-molecule magnet behavior.[24] This phenomenon was attributed to an overall molecular easy-axis anisotropy that stems from the presence of peripheral hard-axis type Fe^{III} centers, whose anisotropy tensors align orthogonal to the threefold molecular axis. Note that in all of these cases, the barrier to spin relaxation is still a consequence of D, albeit positive in sign. As such, to our knowledge, **4** represents the first example of a compound in which slow magnetic relaxation arises due to E.

3.4 Conclusions and Outlook

The foregoing results demonstrate that slow magnetic relaxation in coordination compounds can arise from transverse anisotropy. In particular, high-field, high-frequency EPR measurements on a series of model compounds show that the magnetic relaxation in the single-chain magnet $(DMF)_4MnReCl_4(CN)_2$ is governed by a nonzero E term, despite the presence of a positive D. Furthermore, the anisotropy energy of the compound can be expressed as $\Delta_A = 2|E|S^2$ to give a value of $\Delta_A = 9.8$ cm^{-1}. The overall relaxation barrier can then be expressed as $D\tau = D_A + D\xi$, to give a value of $D\tau = 29$ cm^{-1}. Remarkably, this value is in excellent agreement with the experimentally determined value of $D\tau = 31$ cm^{-1}. The observation of slow relaxation arising from E is, to our knowledge, an unprecedented phenomenon in molecular magnetism, and it represents a potentially new design strategy toward constructing low-dimensional magnetic materials. Future work will focus on further understanding the effects of large transverse anisotropy on related compounds, in particular molecular systems where quantum tunneling of the magnetization is still a significant contributor to overall magnetic relaxation. In addition, work is underway to design new molecular building units that feature large positive D and significant E, in order to direct the formation of new single-chain magnets with high relaxation barriers.

3.6 Acknowledgement

This research was funded by DoE/LBNL grant 403801(synthesis) and NSF grants CHE-1111900 (magnetism) andDMR-0804408 (EPR). A portion of the work was performed at the National High Magnetic Field Laboratory which is supported by the NSF (DMR-0654118) and the State of Florida. I thank Prof. R. Clérac for helpful discussions. I also thank Dr. T. D. Harris and Dr. J. M. Zadrozny for experimental assistance.

3.7 References

1. (a) Sessoli, R.; Tsai, H. L.; Schake, A. R.; Wang, S.; Vincent, J. B.; Folting, K.; Gatteschi, D.; Christou, G.; Hendrickson, D. N. *J. Am. Chem. Soc.* **1993**, *115*, 1804. (b) Sessoli, R.; Gatteschi, D.; Caneschi, A.; Novak, M. A. *Nature* **1993**, *365*, 141. (c) Gatteschi D.; Sessoli R.; Villain J. *Molecular Nanomagnets*, Oxford University Press: New York, **2006** and references therein. (d) Milios, C. J.; Vinslava, A.; Wernsdorfer, W.; Moggach, S.; Parsons, S.; Perlepes, S. P.; Christou, G.; Brechin, E. K. *J. Am. Chem. Soc.* **2007**, *129*, 2754. (e) Freedman, D. E.; Jenkins, D. M.; Iavarone, A. T.; Long, J. R. *J. Am. Chem. Soc.* **2008**, *130*, 2884. (f) Yoshihara, D.; Karasawa, S.; Koga, N. *J. Am. Chem. Soc.* **2008**, *130*, 10460. (g) Freedman, D. E.; Harman, W. H.; Harris, T. D.; Long, G. J.; Chang, C. J.; Long, J. R., *J. Am. Chem. Soc.* **2010**, *132*, 1224; (h) Zhang, Y. Z.; Wang, B. W.; Sato, O.; Gao, S. *Chem. Commun.* **2010**, *46*, 6959; (i) Harman, W. H.; Harris, T. D.; Freedman, D. E.; Fong, H.; Chang, A.; Rinehart, J. D.; Ozarowski, A.; Sougrati, M. T.; Grandjean, F.; Long, G. J.; Long, J. R., *J. Am. Chem. Soc.* **2010**, *132*, 18115; (j) Zadrozny, J. M.; Freedman, D. E.; Jenkins, D. M.; Harris, T. D.; Iavarone, A. T.; Mathoniere, C.; Clérac, R.; Long, J. R. *Inorg. Chem.* **2010**, *49*, 8886; (k) Pedersen, K. S.; Dreiser, J.; Nehrkorn, J.; Gysler, M.; Schau-Magnussen, M.; Schnegg, A.; Holldack, K.; Robert, B.; Stergios, P.; Weihe, H.; Tregenna-Piggott, P.; Waldmann, Oliver.; Bendix, J. *Chem. Commun.* **2011**, *47*, 6918; (l) Das, A.; Gieb, K.; Krupskaya, Y.; Demeshko, S.; Sebastian, D.; Klingeler, R.; Kataev, V.; Buchner, B.; Muller, P.; Meyer, F. *J. Am. Chem. Soc.* **2011**, *133*, 3433; (m) Rinehart, J. D.; Fang, M.; Evans, W. J.; Long, J. R. *Nat. Chem.* **2011**, *3*, 538; (n) Rinehart, J. D.; Fang, M.; Evans, W. J.; Long, J. R.; *J. Am. Chem. Soc.* **2011**, *133*, 14236; (o) Zadrozny, J. M.; Long, J. R. *J. Am. Chem. Soc.* **2011**, *133*, 20732.
2. (a) Garanin, D. A.; Chudnovsky, E. M.; *Phys. Rev. B* **1997**, *56*, 11102; (b) Leuenberger, M. N.; Loss, D., *Nature* **2001**, *410*, 789; (c) Jo, M.-H.; Grose, J. E.; Liang, W.; Baheti, K.; Deshmukh, M. M.; Sokol, J. J.; Rumberger, E. M.; Hendrickson, D. N.; Long, J. R.; Park H.; Ralph, D. C., *Nano Lett.* **2006**, *6*, 2014. (d) Ardavan, A.; Rival, O.; Morton, J. J. L.; Blundell, S. J.; Tyryshkin, A. M.; Timco, G. A.; Winpenny, R. E. P. *Phys. Rev. Lett.* **2007**, *98*, 57201. (e) Bogani, L.; Wernsdorfer, W., *Nat. Mater.* **2008**, *7*, 179. (f) Stamp, P. C. E.; Gaita-Arino, A., *J. Mater. Chem.* **2009**, *19*, 1718. (g) Loth, S.; von Bergmann, K.; Ternes, M.; Otte, A. F.; Lutz, C. P.; Heinrich, A. J., *Nat. Phys.* **2010**, *6*, 340.
3. (a) Caneschi, A.; Gatteschi, D.; Lalioti, N.; Sangregorio, C.; Sessoli, R.; Venturi, G.; Vindigni, A.; Rettori, A.; Pini, M. G.; Novak, M. A., *Angew. Chem., Int. Ed.* **2001**, *40*, 1760. (b) Clérac, R.; Miyasaka, H.; Yamashita, M.; Coulon, C., *J. Am. Chem. Soc.* **2002**, *124*, 12837. (c) Lescouëzec, R.; Vaissermann, J.; Ruiz-Pérez, C.; Lloret, F.; Carrasco, R.; Julve, M.; Verdaguer, M.; Dromzée, Y.; Gatteschi, D.; Wernsdorfer, W. *Angew. Chem., Int. Ed.* **2003**, *42*, 1483. (d) Liu, T. F.; Fu, D.; Gao, S.; Zhang, Y. Z.; Sun, H. L.; Su, G.; Liu, Y. J., *J. Am. Chem. Soc.* **2003**, *125*, 13976. (e) Wang, S.; Zuo, J.-L.; Gao, S.; Song, Y.; Zhou, H.-C.; Zhang, Y.-Z.; You, X.-Z., *J. Am. Chem. Soc.* **2004**, *126*, 8900. (f) Ferbinteanu, M.; Miyasaka, H. Wernsdorfer, W.; Nakata, K.; Sugiura, K.; Yamashita, M.; Coulon, C.; Clérac, R., *J. Am. Chem. Soc.* **2005**, *127*, 3090. (g) Coulon, C.; Miyasaka, H.; Clérac, R. *Struct. Bonding (Berlin)* **2006**, *122*,

163. (h) Bernot, K.; Bogani, L.; Caneschi, A.; Gatteschi, D.; Sessoli, R., *J. Am. Chem. Soc.* **2006**, *128*, 7947. (i) Miyasaka, H.; Madanbashi, T.; Sugimoto, K.; Nakazawa, Y.; Wernsdorfer, W.; Sugiura, K.; Yamashita, M.; Coulon, C.; Clérac, R., *Chem.−Eur. J.* **2006**, *12*, 7028. (j) Miyasaka, H.; Julve, M.； Yamashita, M.； Clérac, R. *Inorg. Chem.* **2009**, *48*, 3420 and references therein. (k) Feng, X.; Harris, T. D.; Long, J. R. *Chem. Sci.* **2011**, *2*, 1688-1694. (l) Yoon, J. H.; Lee, J. W.; Won, R. D.; Choi, S. Y.; Yoon, S. W.; Suh, B. J.; Koh, E. K.; Kim, H. C.; Hong, C. S. *Inorg. Chem.* **2011**, *50*, 11306; (m) Escuer, A.; Vlahopoulout, G.; Mautner, F. A. *Inorg. Chem.* **2011**, *50*, 2717; (n) Ding, M.; Wang, B.; Wang, Z.; Zhang, J.; Fuhr, O.; Fenske, D.; Gao, S. *Chem.- Eur. J.* **2012**, *18*, 915.

4. Harris, T. D.; Bennett, M. V.; Clérac, R.; Long, J. R., *J. Am. Chem. Soc.* **2010**, *132*, 3980.
5. Glauber, R. J., *J. Math. Phys.* **1963**, *4*, 294.
6. (a) Suzuki, M.; Kubo, R., *J. Phys. Soc. Jpn.*, 1968, *24*, 51. (b) Coulon, C.; Clérac, R.; Lecren, L.; Wernsdorfer, W.; Miyasaka, H., *Phys. Rev. B* **2004**, *69,* 132408.
7. (a) Caneschi, A.; Gatteschi, D.; Sessoli, R.; Barra, A. L.; Brunel, L. C.; Guillot, *J. Am. Soc.*, **1991**, 113, 5873-5874; (b) Barra, A. L.; Gatteschi, D.; Sessoli, R., *Phys. Rev. B* **1997**, 56, 8192; (c) Hill, S.; Edwards, R. S.; Aliaga-Alcalde, N.; Christou, G., *Science* **2003**, 302, 1015-1018; (d) Inglis, R.; Jones, L. F.; Milios, C. J.; Datta, S.; Collins, A.; Parsons, S.; Wernsdorfer, W.; Hill, S.; Perlepes, S. P.; Piligkos, S.; Brechin, E. K., *Dalton Trans.* **2009**, 3403-3412.
8. Yang, E.-C.; Kirman, C.; Lawrence, J.; Zakharov, L. N.; Rheingold, A. L.; Hill, S.; Hendrickson, D. N. *Inorg. Chem.* **2005**, *44*, 3827.
9. *SMARTSoftware Users Guide*, *Version 5.1*; Bruker Analytical X-Ray Systems: Madison, WI, **1999**.
10. APEX2 v.2009; Bruker Analytical, Version 7.0; Bruker Analytical X-Ray System: Madison, WI, **1999**.
11. *SAINT Software Users Guide*, Version 7.0; Bruker Analytical X-Ray Systems: Madison, WI, **1999**.
12. Sheldrick, G. M. SADABS, Version 2.03; Bruker Analytical X-Ray Systems, Madison, WI, **2000**.
13. Sheldrick, G. M. SHELXTL, Version 6.12; Bruker Analytical X-Ray Systems, Madison, WI, **2000**.
14. Takahashi, S.; Hill, S., *Rev. Sci. Instrum.* **2005**, *76* (2), 023114-10.
15. (a) Park, K.; Novotny, M. A.; Dalal, N. S.; Hill, S.; Rikvold, P. A., *Phys. Rev. B* **2001**, *65* (1), 014426;(b) Hill, S.; Maccagnano, S.; Park, K.; Achey, R. M.; North, J. M.; Dalal, N. S., *Phys. Rev. B***2002**, *65* (22), 224410.
16. Oshima, Y.; Nojiri, H.; Asakura, K.; Sakai, T.; Yamashita, M.; Miyasaka, H., *Phys. Rev. B* **2006**, *73* (21), 214435.
17. Schmitt, E. A. PhD Thesis, University of Illinois at Urbana-Champaign, **1995**.
18. (a) Hill, S.; Datta, S.; Liu, J.; Inglis, R.; Milios, C. J.; Feng, P. L.; Henderson, J. J.; del Barco, E.; Brechin, E. K.; Hendrickson, D. N., *Dalton Trans.* **2010**, *39*, 4693; (b) Quddusi, H. M.; Liu, J.; Singh, S.; Heroux, K. J.; del Barco, E.; Hill, S.; Hendrickson, D. N., *Phys. Rev. Lett.* **2011**, *106*, 227201; (c) Heroux, K. J.; Quddusi, H. M.; Liu, J.; O'Brien, J. R.; Nakano, M.; del Barco, E.; Hill, S.; Hendrickson, D. H., *Inorg. Chem.* **2011**, *50*, 7367.

19. *Electron Paramagnetic Resonance of Exchange Coupled Clusters*, A. Bencini, D. Gatteschi, Springer, Berlin, **1990**.
20. Krzystek, J.; Ozarowski, A.; Telser, J., *Coord. Chem. Rev.* **2006**, *250* (17-18), 2308.
21. Kajiwara, T.; Nakano, M.; Kaneko, Y.; Takaishi, S.; Ito, T.;Yamashita, M.; Igashira-Kamiyama, A.; Nojiri, H.; Ono, Y.; Kojima, N. *J. Am. Chem. Soc* .**2005**, 127, 10150.
22. Sanakis,Y.; Pissas, M.; Krzystek, J.; Telser, J.;Raptis, R. G. *Chem. Phys. Lett.* **2010**, 493, 185
23. Zadrozny, J. M.; Liu, J.; Piro, N. A.; Chang, C. J.; Hill, S.; Long, J. R. *Chem. Commun.* **2012**, 48, 3927.
24. Tancini, E.; Rodriguez-Douton, M. J.; Sorace, L.; Barra, A.-L.; Sessoli, R.; Cornia, A., *Chem.- Eur. J.* **2010**, *16*, 10482.

3.9 Supporting Information

Table S1. Crystallographic data[a] for $(DMF)_4ZnReCl_4(CN)_2$ and $[(PY5Me_2)Mn]_2[ReCl_4(CN)_2](PF_6)_2$

	2	**3**
formula	$C_{14}H_{28}Cl_4ZnN_6O_4Re$	$C_{56}H_{50}N_{12}P_2F_{12}Cl_4MnRe$
fw	737.81	1064.91
T, K	100	100
space group	$P\,1$	$P2(1)/c$
Z	1	2
a, Å	8.6226(8)	13.7430(2)
b, Å	10.3074(10)	21.9421(2)
c, Å	10.4929(10)	12.8569(1)
α, deg	104.878(4)	90.000
β, deg	92.699(4)	107.514(3)
γ, deg	101.666(4)	90.000
V, Å^3	877.85(14)	3697.28 (10)
d_{calc}, g/cm^3	1.592	1.451
R_1 (wR_2), %[b]	2.15 (5.70)	5.45 (14.20)

[a]Obtained with graphite-monochromated Cu Kα (λ = 1.5406 Å) for **2** and **3**. [b] $R_1 = \Sigma||F_o| - |F_c||/\Sigma|F_o|$, $wR_2 = \{\Sigma\,[w(F_o^2 - F_c^2)^2]\}^{1/2}$.

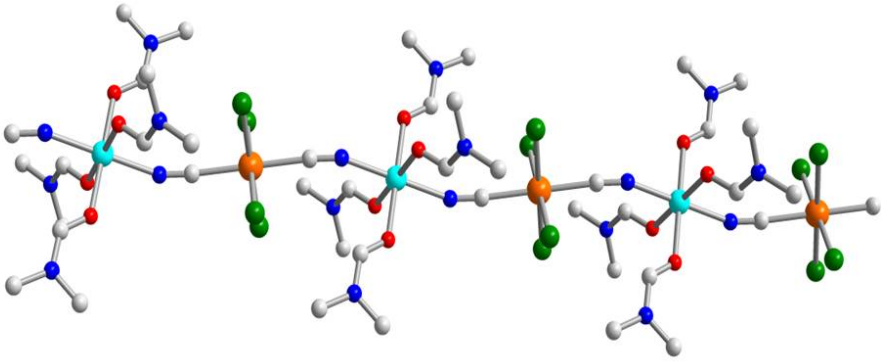

Figure S1. Crystal structure of $(DMF)_4ZnReCl_4(CN)_2$ **2** chain. Orange, cyan, green, red, blue, and gray spheres represent rhenium, zinc, chlorine, oxygen, nitrogen, and carbon atoms, respectively; hydrogen atoms have been omitted for clarity.

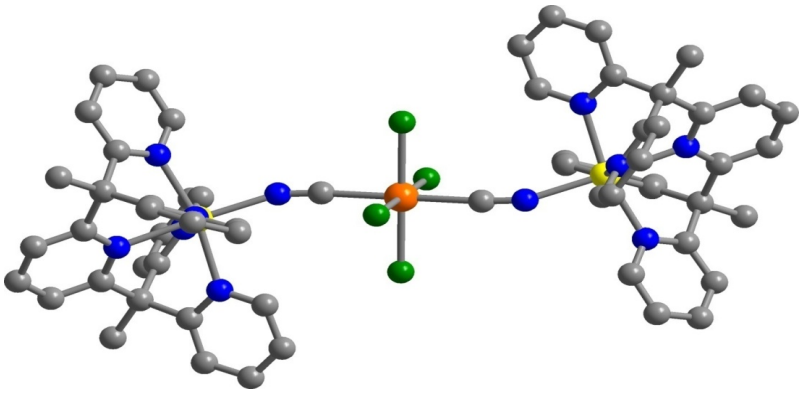

Figure S2. Crystal structure of $\{[(PY5Me_2)Mn]_2[ReCl_4(CN)_2]\}^{2+}$ (**3**). Orange, yellow, green, blue, and gray spheres represent rhenium, manganese, chlorine, nitrogen, and carbon atoms, respectively; hydrogen atoms have been omitted for clarity.

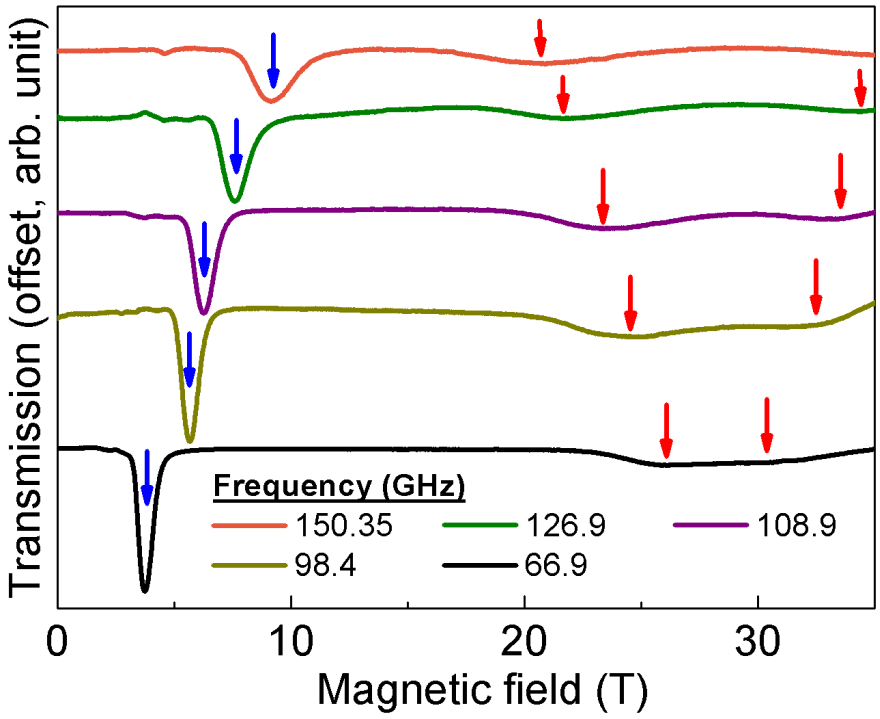

Figure S3. Single-crystal high-field EPR spectra collected at various frequencies in the range from 66.9 to 150 GHz and at T = 1.4 K, with the field applied 3° away from the molecular z-axis. The spectra are normalized according to the weight (area) associated with the low-field intra-Kramers resonance (indicated by the blue arrows). The observation of three resonances between 66 GHz and 127 GHz (one intra-Kramers and two broad inter-Kramers transitions denoted by red arrows) provides unambiguous evidence for the easy-plane anisotropy; a more detailed discussion is given in the main text and in the caption to Figure S4.

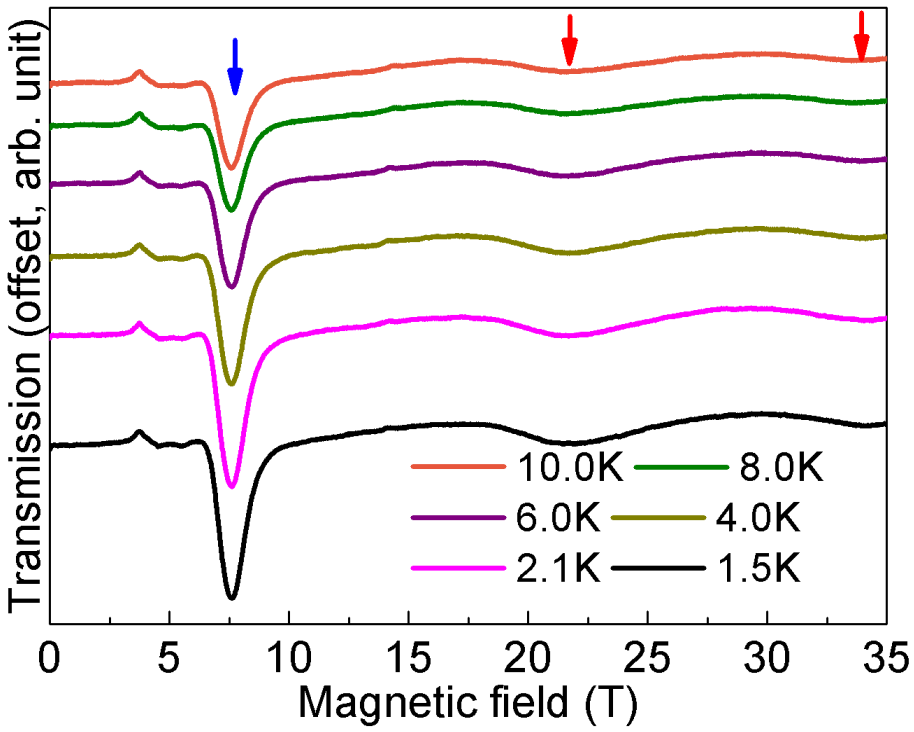

Figure S4. Temperature dependence spectra collected at f = 126.9 GHz. All three resonances strengthen and persist to the lowest temperature, where $k_BT << hf$. This indicates that of all the transitions correspond to excitations from the ground state of the molecule, with the blue and red arrows denoting intra- and inter-Kramers transitions, respectively.

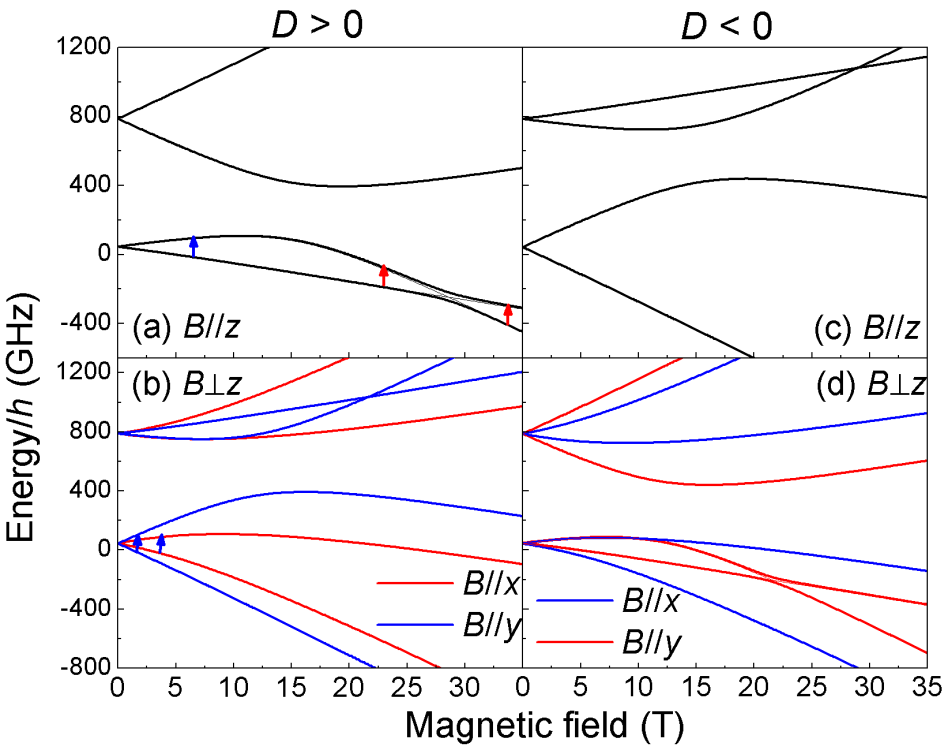

Figure S5. Simulations of the Zeeman diagrams based on the Hamiltonian of Eqn. (1), with B//z [(a) and (c)] and B⊥z [(b) and (d)], for the two cases D > 0 [(a) and (b)] and D < 0 [(c) and (d)]. The employed magnitudes of the employed parameters are those determined for complex **1** given in the main text. Panel (a) corresponds exactly to the black curves in Fig. 3; the thick black curve includes a 3° misalignment of the applied field, corresponding to the actual experimental situation. The red and blue arrows in (a) correspond to allowed EPR transitions of ~100 GHz, illustrating the intra-Kramers transition (red) and the two inter-Kramers (blue) transitions observed in the single-crystal EPR studies. Panel (b) displays the Zeeman diagrams with B//x and B//y; the blue arrows denote the ~100 GHz intra-Kramers x & y components of the powder spectra seen in Figs. 2 and S4. As can be seen, panels (a) and (b) reproduce all aspects of the single-crystal and powder EPR experiments remarkably well. Panels (c) and (d) depict the corresponding Zeeman diagrams generated with D < 0. As seen in (d), it is possible to produce a spectrum consisting of three ground state resonances for the D < 0, B//x case. However, in order to obtain quantitative agreement with the single-crystal and powder EPR data, unphysical E (> | D | /3) and/or g (> 2) parameters are obtained. This rules out the D < 0 parameterization – see main article for a more detailed discussion.

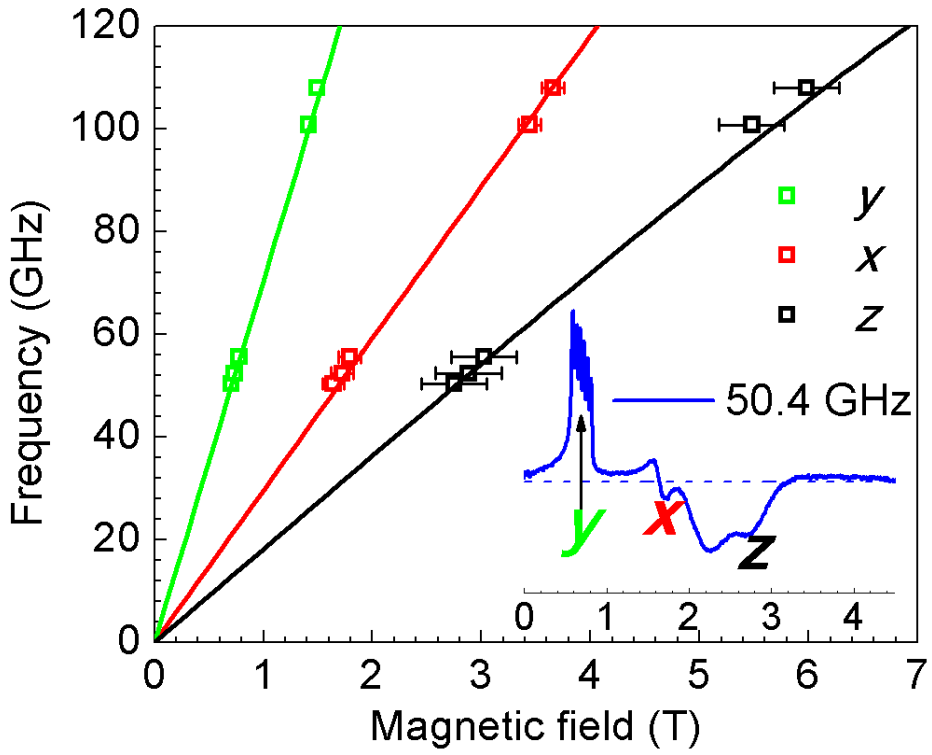

Figure S6. Frequency dependence of the high-frequency EPR peak positions deduced from studies of a powder sample of **1** at 5 K; a representative spectrum collected in the first-derivative mode at 50.4 GHz is displayed in the inset. Three branches of the resonances are observed, corresponding to the three principal components of the effective Lande g tensor associated with lowest Kramers doublet (field parallel to x, y and z). The fine structure seen in the y-component is due to nuclear hyperfine splitting; the resonance position is chosen at the center of the fine structure spectrum. The solid lines in the main panel are simulations of the three resonance branches employing Eqn. (1) and the unique set of parameters given in the main article. The fine structure seen in the **y**-component is due to nuclear hyperfine splitting; the resonance position is chosen at the center of the fine structure spectrum. We note that the hyperfine splitting is not observed in the x or z components, or in the y component at higher frequencies, suggesting that it is washed out at higher fields due to g-strain.

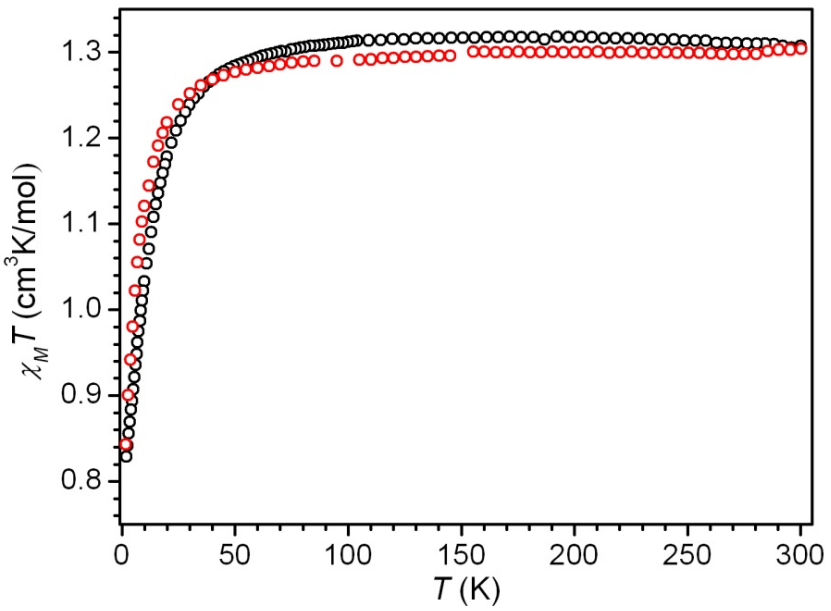

Figure S7. Variable-temperature dc magnetic susceptibility data for $(Bu_4N)_2[ReCl_4(CN)_2]\cdot 2DMA$ (**1**, black) and $(DMF)_4ZnReCl_4(CN)_2$ (**2**, red), collected in an applied field of 1000 Oe. The nearly superimposable data sets indicate that the Re^{IV} ions well-isolated magnetically in both **1** and **2**.

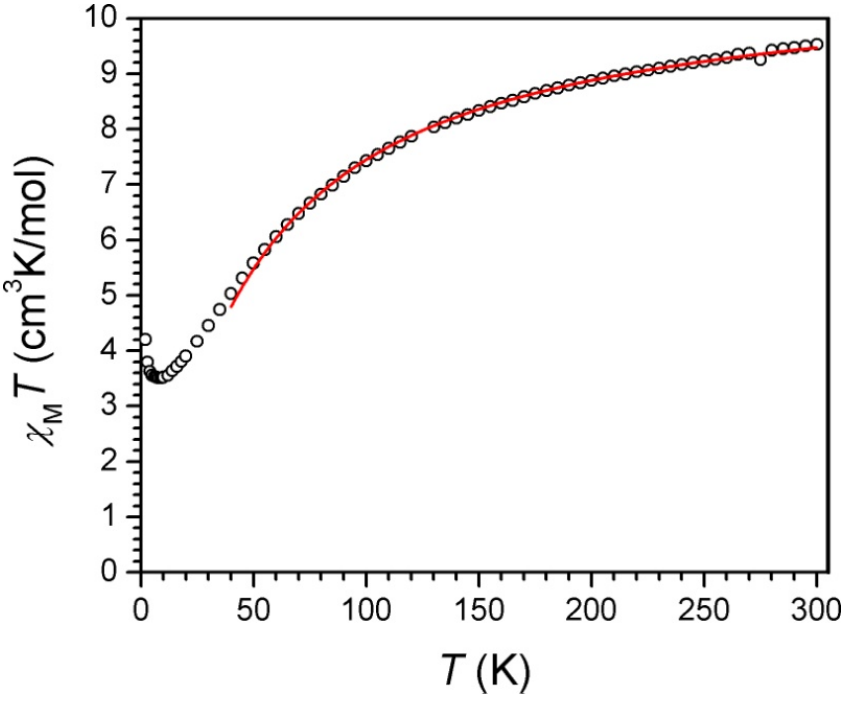

Figure S8. Variable-temperature dc magnetic susceptibility data for $[(PY5Me_2)_2Mn]_2ReCl_4(CN)_2](PF_6)_2$ (**3**), collected in an applied field of 1000 Oe. The solid red line corresponds to a fit to the data, with J = −3.0 cm^{-1} and g = 1.98

Chapter 4: Tristability in a Light Actuated Single-Molecule Magnet

4.1 Introduction

Silicon-based electronics may ultimately be replaced by circuits and devices comprised of molecular-scale components capable of switching between distinct states at high speeds with minimal energy input.[1-4] As a result, researchers are actively seeking molecules exhibiting bistable physical states that can be interchanged via external stimuli, such as temperature, light, electric or magnetic fields, or pressure. Here, molecules capable of interconverting between two stable magnetic polarization directions, known as single-molecule magnets, are of particular interest, owing to the prominent use of magnetic field-based switching in information storage over the past half-century. The introduction of additional physical states that can be accessed in such molecules via other stimuli stands as a challenge that could enable access to increased information density and, for the interesting case of light-based switching, potentially even result in molecular manifestations of magneto-optical effects observed in solids. Herein, we provide an initial demonstration of how spin-crossover behavior in a transition metal complex can give rise to a photoswitchable single-molecule magnet exhibiting tristability.

Spin-crossover complexes of $3d^4$ to $3d^7$ metal ions have been a focus of research for nearly eighty years,[5-7] due in part to their potential applications as molecular memory media, switches, displays, and sensors.[8] Of these, by far the majority are pseudo-octahedral $3d^6$ iron(II) complexes possessing coordination geometries dominated by N-donor ligands that place the ligand field splitting energy near the spin pairing energy.[9] For molecules of this type, the low-spin $t_{2g}^6e_g^0$ electron configuration with $S = 0$ is the ground state at low temperature, but at higher temperatures the high-spin $t_{2g}^4e_g^2$ electron configuration with $S = 2$ becomes significantly thermally populated, owing to differences in the entropy contributions to the Gibbs free energy associated with the spin degrees of freedom. Importantly, in some instances it is possible to switch between the two states using light irradiation, a phenomenon known as light-induced excited spin state trapping or the LIESST effect.[10-12] Thus, certain spin-crossover complexes can offer optically switchable bistability.

Another type of magnetic bistability is found in single-molecule magnets, molecules for which the magnetic dipole associated with a high spin ground state prefers to align along a unique axis.[13-15] Here, an axial magnetic anisotropy creates an energy barrier for converting between up ($M_S = +S$) and down ($M_S = -S$) orientations of the spin, as described by the zero-field splitting Hamiltonian $H = DS_z^2 + E(S_x^2 - S_y^2)$ with usually D large and negative, and E small. As a result, at low temperatures, these molecules exhibit slow relaxation of their magnetization and magnetic hysteresis associated with switching between the two states via application of a magnetic field. While most single-molecule magnets are polynuclear complexes, it was recently discovered that high-spin iron(II) complexes with an appropriate axial ligand field could also behave in this fashion.[16-20] These results motivated us to search for photoactive spin-crossover complexes that might additionally behave as single-molecule magnets when switched into their high-spin configuration. Amongst the possibilities, the compound $[Fe(ptz)_6](BF_4)_2$ (ptz = 1-propyltetrazole), representing the first system ever shown to exhibit the LIESST effect in the solid state,[10,11,21-27] caught our attention, owing to its remarkable photo-sensitivity and

the axial symmetry of its photoinduced high-spin state. Indeed, this molecular salt now provides the first example of a light actuated single-molecule magnet based on a spin-crossover phenomenon.

Over the course of the past twenty years, a series of crystallographic studies were carried out on $[Fe(ptz)_6](BF_4)_2$, revealing the details of the structures of the octahedral complex $[Fe(ptz)_6]^{2+}$ in its various physical states (Figure 1).[22-27] Above its spin-transition temperature of ~130 K, this compound crystallizes in a high symmetry $R\bar{3}$ structure (here denoted $\mathbf{HS_\alpha}$), wherein the high-spin iron(II) centers experience a D_{3d} local symmetry.[22] Upon cooling gradually to below 130 K, the symmetry of the structure (designated $\mathbf{LS_\alpha}$) is reduced to $P\bar{1}$ as a result of the ligands relaxing about the iron(II) centers to give C_i local symmetry upon conversion to a low spin configuration.[26] Intriguingly, however, it was found that by rapidly cooling below the spin-transition temperature, a form of the compound (designated $\mathbf{LS_\beta}$) could be obtained in which the $R\bar{3}$ symmetry of the parent structure is preserved, resulting in low-spin iron(II) centers that maintain an axial D_{3d} local symmetry.[21,23,25] By photo-exciting the $\mathbf{LS_\alpha}$ and $\mathbf{LS_\beta}$ phases, the compound is selectively converted into long-lived metastable high-spin phases (designated $\mathbf{HS_\alpha}$* and $\mathbf{HS_\beta}$*, respectively). Further structural studies performed under irradiation indicate $\mathbf{HS_\beta}$* to retain $R\bar{3}$ symmetry[24,25,27] and suggest that $\mathbf{HS_\alpha}$* has a similar low symmetry structure to $\mathbf{LS_\alpha}$.[26] In particular, the clear axial symmetry of $\mathbf{HS_\beta}$* provides the tantalizing prospect of enabling the large magnetic anisotropy required for a single-molecule magnet to develop.

4.2 Experimental Section

4.2.1 Synthesis of $[Fe(ptz)_6](BF_4)_2$: The synthesis of 1-propyltetrazole (ptz) was performed as previously reported with slight modifications.[1,2] Equimolar amounts of n-propylamine, sodium azide and triethyl orthoformate were dissolved in 30 M equiv. of 99.5% acetic acid and stirred at 90°C overnight. 80 M equiv. of 4 N HCl solution was added after removing the solvent under vacumm. The resulting solution was extracted three times with ethyl acetate. The organic phase was neutralized with $NaHCO_3$. Then, the organic phase was filtered and dried with $MgSO_4$ overnight. Afterwards, the solvent was removed under vacumm. The resulting oil was distilled in a Kugelrohr apparatus at 150 °C and a pressure of 1 hPa yielding colourless oil. All other reagents were obtained from commercial sources and used without further purification. The synthesis of $[Fe(ptz)_6](BF_4)_2$ was performed under nitrogen atmosphere according to the literature, using Schlenk technique as described in the following procedure. 1 mmol of $Fe(BF_4)_2 \cdot 6H_2O$ was dissolved in 3 ml of ethanol. A solution of 6 mmol of 1-propyltetrazole in 3 ml of ethanol was then added drop-wise. The resulting colorless solution was allowed to stir for 1 h to afford white crystalline powder of $[Fe(ptz)_6](BF_4)_2$. The white precipitate was collected by filtration, washed with successive aliquots of Et_2O and dried in air to afford 0.62 g (69%) of product. Anal. Calcd for $FeC_{24}N_{24}H_{48}B_2F_8$: C, 31.94; N: 37.26; H: 5.36. Found: C, 32.02; N: 37.75; H: 5.55. IR (300 K): $\bar{\nu}$ ($C\text{-}H_{ring}$) 3146 cm^{-1}, $\bar{\nu}$ ($C\text{-}H_{alkyl}$) 2972 cm^{-1}, 2941 cm^{-1}, 2883 cm^{-1} Previous Reported: $\bar{\nu}$ ($C\text{-}H_{ring}$) 3144 cm^{-1}, $\bar{\nu}$ ($C\text{-}H_{alkyl}$) 2980 cm^{-1}, 2940 cm^{-1}, 2882 cm^{-1}.[2]

4.2.2 Magnetic Measurements: The magnetic susceptibility measurements were obtained with the use of a Quantum Design SQUID magnetometer MPMS-XL housed at the Centre de Recherche Paul Pascal. This magnetometer works between 1.8 and 400 K

for dc applied fields ranging from -7 to 7 T. Static magnetic measurements were performed on a polycrystalline sample of 21.81 mg introduced in a polyethylene bag (3 × 0.5 × 0.02 cm). For these experiments, the magnetic data were corrected for the sample holder (plastic bag) and the diamagnetic contribution. The photomagnetic experiments were performed with different light sources coupled through an optical fiber directed into the magnetometer cavity. Powdered samples of 10.66 and 6.87 mg were packed in thermo-formed straw maintained at 3 mm to the optical fiber. For all these experiments, the magnetic data were corrected for the sample holder and the diamagnetic contribution. The irradiation is obtained with two LEDs at 505 nm (10 and 25 mW/cm^2) and 850 nm (10, 25 and 40 mW/cm^2). The thermal heating of the compound under irradiation was systematically corrected and did not exceed 0.2 K.

4.2.3 Electron Paramagnetic Resonance: High-field EPR data were collected in a transmission-type spectrometer based on a 17-T superconducting magnet at National High Magnetic Field Laboratory. A phase-locked Virginia Diodes 13-GHz solid-state oscillator, followed by a cascade of frequency multipliers, was employed as the microwave source. Frequencies over the range 100-640 GHz were generated. Ushio lamp USH-102D was used for sample irradiation with a Newport glass filter FSR-BG39. In X-band EPR a powder sample was placed in a standard 3-mm Quartz tube and was irradiated through the cavity window for a few minutes. In high-field EPR a hexagonally shaped crystal of ca. 6-mm length/width and 1 mm height was placed in the waveguide with its hexagonal plane perpendicular to the magnetic field.[3] The same lamp and filter as in the X-band experiment were used and the light followed the waveguide that normally

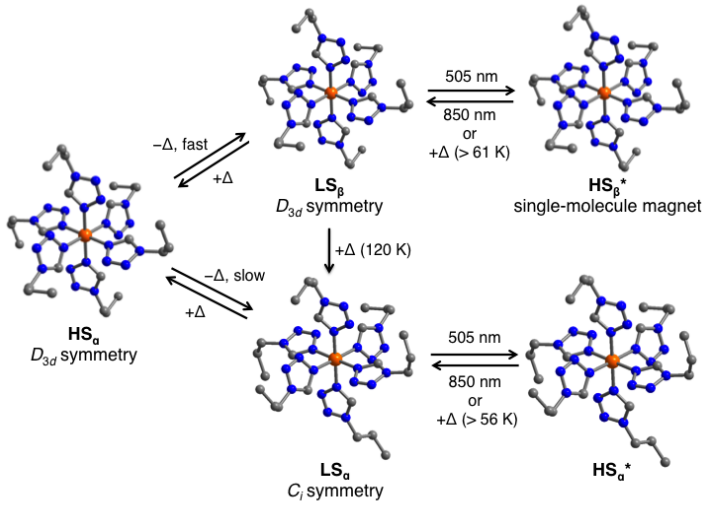

Figure 1. Interconversions between five different states of the octahedral iron(II) complexes in $[Fe(ptz)_6](BF_4)_2$. Orange, gray, and blue spheres represent Fe, C, and N atoms, respectively; H atoms are omitted for clarity. The conversions between the various high-spin (HS) and low-spin (LS) forms of the complex can be affected through application of heat (Δ) or in some cases by irradiation with light of 505 or 850-nm wavelength. With the exception of **HSα***, all of the structures have been well-characterized crystallographically.[11-13,22-27] In these crystal structures, the Fe-N distances are 1.97(1), 2.01(1), and 2.03(1) Å for **LSα**, 1.99(2) Å for **LSβ**, 2.20(2) Å for **HSα**, and 2.18(2) Å at 10 K for **HSβ***, reflecting the differences in spin configuration and local symmetry at the iron(II) center.

transmits the microwaves, irradiating the hexagonal crystal plane. The time of irradiation was 2 hours. EPR spectra were collected afterwards with light turned off.

4.2.4 Other Physical Measurements. Infrared spectra were obtained on a Perkin-Elmer Spectrum 400 FTIR spectrometer equipped with an attenuated total reflectance (ATR) accessory. Carbon, hydrogen, and nitrogen analyses were obtained from the Microanalytical Laboratory of the University of California, Berkeley.

4.3 Results and Discussion

The synthesis and characterization of $[Fe(ptz)_6](BF_4)_2$ proceeded as expected (details are provided in the Supplementary Materials), and its magnetic properties were investigated, with particular attention to the low temperature magnetization dynamics for the photo-induced $\mathbf{HS_\alpha}$* and $\mathbf{HS_\beta}$* phases. Static magnetic susceptibility data collected for a powder sample of the compound yielded c_MT = 3.9 cm^3K/mol at 300 K (Figure S1), corresponding to an $S = 2$ spin state with a g factor of 2.3. Upon lowering the temperature at a rate of 0.4 K/min, an abrupt decrease in c_MT product is observed between 140 and 110 K, indicative of a magnetic and structural phase transition between the $\mathbf{HS_\alpha}$ ($S = 2$) and $\mathbf{LS_\alpha}$ ($S = 0$) phases. These data are in good agreement with previously reported results.[11,26] The sample was then cooled to 10 K and irradiated with 505-nm LED light (P = 10 mW/cm^2) for 9 h, whereupon the c_MT value increased abruptly before reaching a plateau at ~3.6 cm^3K/mol (Figure S2). Under such treatment, $[Fe(ptz)_6](BF_4)_2$ is fully converted from $\mathbf{LS_\alpha}$ to the $\mathbf{HS_\alpha}$* phase.[11,26] After irradiation, ac magnetic susceptibility data as a function of frequency were measured in the dark at 1.9 K to check for slow magnetization dynamics, including in the presence of dc fields of up to 3000 Oe. The results showed no significant out-of phase signal, consistent with an absence of single-molecule magnet behavior for the low-symmetry form of the high-spin iron(II) complex (Figure S3).

To investigate the magnetic properties of $\mathbf{HS_\beta}$*, a sample of $[Fe(ptz)_6](BF_4)_2$ was cooled rapidly at ~100 K/min from 300 to 10 K, and irradiated with 505-nm LED light (P = 10 mW/cm^2) to initiate photoconversion. After 7 h, the c_MT value reached a plateau at 4.4 cm^3K/mol (Figs. S4 and S5). Maintaining a temperature of 10 K, the metastable $\mathbf{HS_\beta}$* phase obtained in this way showed no significant decay over time after switching off the light. To check for possible slow dynamics, ac magnetic susceptibility measurements were carried out from 10 K down to 1.8 K. Under zero applied dc field, no significant out-of-phase susceptibility signal was observed (Figure S6); however, upon application of a small dc field, a frequency-dependent signal indicative of a slowly relaxing single-molecule magnet became apparent. This behavior is typical for mononuclear iron(II) single-molecule magnets, in which fast ground state quantum tunneling of the magnetization short-cuts the thermal relaxation barrier under zero magnetic field, but is minimized upon application of a dc field to break the energy degeneracy of the $\pm M_S$ states.[16-20]

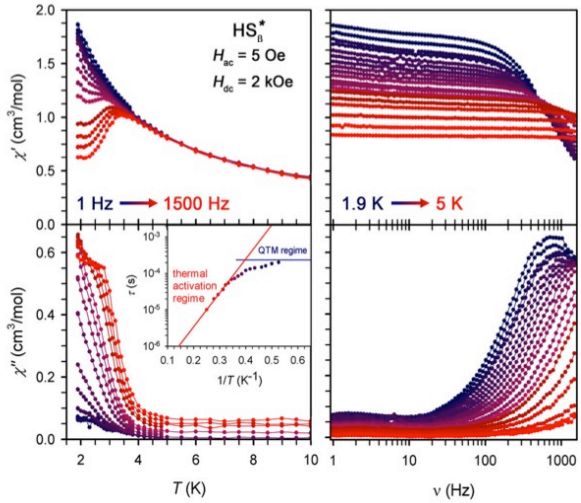

Figure 2. Temperature (left) and frequency (right) dependence of the in-phase (χ', top) and out-of-phase (χ'', bottom) components of the ac magnetic susceptibility data for **HS$_\beta$*** at oscillating frequencies between 1 and 1500 Hz and temperatures between 1.9 and 5 K. Measurements were performed with a 5-Oe ac field and a 2000-Oe dc field. The solid lines are guides for the eye. Inset: Arrhenius plot showing the dependence of the magnetization relaxation time τ upon inverse temperature, as obtained from the χ'' vs ν data. The solid red line corresponds to a linear fit to the data above 3 K, where relaxation can occur via a thermally activated process is accessed. At lower temperatures, relaxation becomes dominated by quantum tunneling of the magnetization (QTM).

Ac magnetic susceptibility data collected at applied fields as high as 7000 Oe enabled quantification of the effective spin reversal barrier associated with the single-molecule magnet behavior of **HS$_\beta$*** (Figure S7). Figure 2 shows the frequency and temperature dependence of the data obtained under an optimum dc field of 2000 Oe (i.e. that minimizes the quantum relaxation pathway of relaxation; Figure S8). Based on the frequency dependence of these data, the temperature dependence of the relaxation time τ was determined experimentally. This was accomplished by utilizing the maxima of the $\chi''(\nu)$ curves at a given temperature, for which $\tau = (2\pi\nu_{max})^{-1}$, and, for portions of the data where a maximum could not be observed, by applying a classical scaling method[28] (Figure S9). For a single-molecule magnet, τ follows a thermally activated relaxation process, resulting in an exponential increase with decreasing temperature. Accordingly, the corresponding plot of $\ln(\tau)$ vs $1/T$ should feature a linear region with the slope giving the relaxation energy barrier. Indeed, the Arrhenius plot shown in Figure 2 features a linear region above 3 K, indicative of a thermally activated relaxation time, and a fit to the data affords a relaxation barrier of U_{eff} = 15 cm^{-1} (22 K) and $t_o = 4.2 \times 10^{-8}$ s. The value of τ_0 provides a quantitative measure of the attempt time of relaxation, and the value obtained here is comparable to those found for other single-molecule magnets.[13-20] Below 3 K, the relaxation time becomes progressively less temperature dependent, as expected in the vicinity of a quantum relaxation regime, with a relaxation time of 2.4×10^{-4} s. Consistent with the measured relaxation times, no magnetic hysteresis was observed at temperatures down to 1.9 K employing the field sweep rates of 100-300 Oe/min attainable with a conventional SQUID magnetometer.

An important characteristic of the **HS$_\beta$*** phase is the presence of D_{3d} symmetry at the iron(II) sites,[24,25,27] which provides a substantial axial magnetic anisotropy D and limits the development of transverse anisotropy E. As a result, the rate of quantum tunneling is reduced significantly. Nevertheless, as shown in Figure 2, the system maintains some

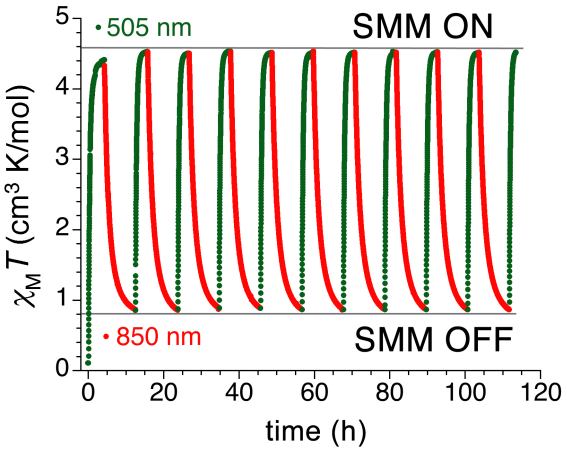

Figure 3. Excitation-deexcitation cycling between the $\mathbf{LS_\beta}$ and $\mathbf{HS_\beta}$* forms of $[Fe(ptz)_6](BF_4)_2$ at 10 K, as probed by dc magnetic susceptibility measurements performed under a 5000-Oe field. Irradiation with a 505-nm LED light source operating at 25 mW/cm^2 converts $\mathbf{LS_\beta}$ to $\mathbf{HS_\beta}$* over the course of 3 h, thereby switching on single-molecule magnet (SMM) behavior (as confirmed by ac magnetic susceptibility measurements). Subsequent irradiation with 850-nm LED light source operating at 40 mW/cm^2 converts $\mathbf{HS_\beta}$* back to $\mathbf{LS_\beta}$ over the course of 8 h, thereby switching off single-molecule magnet behavior. The gray lines are guides to the eye that help show the reproducibility of the cycling.

probability of quantum tunneling below 3 K, suggesting the possibility of an undetected local structural distortion to lower the symmetry at the iron(II) centers at low temperatures. Indeed, the much lower symmetry likely present in $\mathbf{HS_\alpha}$* appears to suppress the single-molecule magnet behavior entirely.

As a direct probe of the magnetic anisotropy, high-field high-frequency EPR spectra were collected at 10 K for the photoinduced $\mathbf{HS_\alpha}$* and $\mathbf{HS_\beta}$* forms of $[Fe(ptz)_6](BF_4)_2$. The spectra for the latter, higher-symmetry phase display the forbidden $\Delta M_S = 4$ transition expected for a high-spin iron(II) metal center (Figure S10), but well-resolved peaks corresponding to allowed transitions were not observed even at magnetic fields of up to 14 T and frequencies of up to 600 GHz. The absence of observable allowed transitions in the spectra is indicative of a remarkably large axial zero-field splitting parameter, while the presence of the $\Delta M_S = 4$ transition at very low temperatures indicates that the sign of D is negative. The only visible transition, from $M_S = -2$ to $M_S = +2$ can be simulated with many pairs of D and E parameters over a wide energy range, but the magnitude of $|D|$ is constrained to be less than ~15 cm^{-1}. Close to this limiting value, the set of parameters $D = -14.8$ cm^{-1} (-21.3 K), $E = -0.95$ cm^{-1} (-1.4 K), and $g_z = 2.3$ is found to be consistent with both the frequency dependencies (Figure S11) and the X-band EPR spectrum (Figure S12). These anisotropy parameters are in agreement with the observation of single-molecule magnet behavior for $\mathbf{HS_\beta}$*, and indicate a total spin reversal barrier of $U = S^2|D| = 50$ cm^{-1} (72 K). The observation of a somewhat reduced effective relaxation barrier of 15 cm^{-1} through ac magnetic susceptibility experiments is typical for mononuclear single-molecule magnets, and can generally be attributed to the presence of vibronic coupling.[29] EPR spectra obtained for $\mathbf{HS_\alpha}$* show the forbidden $\Delta M_S = 4$ resonance moving to lower field, suggesting a reduction in symmetry at the iron(II) centers and a significant transverse anisotropy (Figure S12). These observations are consistent with the absence of single-molecule magnet behavior for the phase. It should be noted that this work represents the first high-field EPR study performed on a photoinduced phase of a spin-crossover system.

The ability to utilize light in reversibly switching "on" and "off" the single-molecule magnet properties of $[Fe(ptz)_6](BF_4)_2$ was also investigated. Since the compound is known to show a reverse LIESST effect (i.e., a conversion back to the low-spin ground state) when the high-spin photoexcited state is irradiated with the longer wavelength light,[12] these experiments involved excitation to form $\mathbf{HS_\beta^*}$ and deexcitation back to $\mathbf{LS_\beta}$ via irradiation using LED light with wavelengths of 505 and 850 nm, respectively. Figure 4 plots c_MT as a function of time, demonstrating reversible excitation-deexcitation cycles during successive irradiations at 10 K. After a first complete conversion of $\mathbf{LS_\beta}$ to $\mathbf{HS_\beta^*}$ using 505-nm light, c_MT decreases under irradiation with 850-nm light, reaching a value of 0.8 cm^3K/mol after 8 h. This value indicates a nearly complete deexcitation, with only 17% of the iron(II) centers remaining in the high-spin configuration. To verify the reproducibility of the switching properties, ten excitation-deexcitation cycles were performed, yielding a sequence of essentially identical c_MT versus time traces. Ac magnetic susceptibility data were collected before the cycling, after the first excitation at 505 nm, after the first deexcitation at 850 nm, and after the last excitation at 505 nm. Remarkably, these data confirm the ability of the system to recover precisely the single-molecule magnet behavior of $\mathbf{HS_\beta^*}$ (Figure 2) upon reexcitation, and to negate that behavior upon subsequent deexcitation (Figure S13). Thus, the octahedral iron(II) complexes in $[Fe(ptz)_6](BF_4)_2$ are seen to exhibit tristability, with the application of light and a magnetic field at low temperature enabling switching between three long-lived states: $|0>$, $|+2>$, and $|-2>$.

4.4 Conclusions and Outlook

The foregoing results represent the first example of light actuated single-molecule magnets based on LIESST effect. The tristability offered by this system intimates the possibility of one day using molecules for ternary information storage.[30] Indeed, the manipulation of the information states for the molecules could potentially be carried out in direct analogy to current binary storage systems that employ magnetic switching and the magneto-optical Kerr effect (MOKE) as write and read mechanisms (see Figure S14). Here, starting with the molecules in the "0" low-spin state, one could write a "1" or a "2" by application of short-wavelength light in combination with a magnetic field to convert it to a high-spin state with the moment polarized either up or down along the easy axis. Information could then be read through application of the magneto-optical Kerr effect, wherein the moment of the molecule shifts the phase of polarized light either not at all for a "0" or in a positive or negative sense for a "1" or a "2". Information could be erased by irradiation with long-wavelength light to return the molecules to their low-spin form. Among other challenges, implementation of such a computing scheme would require significant further developments in the confinement of light at a molecular level[31] and the synthesis of new molecules of the type established here with larger relaxation barriers and longer polarization lifetimes.

4.5 Reference

1. Mannini, M.; Pineider, F.; Sainctavit, P.; Danieli, C.; Otero, E. Sciancalepore, C.; Talarico, A. M.; Arrio, M.-A.; Cornia, A.; Gatteschi, D.; Sessoli, R. *Nat. Mater.* 2009, *8*, 194-197.

2. Mannini, M.; Pineider, F.; Danieli, C.; Totti, F.; Sorace, L.; Sainctavit, P.; Arrio, M.-A.; Otero, E.; Joly, L.; Cezar, J. C.; Cornia, A.; Sessoli, R. *Nature* 2010, *468*, 417-421.
3. Vincent, R.; Klyatskaya, S.; Ruben, M.; Wernsdorfer, W.; Balestro, F. *Nature* 2012, *488*, 357-359.
4. Coskun, A.; Spruell, J. M.; Barin, G.; Dichtel, W. R.; Flood, A. H.; Botros, Y. Y.; Stoddart, J. F. *Chem. Soc. Rev.* 2012, *41*, 4827–4859.
5. Cambi, L.; Szego, L. *Chem. Ber. Dtsch. Ges*. 1931, *64*, 2591-2598.
6. Franke, P. L.; Haasnoot, J. G.; Zuur, A. P. *Inorg. Chim. Acta.*, 1982 *59*, 5-9.
7. Bousseksou, A.; Molnar, G.; Salmon, L.; Nicolazzi, W. *Chem. Soc. Rev.* 2011, *40*, 3313-3335.
8. Kahn, O.; Martinez, C. J. *Science* 1998, *279*, 44-48.
9. Halcrow, M. A. *Polyhedron* 2007, *26*, 3523-3576.
10. Decurtins, S.; Gütlich, P.; Kohler, C. P.; Spiering, H.; Hauser, A. *Chem. Phys. Lett.* 1984, *105*, 1-4.
11. Decurtins, S.; Gütlich, P.; Hasselbach, K. M.; Hauser, A.; Spiering, H. *Inorg. Chem.*, 1985, *24*, 2174-2178.
12. Hauser, A. *Chem. Phys. Lett.* 1986, *124*, 543-548.
13. Sessoli, R.; Tsai, H. L.; Schake, A. R.; Wang, S.; Vincent, J. B.; Folting, K.; Gatteschi, D.; Christou, G.; Hendrickson, D. N. *J. Am. Chem. Soc.* 1993, *115*, 1804-1816.
14. Sessoli, R.; Gatteschi, D.; Caneschi, A.; Novak, M. A. *Nature* 1993, *365*, 141-143.
15. Sessoli, R. ; Villain, J. ; Gatteschi, D. *Molecular Nanomagnets*, Oxford University Press, Oxford, 2006.
16. Freedman, D. E.; Harman, W. H.; Harris, T. D.; Long, G. J.; Chang, C. J.; Long, J. R. *J. Am. Chem. Soc.* 2010, *132*, 1224-1225.
17. Harman, W. H.; Harris, T. D.; Freeman, D. E.; Fong, H.; Chang, A.; Rinehart, J. D.; Ozarowski, A.; Sougrati, M. T.; Grandjean, F.; Long, G. J.; Long, J. R.; Chang, C. J. *J. Am. Chem. Soc*. 2010, *132*, 18115-18126.
18. Lin, P. H.; Smythe, N. C.; Gorelsky, S. I.; Maguire, S.; Henson, N. J.; Korobkov, I.; Scott, B. L.; Gordon, J. C.; Baker, R. T.; Murugesu, M. *J. Am. Chem. Soc*. 2011, *133*, 15806-15809.
19. Weismann, D.; Sun, Y.; Lan, Y.; Wolmershauser, G.; Powell, A. K.; Sitzmann, H. *Chem. Eur. J.* 2011, *17*, 4700-4704.
20. Zadrozny, J. M.; Atanasov, M.; Bryan, A. M.; Lin, C.-Y.; Rekken, B. D.; Power, P. P.; Neese, F.; Long, J. R. *Chem. Sci.* 2012, *4*, 125-138.
21. Ozarowski, A.; McGarvey, B. R. *Inorg. Chem.* 1989, *28*, 2262-2266.
22. Wiehl, L. *Acta. Cryst.* 1993, *B49*, 289-303.
23. Moritomo, Y.; Kato, K.; Nakamoto, A.; Kojima, N.; Nishibori, E.; Takata, M.; Sakata, M. *J. Phys. Soc. Jpn*. 2002, *71*, 1015-1018.
24. Jeftic, J.; Gillon, B.; Goujon, A.; Nau, Q.; Gukasov, A.; Codjovi, E.; Varret, F. *Polyhedron* 2003, 22, 2155-2160.
25. Kusz, J., Gütlich, P.; Spiering, H. *Top. Curr. Chem.* 2004, *234*, 129-153.
26. Kusz, J., Zubko, M., Neder, R. B.; Gütlich, P. *Acta. Cryst.* 2012, *B68*, 40-56.
27. Kusz, J., Spiering, H. ; Gütlich, P. *J. Applied Cryst.* 2004, *37*, 589-595.
28. Labarta, A., Iglesias, O., Balcells, L.; Badia, F. *Phys. Rev. B*, 1993, *48*, 10240-10246.

29. Atanasov, M., Zadrozny, J. M., Long, J. R.; Neese, F. *Chem. Sci.* 2013, *4*, 139-156.
30. (a) Sakamoto, R.; Murata, M.; Kume, S.; Sampei, H.; Sugimoto, M.; Nishihara, H. *Chem. Commun.* 2005, 1215-1217. (b) Schaniel, D.; Woike, Th.; Schefer, J.; Petricek, V.; Kranmer, K. W.; Gudel, H. U. *Phys, Rev. B* 2006, *73*, 174108. (c) Ould Moussa, N. O.; Trzop, E.; Mouri, S.; Zein, S.; Molnar, G.; Gaspar, A. B.; Collet, E.; Buron-Le Cointe, M.; Real, J. A.; Borshch, S.; Tanaka, K.; Cailleau, H.; Bousseksou, A. *Phys. Rev. B* 2007, *75*, 054101. (d) Mossin, S.; Tran, B. L.; Adhikari, D.; Pink, M.; Heinemann, F. W.; Sutter, J.; Szilagyi, R. K.; Meyer, K.; Mindiola, D. J. *J. Am. Chem. Soc.* 2012, *134*, 13651-13661. (e) Nihei, M.; Okamoto, Y.; Sekine, Y.; Hoshino, N.; Shiga, T.; Liu, I. P.-C.; Oshio, H. *Angew. Chem. Int. Ed.* 2012, *51*, 6361-6364.
31. Bao, W.; Melli, M.; Caselli, N.; Riboli, F.; Wiersma, D. S.; Staffaroni, M.; Choo, H.; Ogletree, D. F.; Aloni, S.; Bokor, J.; Cabrini, S.; Intonti, F.; Salmeron, M. B.; Yablonovitch, E.; Schuck, P. J.; Weber-Bargioni, A. *Science* 2012, *338*, 1317-1321.

4.6 Supporting Information

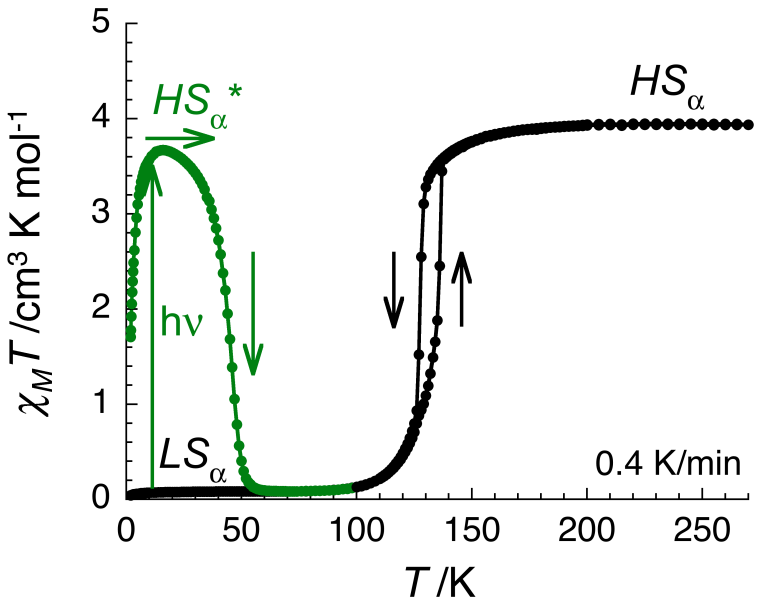

Figure S1 Temperature dependence of the $c_M T$ product (with c_M being the molar magnetic susceptibility defined as M/H per complex at 0.4 K/min) for $[Fe(ptz)_6](BF_4)_2$ between 1.8 and 270 K (H = 5000 Oe) before (black) and after (green) 505-nm irradiation (10 mW/cm^2) at 10 K for 9 hours (see Fig. S2). The solid lines are guides for the eye.

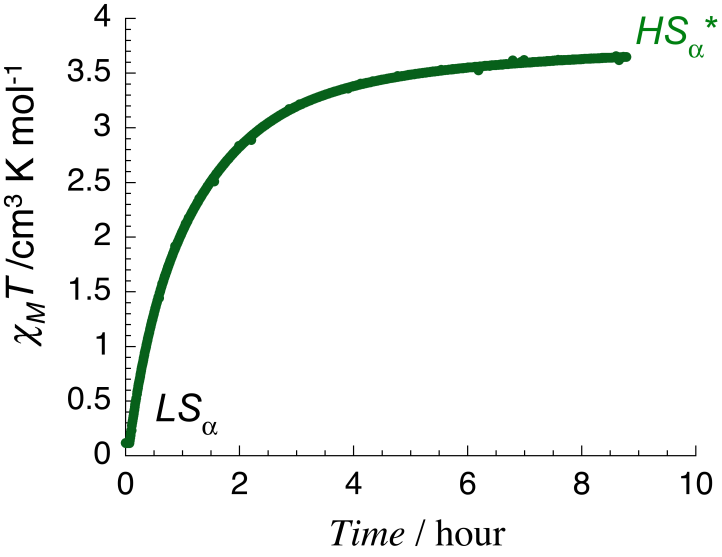

Figure S2 Time evolution of the $\chi_M T$ product (with χ_M being the molar magnetic susceptibility defined as M/H per complex) for $[Fe(ptz)_6](BF_4)_2$ during the 505-nm irradiation (10 mW/cm^2) at 10 K (H = 5000 Oe).

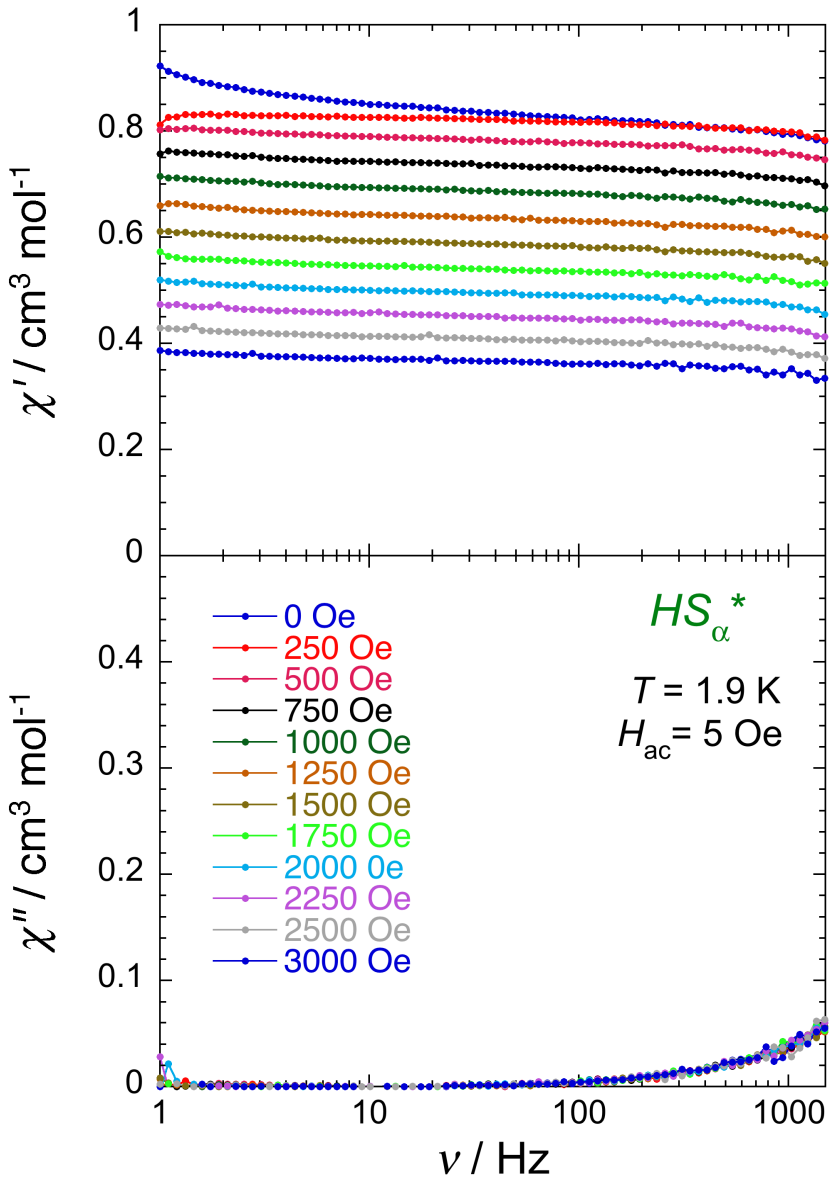

Figure S3 Frequency dependence of the in-phase (χ', top) and out-of-phase (χ'', bottom) components of the *ac* magnetic susceptibility for $[Fe(ptz)_6](BF_4)_2$ in its HS_α* phase at 1.9 K at different dc field between 0 and 3000 Oe. The solid lines are guides for the eye.

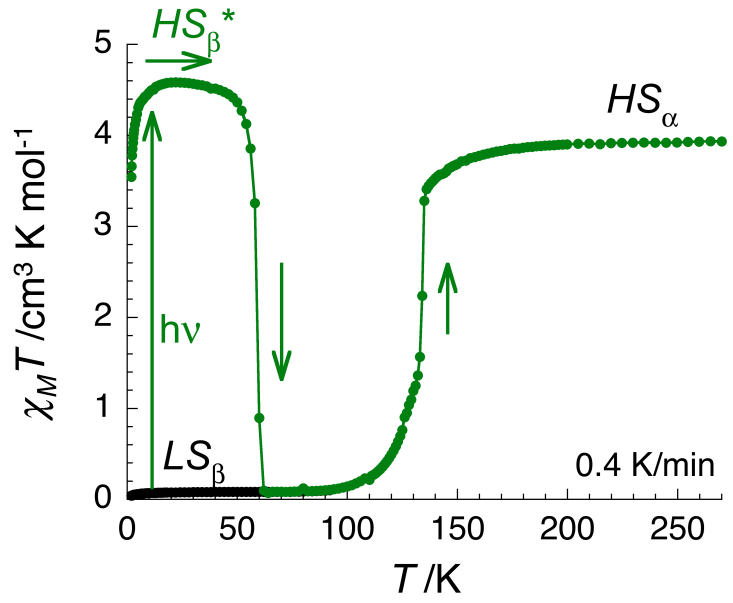

Figure S4 Temperature dependence of the $\chi_M T$ product (with χ_M being the molar magnetic susceptibility defined as M/H per complex at 0.4 K/min) for $[Fe(ptz)_6](BF_4)_2$ after thermal quenched at 10 K (> 100 K/min; H = 5000 Oe) before (black) and after (green) 505-nm irradiation (10 mW/cm^2) at 10 K for 7.5 hours (see Fig. S5). The solid lines are guides for the eye.

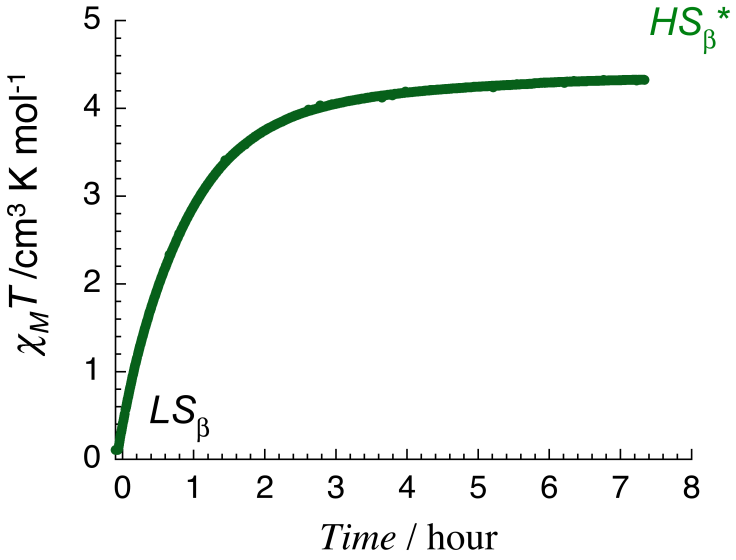

Figure S5 Time evolution of the $\chi_M T$ product (with χ_M being the molar magnetic susceptibility defined as M/H per complex) for $[Fe(ptz)_6](BF_4)_2$ after thermal quenched at 10 K (> 100 K/min; H = 5000 Oe) during the 505-nm irradiation (10 mW/cm^2) at 10 K.

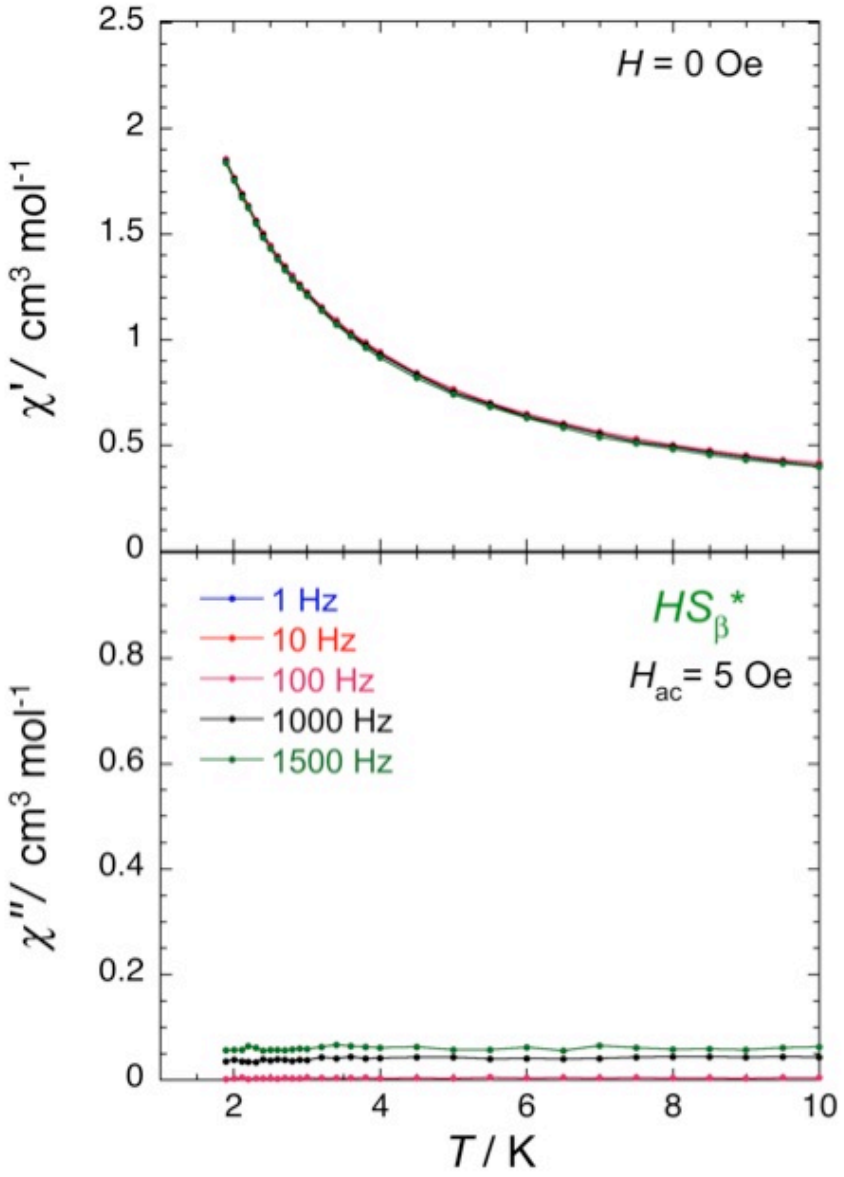

Figure S6 Temperature dependence of the in-phase (χ', top) and out-of-phase (χ'', bottom) components of the *ac* magnetic susceptibility for $[Fe(ptz)_6](BF_4)_2$ in its HS_β* phase in zero-dc field at ac frequencies of 1, 10, 100, 1000, 1500 Hz. The solid lines are guides for the eye.

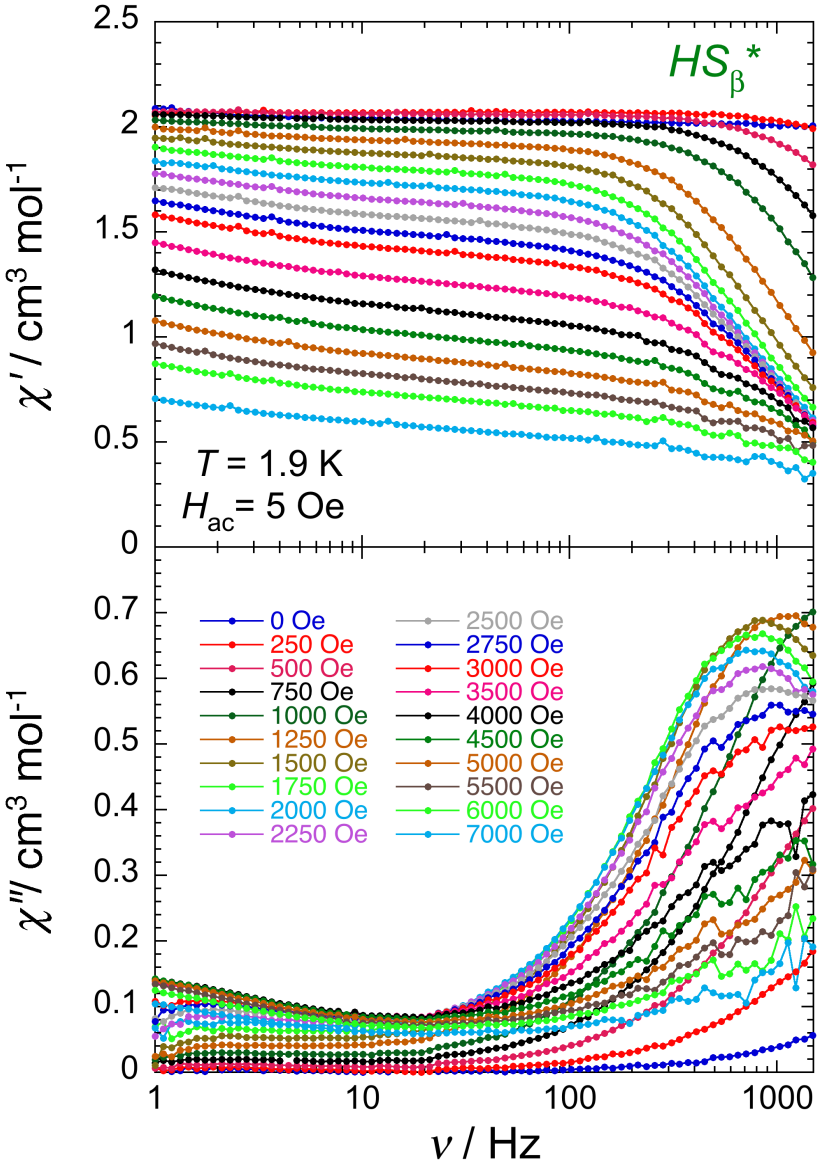

Figure S7 Frequency dependence of the in-phase (χ', top) and out-of-phase (χ'', bottom) components of the *ac* magnetic susceptibility for $[Fe(ptz)_6](BF_4)_2$ in its HS_β* phase at 1.9 K at different dc field between 0 and 7000 Oe. The solid lines are guides for the eye.

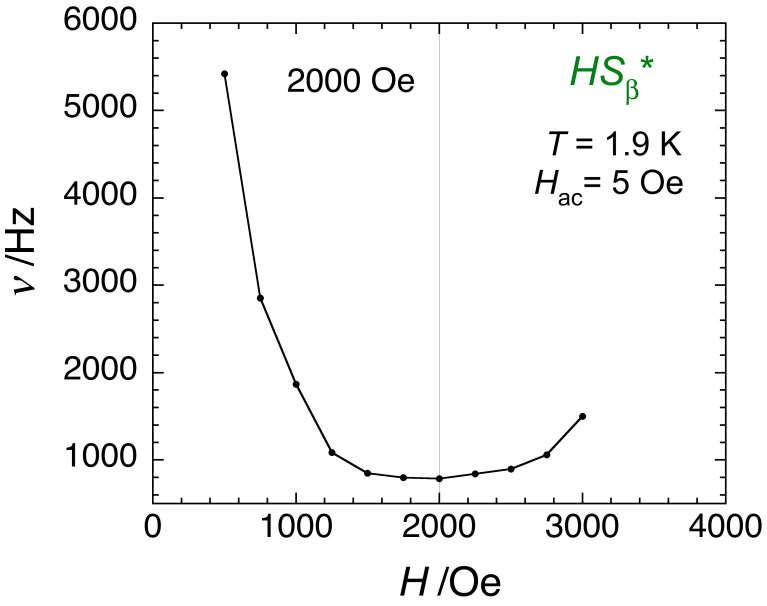

Figure S8 Field dependence of the characteristic relaxation frequency of the magnetization for $[Fe(ptz)_6](BF_4)_2$ in its HS_b* phase at 1.9 K. This plot is deduced from Figures S7. The solid line is a guide for the eye.

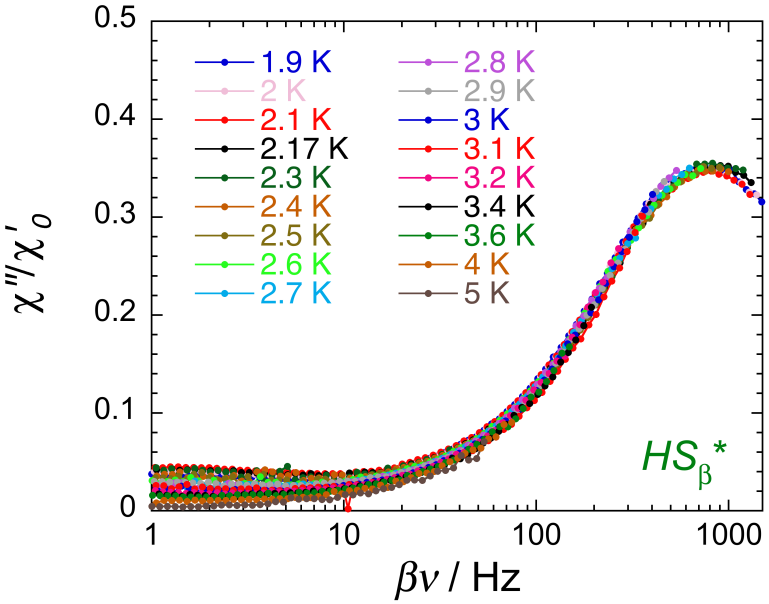

Figure S9 Scaled frequency dependence of the out-of-phase component of the ac susceptibility normalized by the zero-frequency in-phase susceptibility (taken experimentally at 1 Hz) at different temperatures between 1.9 and 5 K (with H_{ac} = 5 Oe and H = 2000 Oe) for $[Fe(ptz)_6](BF_4)_2$ in its HS_b* phase. b is the scaling parameter equals to 1 for the data at 1.9 K.

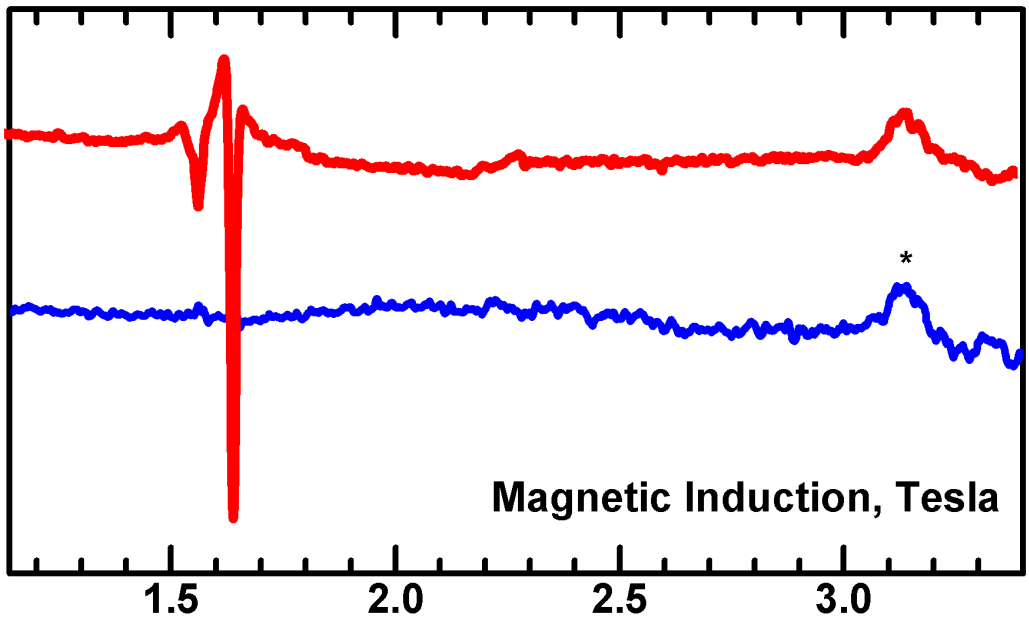

Figure S10 High-field EPR spectra of a crystal sample of $[Fe(ptz)_6](BF_4)_2$, collected at 10 K and 216 GHz in its LS_b phase (blue spectrum) and in its HS_b* phase (red spectrum). The resonance observed at ca. 1.6 T after irradiation moves with the microwave frequency (for example with n = 628.8 GHz it is observed at 4.85 T) showing an almost constant $g_{effective}$ value of 9.25. Accordingly, it can be assigned to a $\Delta M_S = 4$ transition with an intrinsic g value of ~2.3. This observation provides unambiguous evidence of negative sign of zero-field splitting parameter D *(see Figure S11)*. No other resonances, which could be attributable to Fe^{2+}, were observed. The signal marked with an * is due to frozen O_2, often encountered in HF EPR spectra. Magnetic field was perpendicular to the hexagonal crystal plane, which appears to be the z orientation.

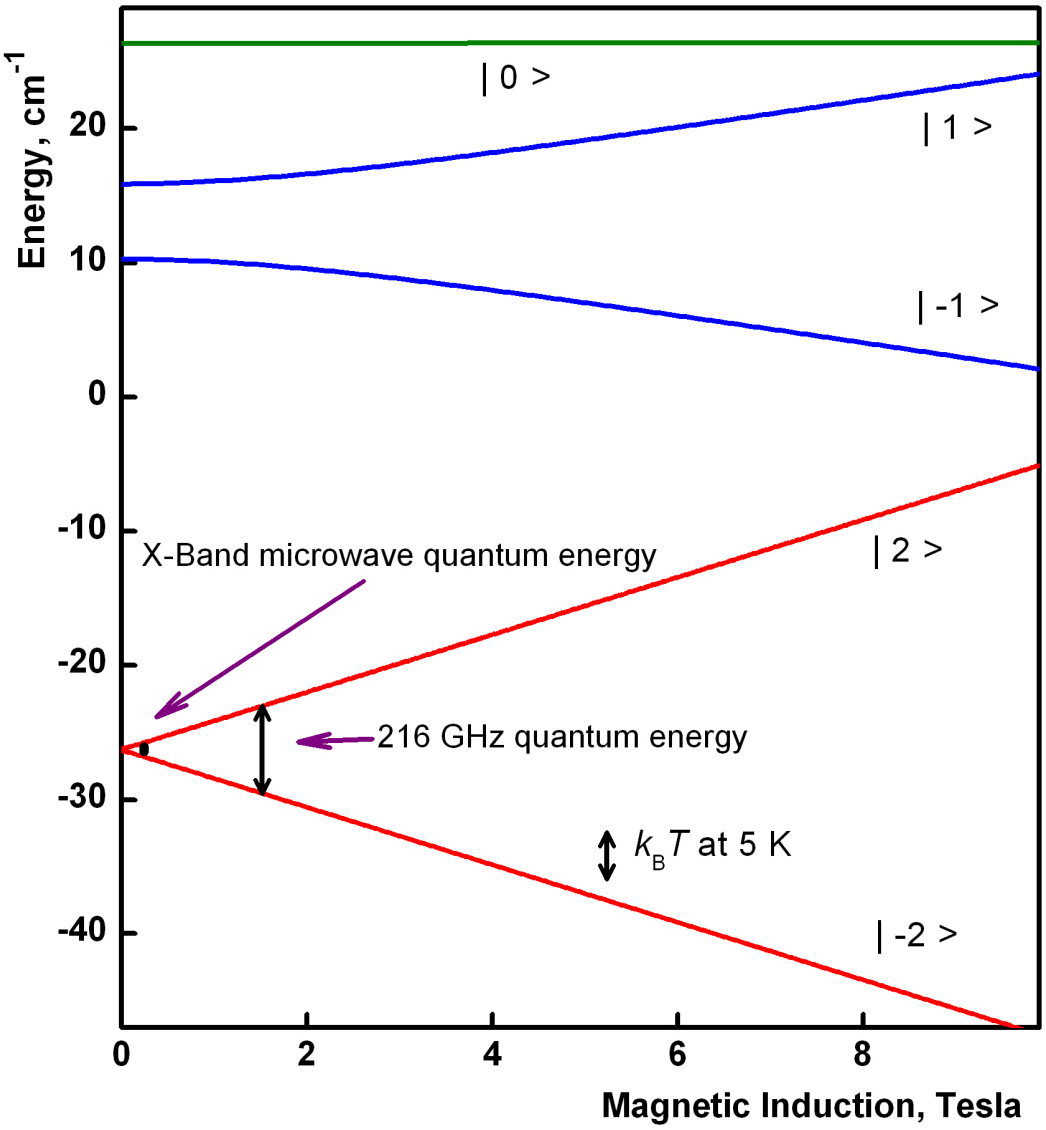

Figure S11 Energy levels of the HS_{II}* phase for $[Fe(ptz)_6](BF_4)_2$, calculated with the magnetic field parallel to z axis (with D = -14.8 cm^{-1} (-21.3 K), E = -0.95 cm^{-1} (-1.4 K) and g_z = 2.3). An arrow of thermal energy k_BT at 5 K demonstrates that only $M_S = \pm 2$ can be populated at 5 K in the case of negative D. The only transition to be observed is the $\Delta M_S = 4$ transition. It is also seen that a huge microwave frequency would be required to invoke an allowed transition from $M_S = \pm 2$ to $M_S = \pm 1$. If the sign of D were positive, this diagram would be reversed and $\Delta M_S = 4$ transition could not be observed. Also, the energies that allowed to observe $\Delta M_S = 4$ transition in high-field EPR and X-band EPR are marked out.

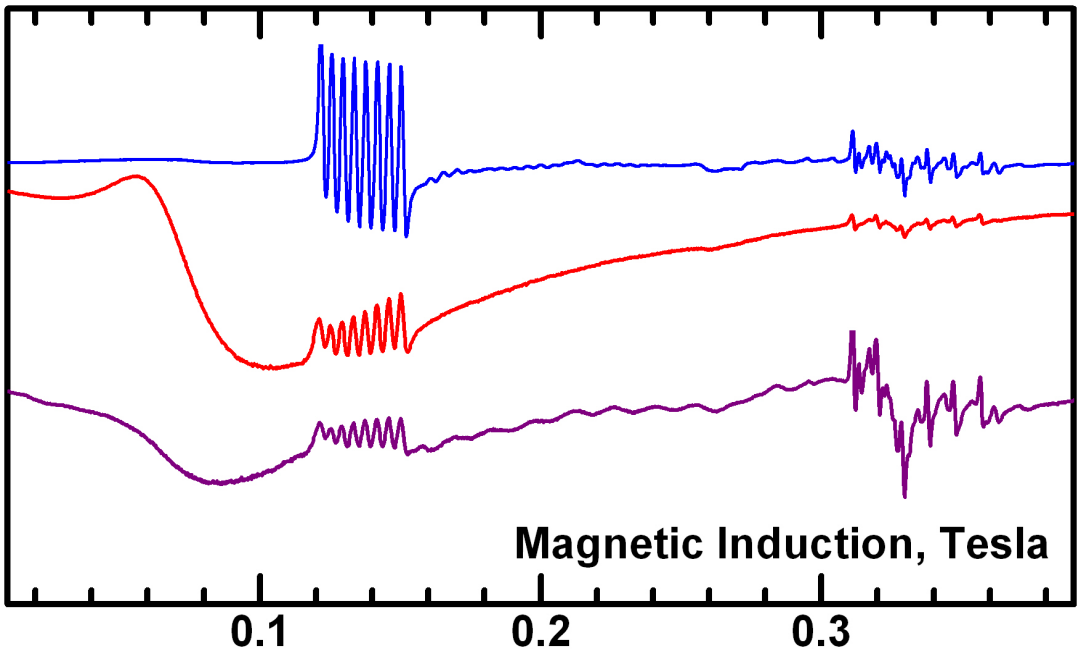

Figure S12 X-band EPR spectra collected for $[Fe(ptz)_6](BF_4)_2$ at 5 K. In the LS_0 phase (blue), only traces of high-spin Co(II) and Mn(II) are seen. Note: the trace amount of Co(II) and Mn(II) impurities are from starting materials and haven't been introduced intentionally. The red plot represents the spectrum of the HS_0* phase after light irradiation (details in section 1.3). The $\Delta M_S = 4$ transition in Fe^{2+}, which was observed in high-field EPR shows up again nicely below 0.1 T. The purple plot is the spectrum of HS_α* phase after light irradiation (details in section 1.3). In this case, the resonance shifts to a lower resonance field and becomes more complicated, which can be interpreted as an increase of transverse anisotropy E due to lower symmetry.

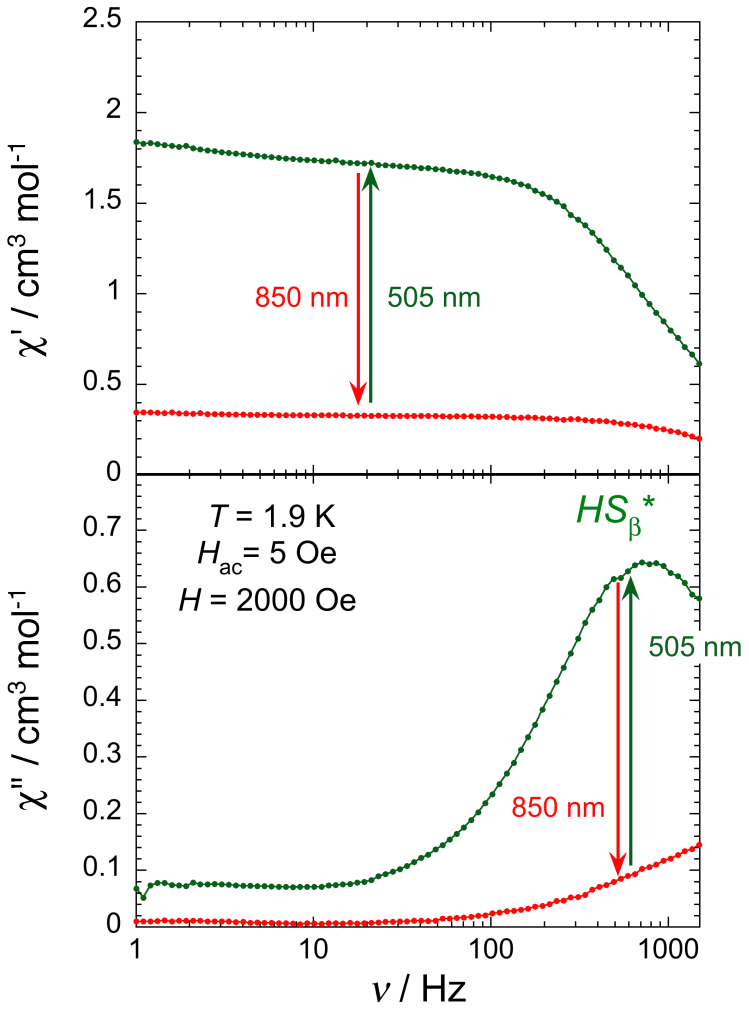

Figure S13 Frequency dependence of the in-phase (χ', top) and out-of-phase (χ'', bottom) components of the *ac* magnetic susceptibility for $[Fe(ptz)_6](BF_4)_2$ after thermal quenched at 10 K (> 100 K/min), measured at 1.9 K under 2000 Oe before irradiation at 505 nm or after irradiation at 850 nm (25 mW/cm^2, 8 hours) (red) and after irradiation at 505 nm (green, 10 mW/cm^2, 3 hours). The solid lines are guides for the eye.

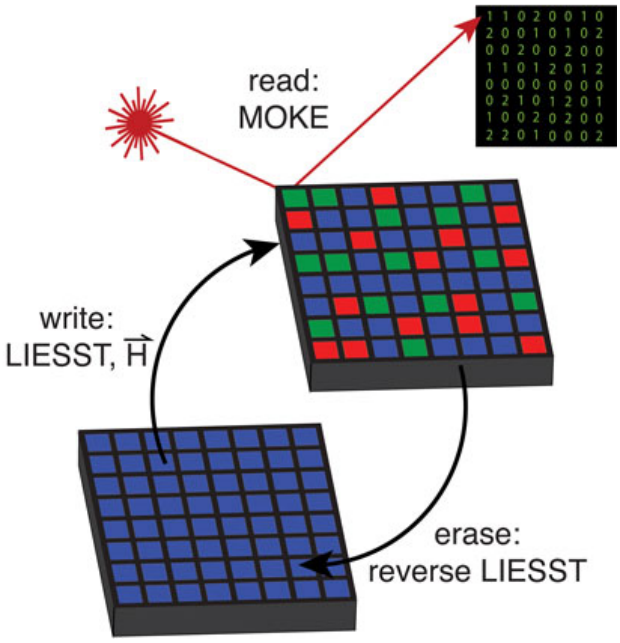

Figure S14 Illustration of a ternary information storage scheme utilizing light actuated single-molecule magnets. Starting with all molecules in the low-spin or "0" state (blue), a "1" or "2" could be written by application of the light-induced electron spin state trapping (LIESST) effect in the presence of an external magnetic field, resulting in a high-spin state magnetized in either an up (green) or down (red) direction. The data could then be read using the magneto-optical Kerr effect (MOKE), by detecting the change of phase of the applied polarized light, with no phase shift indicating a "0", a positive phase shift representing a "1", and a negative phase shift representing a "2". Data could be erased by application of the reverse LIESST effect (i.e., irradiation with lower-frequency light) to return all molecules to their low-spin configuration.

Chapter 5: Electronic Structure and Single-Molecule Magnet Behavior of $[ReCl_4(CN)_2]^{2-}$

5.1 Introduction

Paramagnetic molecules capable of interconverting between two stable magnetic polarization directions, known as single-molecule magnets (SMMs), have received considerable attention as they have been suggested for applications in high-density information storage for the past twenty years.[1]

For molecules with integer spin, to observe slow magnetic relaxation, the sign of zero-field splitting parameter D is required to be negative in order to generate a doubly degenerate ground state. However, for molecules with half-integer spin, a doubly degenerate ground state is always assured by Kramers' Theorem, regardless of the sign of D. Thus, in theory, observation of slow relaxation of magnetization via an Orbach process, involving three real states accompanied with two phonons, is always possible for half-integer spin system irrespective of the M_S composition of the ground doublet. Unlike the single-phonon direct process resonating between only two states, very few cases of single-molecule magnets with easy-plane magnetic anisotropy[2] were reported through an Orbach process which relaxation time grows faster in exponential over decreasing temperature.

Whereas the first generations of single-molecule magnets were characterized by a large spin ground state,[3] recent results have suggested that an increase in spin ground state is usually compensated by a corresponding decrease in total magnetic anisotropy.[4] To overcome such a problem, new approaches have emerged, for example, using molecules containing single paramagnetic lanthanide or actinide ions, known for their pronounced magnetic anisotropy.[5] The effective energy barriers for spin-reversal, U_{eff}, for such molecules have been reported as large as 641 cm^{-1},[6] which is an order of magnitude larger than the archetypal Mn_{12} complex.[7] More recently, it has been shown that mononuclear, first-row transition metal complexes can display large magnetic anisotropy, originating from a near-degenerate ground state where the orbital angular momentum is unquenched.[8] Moreover, taking advantage of the Kramers Theorem,[9] fast quantum tunneling can be effectively avoided by using half-integer spin metal ions. Following this strategy, several mononuclear first-row transition metal single-molecule magnets were reported.[10] For example, a recent linear two-coordinate Fe^{I} molecule has been shown to display a spin reversal barrier of 226 cm^{-1} and magnetic hysteresis up to 6.5 K.[11]

Beside the synthetic challenges of generating low coordinate complexes, compared to lanthanide or actinides, mononuclear single-molecule magnets of first-row transition metals appear to have an inherent disadvantage towards displaying a large magnetic anisotropy, due to their much smaller spin-orbit coupling constant. To meet this challenge, recent attention turned to 5d metal ions combining the strong spin-orbit coupling and tunability through the chemically controllable ligand field and geometry.[12] Recently, the rhenium(IV) complexes $(NBu_4)[Re(ox)X_4]$ (ox = oxalate, X = Cl, Br), $(PPh_4)_2[ReF_6]\cdot 2H_2O$ and $Zn(viz)_4[ReF_6)]_*$ (viz = 1-vinylimidazole) were shown to display slow relaxation of the magnetization (under applied dc fields). Notably, for all four systems, the U_{eff} is much reduced as compared to the expected value determined from the spin-Hamiltonian parameters. In fact, this observation is not reserved for Re^{IV}, and the vast majority of published mononuclear single-molecule magnets show serious

disagreement between the measured U_{eff} and the energy of the first excited electronic state pointing towards the presence of alternative relaxation processes.

Both the magnetic measurements and our previous high-frequency and -field EPR (HF-EPR) study[13] on *trans*-$(Bu_4N)_2[Re^{IV}Cl_4(CN)_2]\cdot 2DMA$ (**1**) reveal the spin-Hamiltonian parameters $D = +11.5$ cm^{-1} and $|E| = 3.1$ cm^{-1}. Despite the positive value of D, we report herein the observation of slow relaxation of magnetization in **1** reminiscent of single-molecule magnet behavior. Remarkably, the experimental energy barrier for slow magnetic relaxation in **1** 26.7 cm^{-1} is in great agreement with the calculated energy barrier from D and E values (25.4 cm^{-1}), representing the highest energy barrier yet observed for a 4d/5d mononuclear single-molecule magnet.

5.2 Experimental Section

5.2.1 Synthesis of *trans*-$(Bu_4N)_2[Re^{IV}Cl_4(CN)_2]\cdot 2DMA$ The synthesis of *trans*-$(Bu_4N)_2[Re^{IV}Cl_4(CN)_2]\cdot 2DMA$ was performed as previous method.[1] 0.4 g dry $(Bu_4N)CN$ was added to a stirred green solution of *cis*-$[ReCl_4(THF)_2]$ (0.2 g) in 2 mL of DMF under nitrogen. The resulting dark brown solution was allowed to stir overnight and then exposed to air. Addition of 25 mL of water to the solution resulted in the formation of a brown precipitate. The precipitate was collected after filtration, washed with water and diethyl ether, and allowed to dry under vacuum for 1h. The pale brown solid was then dissolved in 1.5 mL of N,N-dimethylacetamide (DMA), and the resulting dark yellow solution was filtered through diatomaceous earth. Diffusion of diethyl ether vapor into the resulting filtrate yielded pale blue rod-shaped crystals suitable for X-ray diffraction. Anal. Calcd for $C_{42}H_{90}N_6Cl_4O_2Re$: C, 48.54; N: 8.09; H: 8.73. Found: C, 48.49; N: 8.07; H: 8.63. IR (300 K): ν_{CN} 2120 cm^{-1}.

5.2.2 Magnetic Measurements. Magnetic data were collected on a Quantum Design MPMS-XL7 SQUID magnetometer and on a Quantum Design Physical Property Measurement System (PPMS-9). Dc susceptibility measurements for *trans*-$(Bu_4N)_2[ReCl_4(CN)_2]\cdot 2DMA$ were obtained for a microcrystalline powder restrained in a frozen polyethylene bag. All data were corrected for diamagnetic contributions from the sample holder, as well as for the core diamagnetism of each sample.

5.2.3 Other Physical Measurements. Infrared spectra were obtained on a Perkin-Elmer Spectrum 400 FTIR spectrometer equipped with an attenuated total reflectance (ATR) accessory. Carbon, hydrogen, and nitrogen analyses were obtained from the Microanalytical Laboratory of the University of California, Berkeley.

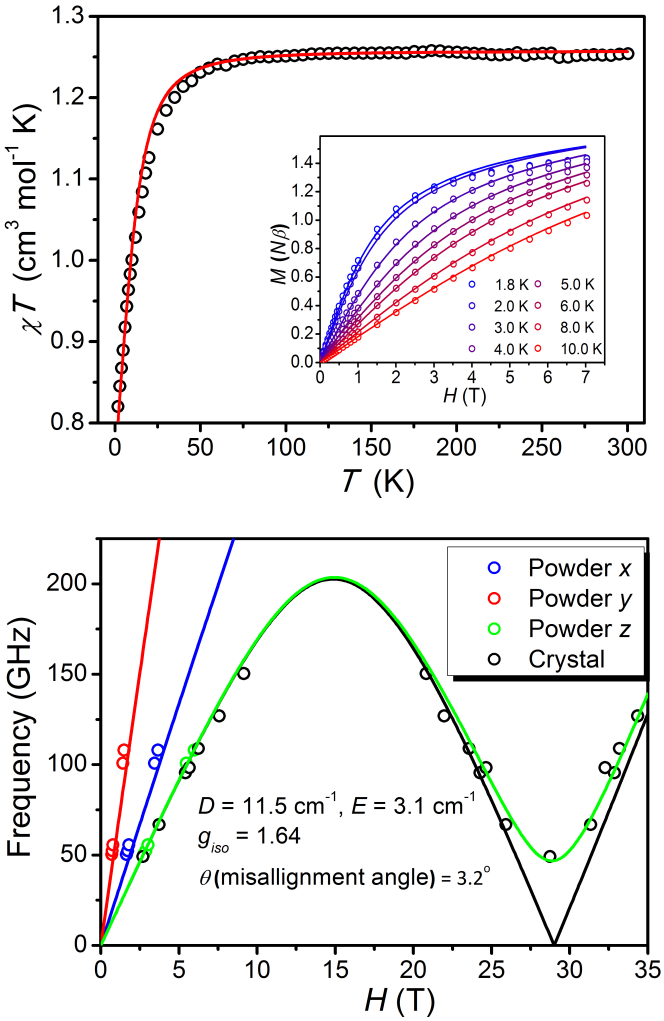

Figure 1. *Top*: χT ($\chi = M/H_{dc}$, H_{dc} = 1000 Oe) product data for polycrystalline **1**. The solid red line is from the best fit. Inset: Field-dependence of the magnetization obtained at selected low temperatures. The solid lines are from the best fit (blue, 1.8 K; red, 10 K). *Bottom*: the EPR peak positions from the powder and the single crystal measurements. The solid green line is from the best fit, and the black line is the simulation with the misalignment angle $\theta = 0^{o}$.

5.3 Results and Discussion

Selected interatomic distances and bond angles for **1** are listed in Table S1. Close inspection of structures at 50 K and 100 K reveals little differences in the local coordination environment of Re^{IV}. The bond distances shrink slightly with decreasing the temperature. The Re-Cl distances are 2.351(1) Å and 2.341(1) Å at 100 K, while at 50 K, these distances are 2.321(2) Å and 2.334(2) Å respectively.

The temperature dependence of the direct current (dc) magnetic susceptibility was measured between 1.8 and 300 K for a crystalline sample of **1** (Figure 1). The $\chi_M T$ product decreases upon lowing temperatures at the presence of zero-field splitting, of which the room-temperature value is 1.25 cm^3 K mol^{-1}. The magnetic data (including $\chi_M T$ vs. T and M vs. H) as well as the HF-EPR peak positions for the powder and the single crystal measurements were simultaneously fitted using the following spin Hamiltonian:

$$\hat{H} = g\mu_B B\hat{S} + D\left(\hat{S}_z{}^2 - \tfrac{1}{3}\hat{S}^2\right) + E\left(\hat{S}_x{}^2 - \hat{S}_y{}^2\right) \qquad \text{(Eq. 1)}$$

where g indicates an isotropic g-factor and the rest of the symbols have their usual meaning. The resulting parameters are $D = 11.5$ cm^{-1}, $|E| = 3.1$ cm^{-1} and $g = 1.64$.

Note that we tried to fit the magnetization data using the full sphere average but they were not well reproduced at high fields, while it was successful to fit them if only using x, y and z directions to average. In order to prevent losing solvents, the measured sample was not fine powder, which may favor some of the specific orientations of the crystals; In order to prevent over-parameterization, the partially unquenched orbital contributions are not explicitly taken into account for the full Hamiltonian, though it could play an role in magnetic and spectroscopic data. These points might be responsible for the small deviations between the measured and the fitted curves.

Alternating current (ac) magnetic susceptibility measurements were performed to detect any slow relaxation of magnetization in **1**. In the absence of an applied dc field, no out-of-phase (χ'') signal is observed at frequencies up to 1500 Hz and temperatures down to 1.8 K. However, application of static field resulted in a clear frequency dependence of χ' and χ'', as shown in Figure 2. Relaxation times were extracted from these peaks by fitting the χ' vs. χ'' data to a generalized Debye model (Figure S2), to obtain α values and relaxation times at different temperatures.[14] Here, α provides a quantitative measure of the distribution of relaxation times. From 1.8 K to 2.65 K, α ranges from 0.04 to 0.09, indicating a narrow distribution of relaxation times. The resulting Arrhenius (ln(τ) vs. T^{-1}) plot (Figure 3) features a linear region at the highest temperature and a fit to the expression $\ln(\tau) = \ln(\tau_0) + U_{eff}/(k_B T)$ yielded an effective barrier of $U_{eff} = 27$ cm^{-1} and a pre-exponential factor of $\tau_0 = 3.9\times10^{-11}$ s.

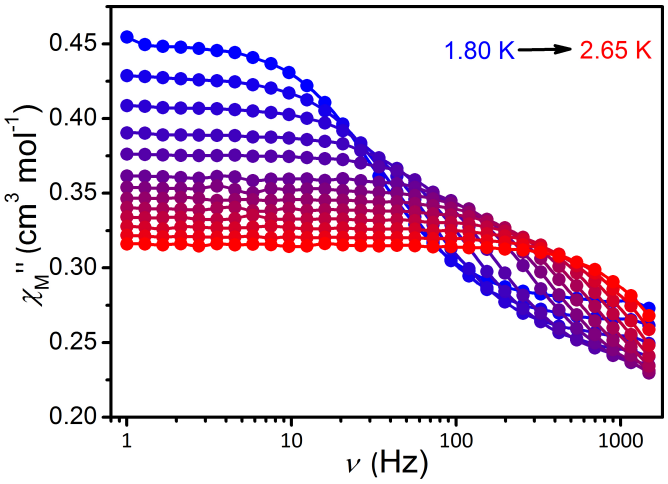

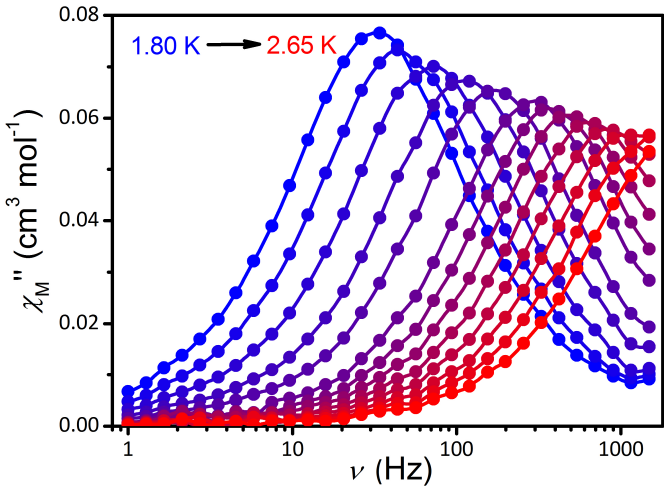

Figure 2. Variable-temperature ac magnetic susceptibility data obtained for **1** in a 1000 Oe dc field from MPMS-XL7. Solid lines are guides for the eye.

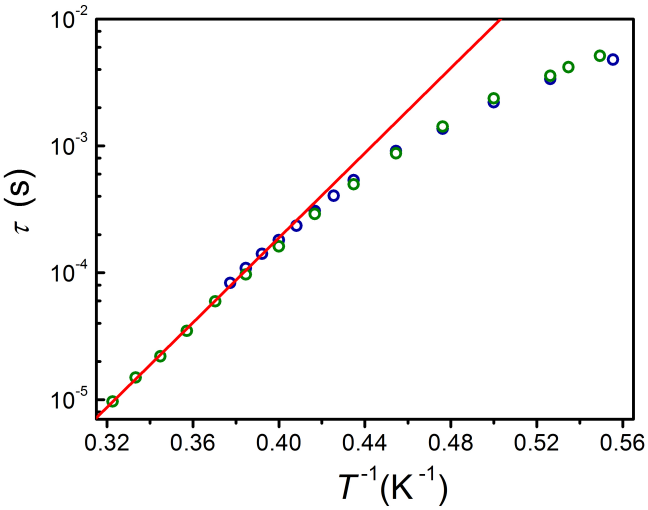

Figure 3. Relaxation time obtained from MPMS-XL7 (blue) and PPMS-9 (green) vs. temperature. The red solid line is for the Arrhenius fit.

In zero applied dc field, any tunneling splitting of the ground doublet is forbidden by Kramers' Theorem. However, quantum tunneling could originate from hyperfine or dipolar interactions, which are possible reasons for the observation of no slow relaxation of magnetization in **1** under zero applied field. Under an applied dc field, for example, 1000 Oe as shown in Figure 2, any hyperfine and dipolar mediated processes is suppressed. In such a situation, the splitting of the ground doublet is *ca.* 0.06 cm^{-1} (when the magnetic field is applied in the *z* direction) and the direct relaxation between them is slower compared to an Orbach process, especially within the high-temperature regime. Using the fitted parameters, the ground and excited doublets can be shown as follows:

$|KD_1\rangle = -0.22\ |-^3/_2\rangle + 0.98\ |^1/_2\rangle$
$|KD_2\rangle = -0.22\ |^3/_2\rangle + 0.98\ |-^1/_2\rangle$
$|KD_3\rangle = +0.22\ |-^1/_2\rangle + 0.98\ |^3/_2\rangle$

$|KD_4\rangle = -0.22\,|^1/_2\rangle - 0.98\,|-^3/_2\rangle$

Thus, the spin will relax via a more efficient Orbach process via mixing the $M_S = \pm^1/_2$ and $M_S = \pm^3/_2$ levels of the opposite sign due to the presence of E.[15] As such, the energy barrier for the reversal of the spin of the Re^{IV} center via this Orbach process is given by $U_{\text{eff}} = 2\sqrt{D^2 + 3E^2}$. Considering the fitted spin-Hamiltonian parameters of D = +11.5 cm^{-1} and $|E|$ = 3.1 cm^{-1}, the expression amounts to U_{eff} = 25.4 cm^{-1}. This value is in excellent agreement with the energy barrier determined from the Arrhenius analysis of the ac magnetic susceptibility data of U_{eff} = 26.7 cm^{-1}, thus suggesting the domination of Orbach-type relaxation in **1**.

To further probe the effect of applied magnetic field on slow relaxation of the magnetization in **1**, relaxation times were extracted from variable-frequency ac susceptibility data obtained at 1.8 K under various dc fields (Figure S4). Besides the Orbach process, of which relaxation rate can be considered field-independent, quantum tunneling and direct processes should be taken into consideration at this low temperature. In the absence of magnetic fields, the relaxation time is so short that no χ'' signals were observed. Upon applying a small static field, significant frequency- and temperature-dependent ac signals were found. On one hand, the axial field suppresses the fast tunneling; On the other hand, the transverse field mixes the microstates with M_S and $M_S \pm 1$, leading to a faster relaxation rate upon increasing field due to the presence of a single-phonon direct process. Under these two competing effects, we could find an optimized field. However, a direct process with transition between $\pm^1/_2$ ($\Delta m_S = 1$) should be more efficient than that between $\pm^3/_2$ ($\Delta M_S = 3$) in the presence of magnetic field. For this reason, in the case of a magnetic system with $D > 0$, the direct process could dominate over quantum tunneling even in the very-low-field regime. That's why the relaxation rate monotonously increases for the title Re^{IV} compound.

5.4 Conclusion

The presented results support that Orbach-type slow relaxation of magnetization in single-molecule magnets can be observed in a mononuclear complex with positive sign of D, not only for the Co^{II} complex[2a] but also for a Re^{IV} complex. Such behavior leads to the observation of slow magnetic relaxation in **1**, which also represents the highest energy barrier yet observed for 4d/5d mononuclear single-molecule magnets. Moreover, for half-integer spin systems ($S \geq {}^3/_2$), as avoided crossing for the ground Kramers doublet is always forbidden in the presence of purely electric fields, regardless of the sign of D, it is possible to observe Orbach-type slow magnetic relaxation under zero applied dc field in positive D systems if hyperfine[16] and dipolar coupling[17] can be quenched. This suggests a broader strategy in designing single-molecule magnets with large spin reversal barriers for Kramers systems.

5.5 Acknowledgement

This work was supported by National Science Foundation under Grant CHE-1111900. Research in France was funded by the Centre National de la Recherche Scientifique (CNRS), the University of Bordeaux, the Conseil Regional d´ 'Aquitaine, GIS Advanced Materials in Aquitaine (COMET Project), the ANR (NT09_469563, AC-MAGnets Project), and Institut Universitaire de France (IUF).

5.6 References

1. Gatteschi, G.; Sessoli, R.; Villain, J. *Molecular Nanomagnets*, Oxford University Press, Oxford, **2006**.
2. (a) Zadrozny, J. M.; Liu, J.; Piro, N. A.; Chang, C. J.; Hill, S.; Long, J. R. *Chem. Commun*., **2012**, *48*, 3927; (b) Liu, J.-L.; Yuan, K.; Leng, J.-D.; Ungur, L.; Wernsdorfer, W.; Guo, F.-S.; Chibotaru, L. F.; Tong, M.-L. *Inorg. Chem.*, **2012**, *51*, 8538.
3. Milios, C. J.; Vinslava, A.; Wernsdorfer, W.; Moggach, S.; Parsons, S.; Perlepes, S. P.; Christou, G.; Brechin, E. K. *J. Am. Chem. Soc*., **2007**, *129*, 2754.
4. (a) Neese. F.; Solomon, E. I. *Inorg. Chem.,* **1998**, *37*, 6568; (b) Waldmann, O. *Inorg. Chem.*, **2007**, *46*, 10035; (c) Neese, F.; Pantazis, D. A. *Faraday Discuss.*, **2011**, *148*, 229.
5. (a) Ishikawa, N.; Sugita, M.； Ishikawa, T.; Koshihara, S. Y.; Kaizu, Y. *J. Am. Chem. Soc.*, **2003**, *125*, 8694. (b) Rinehart, J. D.; Long, J. R. *J. Am. Chem. Soc.*, **2009**, *131*, 12558.
6. (a) Branzoli, F.; Caretta, P.; Filibian, M.; Zoppellaro, G.; Graf, M. J.; Galan-Mascaros, J. R.; Fuhr, O.; Brink. S.; Ruben, M. *J. Am. Chem. Soc.*, **2009**, *131*, 4387; (b) Gonidec, M.; Biagi, R.; Corradini, V.; Moro, F.; De Renzi, V.; del Pennino, U.; Summa, D.; Muccioli, L.; Zannoni, C.; Amabilino, D. B.; Veciana, J. *J. Am. Chem. Soc.*, **2011**, *133*, 6603; (c) Jiang, S.-D.; Wang, B.-W.; Sun, H.-L.; Wang, Z.-M.; Gao, S. *J. Am. Chem. Soc.*, **2011**, *133*, 4730.
7. (a) Sessoli, R.; Tsai, H. L.; Schake, A. R.; Wang, S.; Vincent, J. B.; Folting, K.; Gatteschi, D.; Christou, G.; Hendrickson, D. N. *J. Am. Chem. Soc.*, **1993**, *115*, 1804; (b) Sessoli, R.; Gatteschi, D.; Caneschi, A.; Novak, M. A. *Nature*, **1993**, *365*, 141.
8. Freedman, D. E.; Harman, W. H.; Harris, T. D.; Long, G. J.; Chang, C. J.; Long, J. R. *J. Am. Chem. Soc.*, **2010**, *132*, 1224.
9. Kramers, H. A. *Proc. R. Acad. Sci. Amsterdam*, **1930**, *33*, 959.
10. (a) Zadrozny, J. M.; Long, J. R. *J. Am. Chem. Soc.*, **2011**, *133*, 20732; (b) Mossin, S.; Tran, B. L.; Adhikari, D.; Pink, M.; Heinemann, F. W.; Sutter, J.; Szilagyi, R. K.; Meyer, K.; Mindiola, D. J. *J. Am. Chem. Soc.*, **2012**,*134*, 13651.
11. Zadrozny, J. M.; Xiao, D. J.; Atanasov, M.; Long, G. J.; Grandjean, F.; Neese, F.; Long, J. R. *Nature Chem.*, **2013**, *5*, 577.
12. Wang, X. Y.; Avendano, C.; Dunbar, K. *R. Chem. Soc. Rev.* **2011**, 40, 3212.
13. Feng, X.; Liu, J.; Harris, T. D.; Hill. S.; Long, J. R. *J. Am. Chem. Soc.*, **2012**, *134*, 7521.
14. (a) Cole, K. S. ; Cole, R. H. *J. Chem. Phys*., **1941**, *9*, 341; (b) Boettcher, C. J. F. *Theory of Electric Polarisation; Elsevier: Amsterdam*, **1952**; (c) Aubin, S. M.; Sun, Z.; Pardi, L.; Krzystek, J.; Folting, K.; Brunel, L.-J. Rheingold, A. L.; Christou, G.; Hendrickson, D. N. *Inorg. Chem.*, **1999**, *38*, 5329.
15. Finn, C. B. P.; Orbach, R.; Wolf. W. P. *Proc. Phys. Soc.* **1961**, *77*, 261.
16. (a) Ishikawa, N.; Sugita, M.; Wernsdorfer, W. *Angew. Chem. Int. Ed.,* **2005**, *44*, 2931; (b) Pointillart, F.; Bernot, K.; Golhen, S.; Le Guennic, B.; Guizouarn, T.; Quahab, L.; Cador, O. *Angew. Chem. Int. Ed.*, **2015**, *54*, 1504.

17. (a) Ishikawa, N.; Sugita, M.; Ishikawa, T.; Koshihara, S.-Y.; Kaizu, Y. *J. Am .Chem. Soc*., 2003, **125**, 8694; (b) Meihaus, K. R.; Rinehart, J. D.; Long, J. R. *Inorg. Chem.*, **2011**, *50*, 8484; (c) Zadrozny, J. M.; Long, J. R. *J. Am. Chem. Soc.*, **2011**, *133*, 20732.

5.7 Supporting Information

Table S1. Selected Mean Interatomic Distances (Å) and Angles (°) for *trans*-$(Bu_4N)_2[Re^{IV}Cl_4(CN)_2]\cdot$2DMA at 139 K and 50 K.

	139 K	**50 K**
Re-Cl	2.3509(9) , 2.3407(10)	2.3212(15), 2.3357(15)
Re-C	2.148(4)	2.140(5)
Re-C-N	177.2(3)	177.8(5)
Cl-Re-Cl	90.13(4)	90.18(5)
C-Re-Cl	88.58(10) , 89.57(10)	88.28(15), 89.92(15)

Table S2. Crystallographic data for *trans*-$(Bu_4N)_2[Re^{IV}Cl_4(CN)_2]\cdot$2DMA at 139 K and 50 K.

	139 K	**50 K**
Crystal system	triclinic	
Space group	*P*-1	
***a* / Å**	10.5629(8)	10.4031(6)
***b* / Å**	11.9119(9)	11.9265(7)
***c* / Å**	12.1271(9)	11.9819(7)
***α* / °**	64.8130(10)	64.8219(16)
***β* / °**	75.0150(10)	75.0617(17)
***γ* / °**	82.1510(10)	82.2082(17)
***V* / Å^3**	1333.2(2)	1299.34(13)
Z	1	
***μ* / mm^{-1}**	2.500	2.581
Refl. Coll. / unique	6616 / 4241	23134 / 6646
R_{int}	0.031	0.086
[a] R_1 ($I > 2\sigma(I)$)	0.0337	0.0624
[b] wR_2 (all data)	0.0859	0.1708
Goodness-of-fit	1.045	1.033

[a] $R_1 = \Sigma||F_O|-|F_C||/\Sigma|F_O|$, [b] $wR_2 = [\Sigma w(F_O^2-F_C^2)^2/\Sigma w(F_O^2)^2]^{1/2}$

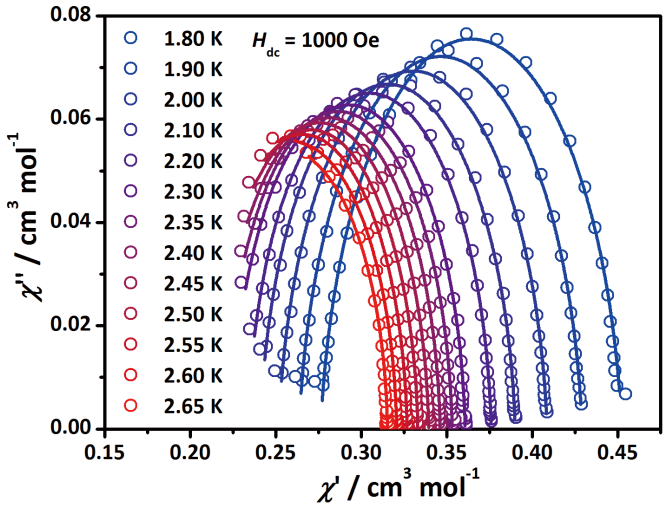

Figure S1 Cole-Cole plots for complex 1 at temperatures from 1.8 K to 2.65 K, under 1000 Oe applied dc field. The solid lines correspond to the fits to the data with α values range from 0.04-0.09, as described in the text.

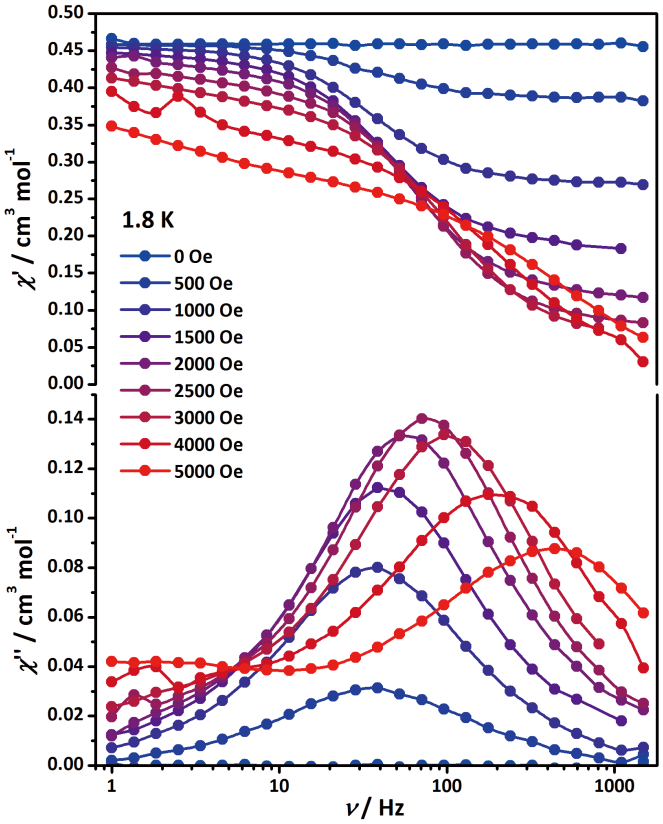

Figure S2 Variable-field ac magnetic susceptibility data obtained for complex 1 at 1.8 K from MPMS-XL7. Solid lines are guides for the eye.

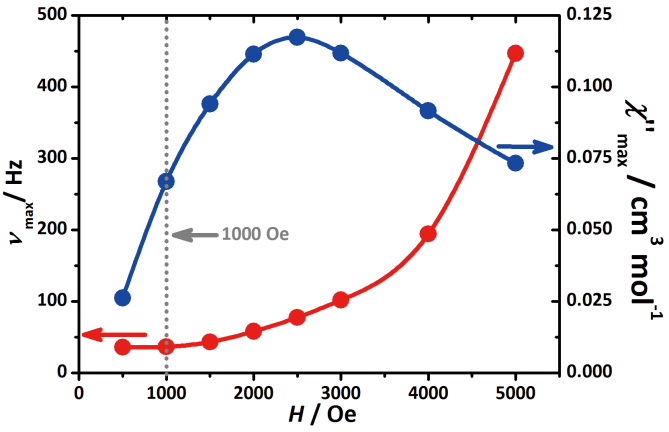

Figure S3 Dc field dependence of the maximum intensity of out-of-phase signals and the relevant frequency at 1.8 K.

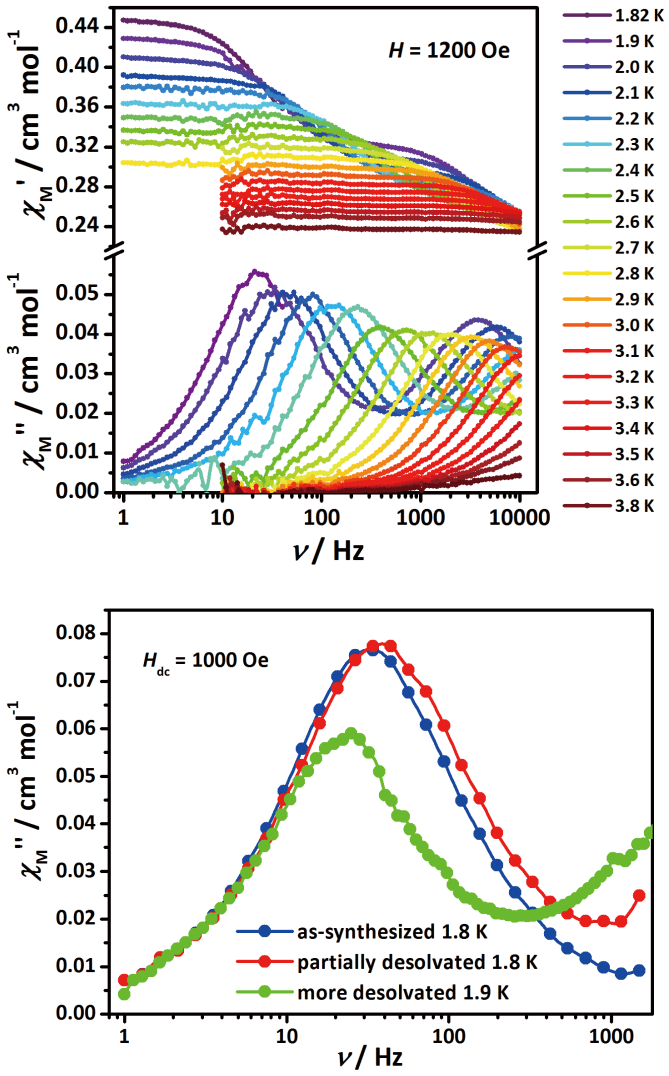

Figure S4 Top: Variable-temperature ac magnetic susceptibility data obtained for 1 in a 1200 Oe dc field from PPMS-9. Bottom: the presence of the higher frequency relaxation process could be due to desolvation for the sample. Solid lines are guides for the eye.

Chapter 6: $Co(hfac)_2$(NITPhenOMe): A Single-Chain Magnet Exhibiting Magnetic Blocking at 12 K

6.1 Introduction

In 2001, slow magnetic relaxation was observed in the one-dimensional chain solid $Co(hfac)_2$(NITPhOMe),[1a] a phenomenon predicted by Glauber nearly half a century ago.[2] Within the solid, slow magnetic relaxation arises from the energy barrier of flipping the net spin generated through antiferromagnetic coupling between anisotropic Co(II) centers (effective S = 1/2) and nitronyl nitroxide radical ligands (S = 1/2). This magnetic behavior is analogous to that observed in single-molecule magnets,[3] and, consequently, chain compounds that exhibit slow magnetic relaxation have come to be known as single-chain magnets.[1b] As a result, these chain compounds have received considerable recent attention, owing to their potential applications such as in spin-based high-density information storage.[4]

In single-chain magnets, the total relaxation barrier can be expressed as $\Delta_\tau = \Delta_A + 2\Delta_\xi$ where Δ_A represents the anisotropy energy barrier and Δ_ξ represents the correlation energy. The anisotropy energy barrier is the energy requirement to overcome the magnetic anisotropy of each individual spin within the chain, analogous to the effective barrier of single molecule magnets (U_{eff}). One prominent feature of single-chain magnets compared to single-molecule magnets is their ability to display a much higher relaxation barrier over their molecular counterparts.[1b] The larger relaxation barriers stem from the short-range magnetic correlation along individual chains, yielding an additional energy component to the overall energy barrier known as correlation energy, Δ_ξ. For an Ising system, where the domain walls within the chain are expected to be narrow ($|D/J|>4/3$), the value of correlation energy barrier is expressed as $\Delta_\xi = 4|J|S^2$. While for the Heisenberg model, where the magnetic anisotropy has to be as small as $|D|<<|J|$, the correlation energy barrier is written as $\Delta_\xi = 4|JD|^{1/2}S^2$. Thus, according to these models, increasing the strength of intrachain exchange coupling should yield higher relaxation barriers in single-chain magnets. Indeed, recent results have shown drastic improvements of single-chain magnets behavior by increasing intrachain magnetic interaction.[5]

Despite the tremendous efforts aimed at synthesizing single-chain magnets with higher relaxation barrier, progress toward this goal has been limited.[1] Indeed, the barrier of 107 cm^{-1} measured for the first single-chain magnet, $Co(hfac)_2$(NITPhOMe), is still considered to be the world record for energy barrier. Clearly, dramatic increases in relaxation energy must be achieved for these compounds to find use in applications at practical temperatures. Recently, we have shown subtle tuning of orbital overlap, and thus exchange strength, can engender a dramatic increase in the relaxation barrier of a series of single-chain magnets of type $LFeReCl_4(CN)_2$.[5] These results inspired us to pursue a new one-dimensional chain compound by modifying the radical ligand of the original single-chain magnet, $Co(hafc)_2$(NITPhOMe). The different steric and electronic properties of the nitronyl nitroxide radicals, along with a different type of crystal packing may provide fine tuning of the orbital overlap between radical ligand and Co(II) centers, and better alignment of anisotropic axes, thereby enhancing significantly the intrachain interactions, and therefore overall magnetic anisotropy and total relaxation barrier. Herein, we demonstrate that such a strategy indeed leads to the observation of a record relaxation

barrier of 251 cm^{-1} in the new single-chain magnet $Co(hfac)_2$(NITPhenOMe), together with blocking temperature at 12 K.

6.2 Experimental Section

The radical ligand NITPhenOMe was prepared by our current collaborators in Prof. Wei Shi's group at Nankai University, compound $Co(hfac)_2$(NITPhenOMe) was synthesized by refluxing $Co(hfac)_2$ salt and NITPhenOMe ligand in heptane under nitrogen atmosphere, according to the previous literature with slight modification.[6,7] Single crystal of compound **1** suitable for x-Ray structure determination was obtained by cooling the resulting hot heptane solution slowly. Treating the single-crystal of **1** under DMF vapor afforded crystalline sample of DMF-dosed compound $Co(hfac)_2$(NITPhenOMe)•xDMF **2**. Crystal structure of compound **1** and powder diffraction pattern of compound **2** are provided in the supporting information (Figure S1 and Figure S2).

Magnetic Susceptibility Measurements. Magnetic data were collected on a Quantum Design MPMS-XL SQUID magnetometer. Measurements for compound **2** were performed on microcrystalline powders restrained in a frozen polyethylene bag. All data were corrected for diamagnetic contributions from the sample holder, as well as for the core diamagnetism of each sample (estimated using Pascal's constants).

Other Physical Measurements. Infrared spectra were obtained on a Nicolet Avatar 360 FTIR with an attenuated total reflectance (ATR) accessory.

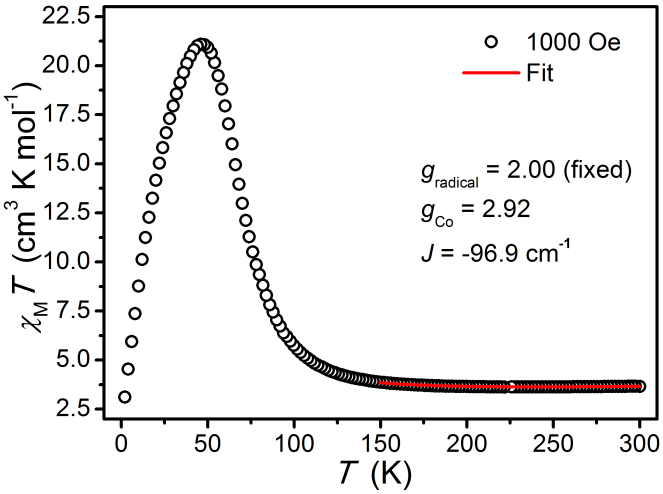

Figure 1. Variable-temperature dc magnetic susceptibility data for **2**, collected in an applied field of 1000 Oe. The solid red line corresponds to a fit to the data, as described in the text, highlighting the

6.3 Results and Discussion

To probe the nature of the magnetic exchange interactions between Co(II) centers and the NITPhenOMe radical ligands in compound **2**, viable temperature dc susceptibility data were collected under an applied field of 1000 Oe, as shown in Figure 1. At 300 K, $\chi_M T$ = 2.73 cm^3K/mol, slightly higher than the calculated value for an isolated S =3/2 Co(II) center together with an S = 1/2 radical center with g = 2.0. When the temperature is

lowered, the value of $\chi_M T$ begins rises gradually at first, then abruptly below 150 K. Finally, $\chi_M T$ reaches maximum at around 50 K and then undergoes a sharp downturn below this temperature, likely due to the magnetic anisotropy of the Co(II) centers. The temperature dependence of $\chi_M T$ data shows clearly a one-dimensional nature as the continuous increase in magnetic moment upon lowering temperature is associated with the correlated magnetic behavior. Furthermore, a dc susceptibility measurement was performed upon cooling the sample with and without applied 100 and 1000 Oe dc fields. Indeed, a sharp divergence was observed at 12 K, as shown in Figure 2, indicating the presence of magnetic blocking, where the magnetic moment is "blocked" due to an energy barrier of spin reorientation.

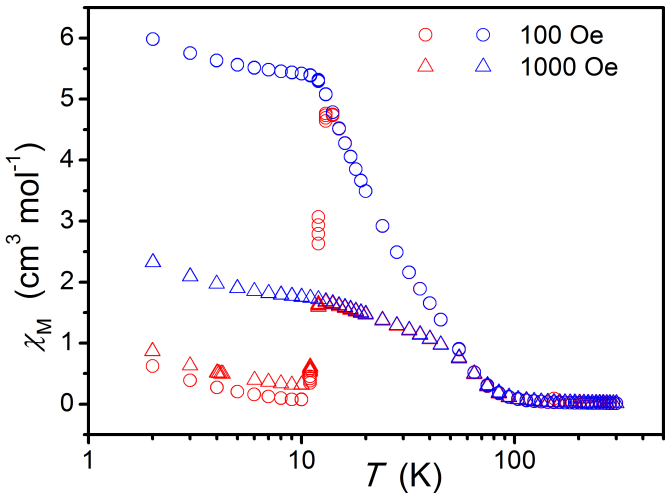

Figure 2. Low temperature dc susceptibility data collect at 1000 and 100 Oe, highlighting divergence at 12 K, indicative of magnetic blocking that arises when the sample is cooled under an applied dc field (FC) compared to cooling under a zero dc field (ZFC).

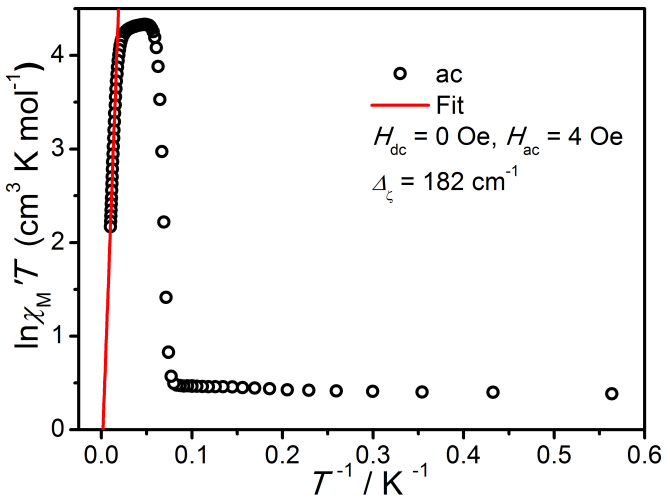

Figure 3. Plot of $\ln(\chi'_M T)$ vs $1/T$ (where χ'_M is the molar component of the ac susceptibility) for 2, collected in zero applied dc field. The solid red line corresponds to a fit to the linear portion of the data, giving Δ_ξ =182 cm^{-1}.

In order to exact the strength of intrachain exchange coupling between Co(II) centers and the NITPhenOMe radical, the $\chi_M T$ data was modeled using the following spin Hamiltonian for a chain consisting of alternating Heisenberg classical spins:

$$H = -2J\sum_{i}^{\infty}(S_i s_i + S_i s_{i+1})$$

where J represents the exchange coupling constant for the interaction between Co^{II} and radical centers, and S and s are the local spins of Co^{II} (S = 3/2) and radical (S = 1/2), respectively. The data were fit in the temperature range of 50-300 K, employing an expression used to describe the magnetic susceptibility of an alternating chain,[8] to give J = -97(1) cm^{-1}, g_{Co} = 2.92, $g_{radical}$ = 2.0 (fixed). The value of J in compound **1** is significantly greater than that of -76 cm^{-1} in the original $Co(hfac)_2$(NITPhOMe) chain compound, indicative of much higher relaxation barrier. Such a drastic increase in the strength of magnetic coupling might come from a better orbital overlap between radical ligand and Co(II) center, due to differences in crystal packing.

For any one-dimensional classical system, the $\chi_M T$ product under zero applied field increases exponentially with decreasing temperature, according to the equation:

$$\chi_M T/C \approx \exp(\Delta_\xi/k_B T)$$

Where C is the effective Curie constant, Δ_ξ is the correlation energy and k_B is the Boltzmann constant.[9] Following this relationship, a plot of $\ln(\chi_M T)$ vs $1/T$ should feature a linear region, with the line of best fit exhibiting a slope corresponding to the correlation energy. Thus, to probe the one-dimensional nature of compound **2**, viable-temperature ac susceptibility data were collected under a 4 Oe ac field oscillating at 1 Hz. Indeed, the resulting plot of $\ln(\chi'_M T)$ vs 1/T displays a linear region between 40-200K, giving Δ_ξ = 182 cm^{-1}. The value of $\ln(\chi'_M T)$ reaches a maximum at 20 K and features a plateau between 12 and 20 K, indicative of the saturation of magnetic correlation for a one-

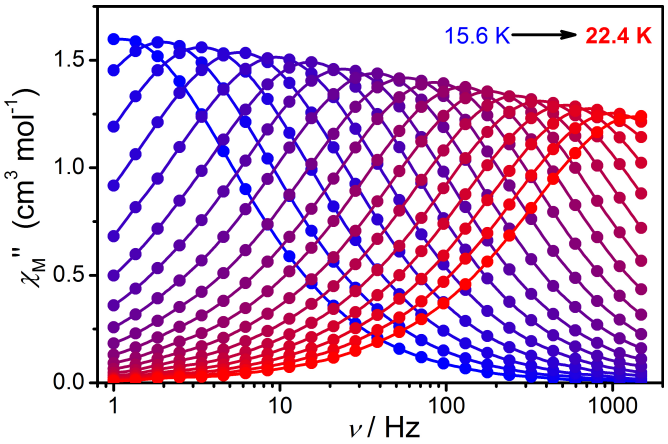

Figure 4. Variable-frequency in-phase (top) and out-of-phase (bottom) ac magnetic susceptibility data for 2, collected in a 4 Oe ac field at temperature range of 15.5 K to 29 K.

.

dimensional chain behavior.

To probe the slow magnetic relaxation in compound **1**, variable temperature ac susceptibility data were collected in the range of 1-1500 Hz under zero applied dc field, revealing strong frequency dependence of both in-phase (χ'_M) and out-of-phase (χ''_M) signals. The relaxation time, τ, was then extracted by fitting the data of χ'_M and χ''_M using a generalized Debye model.[10] For a single-chain magnet, the temperature dependence of relaxation time should follow a thermally activated Arrhenius behavior, where the plot of $\ln(\tau)$ vs $1/T$ is linear with a slope corresponding to the total relaxation barrier Δ_A. Indeed, the plot of $\ln(\tau)$ vs $1/T$ of compound 2 demonstrated a clear Arrhenius behavior, with the best least square fit to the line giving $\Delta_A = 251$ cm^{-1} and $\tau_0 = 1.29\times10^{-11}$s. The value of τ_0 is in good agreement with the value reported for other single-chain magnets.

Notably, the relaxation barrier observed for **2** is among the highest yet observed for single-chain magnets. In comparison, the radical bridged chain compound Co(hfac)$_2$(*p*-butoxyphenyl-NN) was shown to exhibit a relaxation barrier of $\Delta_\tau = 243$ cm^{-1}, but with a much smaller attempt time ($\tau_0 = 6.8 \times 10^{-13}$ s).[11] The authors note that the small τ_0 may be diagnostic of spin glass behavior caused by interchain interactions. Indeed, this hypothesis is supported by a lack frequency dependence in the ac susceptibility upon application of a 500 Oe dc field. Another compound, Co(hfac)2(PyrNN), was reported to exhibit a barrier of $\Delta_\tau = 262$ cm^{-1} and 275 cm^{-1}, with two maxima peaks presented in the ac frequency dependent measurements.[12] As the authors explained, this observation of two sets of ac peaks in one frequency is due to the presence of short and long chains

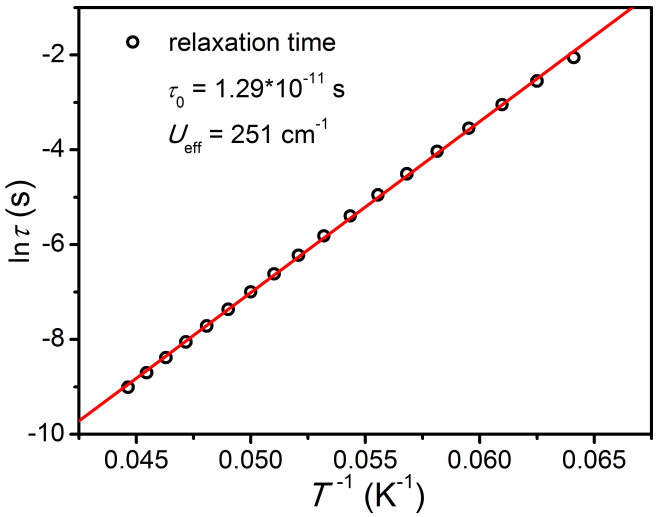

Figure 4. Arrhenius plot of relaxation time for **2**. The solid red line corresponds to a linear fit to the data, giving $\Delta_\tau = 251$ cm^{-1}.

within finite regime. However, previous study has shown no evidence that the chain length within finite regime should have an influence of the relaxation barrier. Thus, this compound deserves further study. Considering chain compounds that show attempt times within the range typically observed for superparamagnets and do not exhibit anomalous relaxation behavior, the highest barrier yet reported belongs to the radical-bridged chain compound Co(hfac)$_2$(NITPhOMe). As such, the relaxation barrier of compound **2** represents the highest barrier for a single-chain magnet.

Extrapolating the Arrhenius plot of compound 2 to low temperatures indicates 100s relaxation time at 12.2 K, suggesting the apparent of magnetic hysteresis behavior below this temperature. Indeed, open magnetic hysteresis was observed from the viable field magnetization measurements performed in the temperature range of 1.8 -12 K, as shown in Figure 5. It is also noted that the significant difference of the shapes between hysteresis blow 6 K and above, which is likely due to either magnetic ordering effect below 6 K or structural phase transition below 6 K. For a molecular magnet, the blocking temperature of always defined by either magnetic hysteresis remains open at zero-field, or the temperature at which the relaxation time is 100 s.[13,14] For the case of compound **2**, both extrapolation of ac susceptibility and hysteresis measurements suggested a blocking temperature of 12 K. Significantly, this blocking temperature represents the highest yet observed for a single-chain magnet.

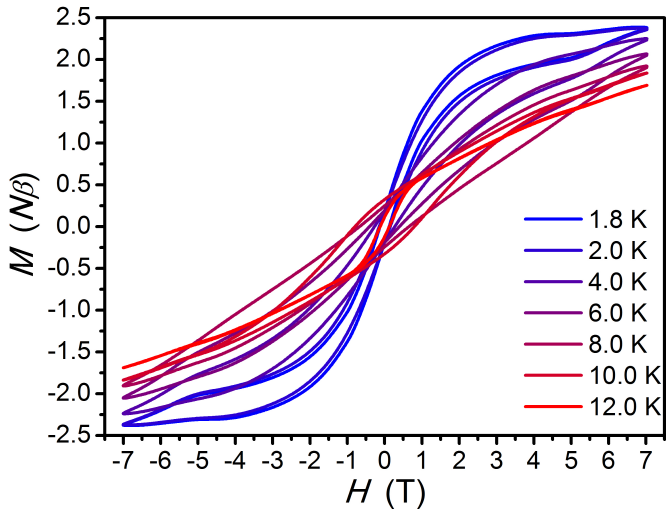

Figure 5. Variable-field magnetization data for **6**, collected at from 2 K to 12 K under a sweep-rate of 100 Oe/min.

6.4 Conclusion and Outlook

Taken all together, the foregoing results demonstrated a new Co(II)-nitronyl nitroxide radical single-chain magnet, with record blocking temperature and relaxation barrier. In particular, compared to the previous $Co(hfac)_2(NITPhOMe)$ chain reported by Gatteschi and co-workers, the increase of magnetic coupling in **1** leads to a significantly increase in correlation energy barrier and thus total relaxation barrier. This result, again, emphasizes the important role of intrachain magnetic coupling to the total relaxation barrier for a single-chain magnet. Efforts are underway to synthesize other nitroxide radical ligands with different substituent groups, to establish a magneto-structural correlation for this kind of one-dimensional chain solid, and to obtain single-chain magnets with higher relaxation barriers. Additionally, extension of the system to lanthanide ions may lead to higher relaxation barriers, as the strong-spin orbit coupling from 4f orbitals can give contribution to much larger magnetic anisotropy, thus increase the anisotropy energy of the total relaxation barrier. For such a strategy, the crucial concern is how to generate strong magnetic coupling between lanthanide ions and radical ligands. Indeed, recent

results have shown strong magnetic coupling can be achieved between lanthanide centers and radicals in single-molecule magnets.[15] It is our hope that such efforts could result in new single-chain magnets with large relaxation barrier, to open the gate for potential application at more practical temperatures.

6.5 Acknowledgement

This research was supported by NSF Grant No. CHE-0617063. I thank Prof. R. Clérac for helpful discussions. I also thank Dr. T. David Harris and Dr. J. M. Zadrozny for experimental assistance.

6.6 Reference

1 Caneschi, A.; Gatteschi, D.; Lalioti, N.; Sangregorio, C.; Sessoli, R.; Venturi, G.; Vindigni, A.; Rettori, A.; Pini, M. G.; Novak, M. A. *Angew. Chem., Int. Ed.* 2001, *40*, 1760. (b) Clérac, R.; Miyasaka, H.; Yamashita, M.; Coulon, C. *J. Am. Chem. Soc.* **2002**, *124*, 12837. (c) Lescouëzec, R.; Vaissermann, J.; Ruiz-Pérez, C.; Lloret, F.; Carrasco, R.; Julve, M.; Verdaguer, M.; Dromzée, Y.; Gatteschi, D.; Wernsdorfer, W. *Angew. Chem., Int. Ed.* **2003**, *42*, 1483. (d) Liu, T. F.; Fu, D.; Gao, S.; Zhang, Y. Z.; Sun, H. L.; Su, G.; Liu, Y. J. *J. Am. Chem. Soc.* **2003**, *125*, 13976. (e) Wang, S.; Zuo, J.-L.; Gao, S.; Song, Y.; Zhou, H.-C.; Zhang, Y.-Z.; You, X.-Z. *J. Am. Chem. Soc.* **2004**, *126*, 8900. (f) Ferbinteanu, M.; Miyasaka, H.; Wernsdorfer, W.; Nakata, K.; Sugiura, K.; Yamashita, M.; Coulon, C.; Clérac, R. *J. Am. Chem. Soc.* **2005**, *127*, 3090. (g) Coulon, C.; Miyasaka, H.; Clérac, R. *Struct. Bonding (Berlin)* **2006**, *122*, 163. (h) Bernot, K.; Bogani, L.; Caneschi, A.; Gatteschi, D.; Sessoli, R. *J. Am. Chem. Soc.* **2006**, *128*, 7947. (i) Miyasaka, H.; Madanbashi, T.; Sugimoto, K.; Nakazawa, Y.; Wernsdorfer, W.; Sugiura, K.; Yamashita, M.; Coulon, C.; Clérac, R. *Chem.−Eur. J.* **2006**, *12*, 7028. (j) Miyasaka, H.; Julve, M.; Yamashita, M.; Clérac, R. *Inorg. Chem.* **2009**, *48*, 3420 and references therein. (k) Venkatakrishnan, T. S.; Sahoo, S.; Brefuel, B.; Duhayon, C.; Paulsen, C.; Barra, A.; Ramasesha, S.; Sutter, J. *J. Am. Chem. Soc.* **2010**, *132*, 6047.

2 Glauber, R. J. *J. Math. Phys.* 1963, 4, 294.

3 (a) Sessoli, R.; Tsai, H. L.; Schake, A. R.; Wang, S.; Vincent, J. B.; Folting, K.; Gatteschi, D.; Christou, G.; Hendrickson, D. N. *J. Am. Chem. Soc.***1993**, *115*, 1804. (b) Sessoli, R.; Gatteschi, D.; Caneschi, A.; Novak, M. A. *Nature* **1993**, *365*, 141. (c) Gatteschi, D.; Sessoli, R.; Villain, J. *Molecular Nanomagnets*, Oxford University Press: New York, **2006** and references therein. (d) Schelter, E. J.; Prosvirin, A. V.; Dunbar, K. R. *J. Am. Chem. Soc.* **2004**, *126*, 15004. (e) Milios, C. J.; Vinslava, A.; Wernsdorfer, W.; Moggach, S.; Parsons, S.; Perlepes, S. P.; Christou, G.; Brechin, E. K. *J. Am. Chem. Soc.* **2007**, *129*, 2754. (f) Freedman, D. E.; Jenkins, D. M.; Iavarone, A. T.; Long, J. R. *J. Am. Chem. Soc.***2008**, *130*, 2884. (g) Yoshihara, D.; Karasawa, S.; Koga, N. *J. Am. Chem. Soc.***2008**, *130*, 10460. (h) Lin, P.-H.; Burchell, T. J.; Ungur, L.; Chibotaru, L.; Wernsdorfer, W.; Murugesu, M. *Angew. Chem. Int. Ed.*, **2009**, *48*, 9489.

4 (a) Garanin D. A. and Chudnovsky, E. M. *Phys. Rev. B*, **1997**, *56*, 11102; (b) Leuenberger M. N. and Loss, D. *Nature*, 2001, **410**, 789; (c) Jo, M.-H.; Grose, J. E.; Liang, W.; Baheti, K.; Deshmukh, M. M.; Sokol, J. J.; Rumberger, E. M.; Hendrickson, D. N.; Long, J. R.; Park H.; Ralph, D. C. *Nano Lett.*, **2006**, *6*, 2014. (d)

Ardavan, A.; Rival, O.; Morton, J. J. L.; Blundell, S. J.; Tyryshkin, A. M.; Timco, G. A.; Winpenny, R. E. P. *Phys. Rev. Lett.* **2007**, *98*, 57201. (e) Bogani, L.; Wernsdorfer, W. *Nat. Mater.* 2008, **7**, 179. (f) Stamp, P. C. E.; Gaita-Arino, A. *J. Mater. Chem.* **2009**, *19*, 1718. (g) Loth, S.; von Bergmann, K.; Ternes, M.; Otte, A. F.; Lutz, C. P.; Heinrich, A. J. *Nat. Phys.* **2010**, *6*, 340.
5 Feng, X.; Harris, T. D.; Long, J. R. *Chem. Sci.* **2011**, *2*, 1688.
6 Caneschi, A.; Gatteschi, D; Rey, P.; Sessoli, R. *Inorg. Chem.* **1991**, *30*, 3936.
7 Private communication between Long group and Wei group.
8 Drillon, M.; Coronado, E.; Beltran, D.; Georges, R. *Chem. Phys.***1983**, *79*, 449. (b) Georges, R.; Borras-Almenar, J. J.; Coronado, E.; Curely, J.; Drillon, M. *Magnetism: Molecules to Materials I: Models and Experiments*, Eds. Miller, J. S.; Drillon, M.; Wiley-VCH: Verlag, **2002**.
9 (a) Coulon, C.; Miyasaka, H.; Clerac, R. *Struct. Bonding (Berlin)* **2006**, *122*, 163. (b) Loveluck, J. M.; Lovesey, S. W.; Aubry, S. *J. Phys. C: Solid State Phys.* **1975**, *8*, 3841. (c) Nakamura, K.; Sasada, T. *J. Phys. C: Solid State Phys.* **1978**, *11*, 331.
10 (a) Cole, K. S.; Cole, R. H. *J. Chem. Phys.* **1941**, *9*, 341. (b) Boettcher, C. J. F. *Theory of Electric Polarisation*; Elsevier: Amsterdam, **1952**. (c) Aubin, S. M.; Sun, Z.; Pardi, L.; Krzystek, J.; Folting, K.; Brunel, L.-J.; Rheingold, A. L.; Christou, G.; Hendrickson, D. N. *Inorg. Chem.* 1999, **38**, 5329.
11 Ishii, N.; Okamura, Y.; Chiba, S.; Nogami, T.; Ishida, T. *J. Am. Chem. Soc.* **2008**, *130*, 24.
12 Vaz, M. G. F.; Cassaro, R. A. A.; Akpinar, H.; Schlueter, J. A.; Lahti, P. M.; Novak, M. A. *Chem. Eur. J.* **2014**, *20*, 5460.
13 Woodruff, D. N.; Winpenny, R. E.; Layfield, R. A. *Chem. Rev.* **2013**, *113*, 5110.
14 Gatteschi, D.; Sessoli, R.; Villain, J. Molecular Nanomagnets; Oxford University Press: Oxford, **2006**.
15 (a) Rinehart, J. D.; Fang, M.; Evans, W. J.; Long, J. R. *Nat. Chem.* **2011**, *3*, 538-542. (b) Rinehart, J. D.; Fang, M.; Evans, W. J.; Long, J. R. *J. Am. Chem. Soc.* **2011**, *133*, 14236-14239. (c) Demir, S.; Zadrozny; J. M.; Nippe, M.; Long, J. R. *J. Am. Chem. Soc.* **2012**, *134*, 18546-18549. (d) Demir, S.; Nippe, M.; Gonzalez, M. I.; Long, J. R. *Chem. Sci.* **2014**, *5*, 4701-4711.

6.7 Supporting Information

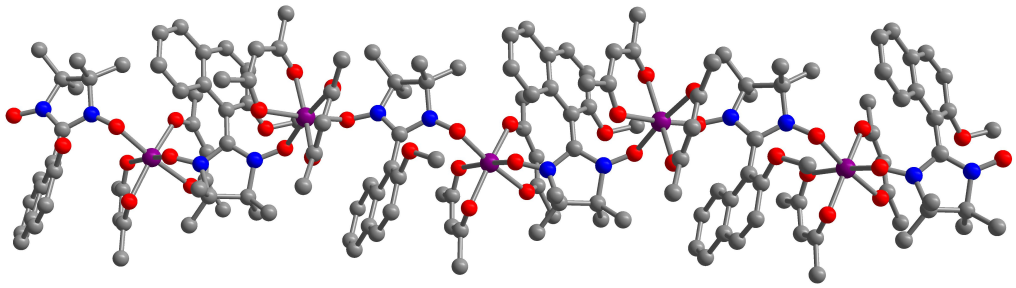

Figure S1. Crystal structure of $Co(hfac)_2(NITPhenOMe)$. Violet, red, blue, and gray spheres represent cobalt, oxygen, nitrogen, and carbon atoms, respectively; hydrogen atoms have been omitted for clarity.

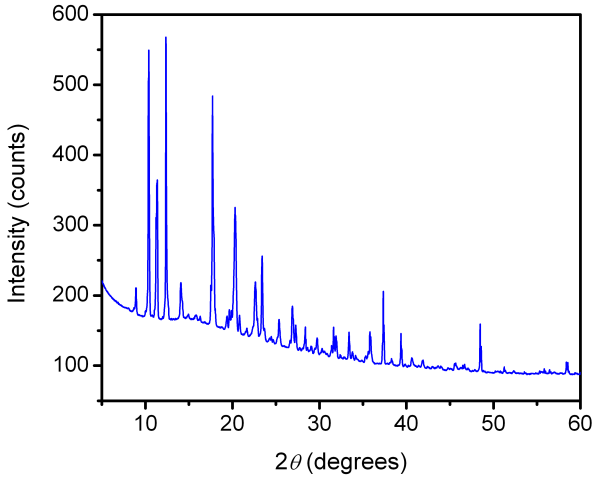

Figure S2. Powder diffraction spectrum of compound 2. Indexing the spectrum yields unit cell parameters a = 6.27 Å, b = 10.09 Å, c = 20.46 Å, α = 98.7°, β = 94.8 °, γ = 65.6°, V = 1163.2 Å^3.